

Dissertation
submitted to the
Combined Faculty of Natural Sciences and Mathematics
of the Ruperto Carola University Heidelberg, Germany
for the degree of
Doctor of Natural Sciences

Presented by
M. Sc. Julia Alexandra Braun
born in: Ulm
Oral examination: 17th December 2018

The Effects of Iron Chelators on the Phenotype of HPV-Positive Cervical Cancer Cells

Referees: Prof. Dr. Walter Nickel

Prof. Dr. Felix Hoppe-Seyler

Table of contents

Summary.....	I
Zusammenfassung	III
Acknowledgements	V
Publications, patents and presentations	VII
1. Introduction	3
1.1 Human Papillomavirus (HPV) and cancer.....	3
1.2 Pathogenesis of HPV-linked cancer	3
1.3 HPV oncogenes <i>E6</i> and <i>E7</i>	5
1.4 Therapy of HPV-positive cervical cancer.....	6
1.5 Tumour hypoxia.....	7
1.6 Hypoxia in cervical cancer.....	8
1.7 Senescence	9
1.8 Iron metabolism	11
1.9 Intracellular iron	13
1.10 Iron and oxygen homoeostasis.....	15
1.11 Iron and cancer.....	15
1.12 Iron chelators	16
1.13 Ciclopirox (CPX).....	17
1.14 Ribonucleotide reductase (RR).....	19
1.15 Research objectives.....	20
2. Results	25
2.1 Iron chelators repress <i>E6</i> and <i>E7</i>	25
2.2 CPX inhibits cell proliferation	29
2.3 CPX induces cell cycle arrest and senescence.....	31
2.4 CPX induces apoptosis	39
2.5 CPX induces mTORC1-independent senescence	44
2.6 CPX exhibits growth inhibitory effects under hypoxic conditions.....	47
2.7 CPX cooperates with RT and CT	50
2.8 Proteome analyses after CPX treatment	51
2.9 HU induces senescence, but not apoptosis	53
3. Discussion.....	59
3.1 Repression of <i>E6/E7</i> by iron chelators	59

3.2 Growth inhibition by CPX	61
3.3 CPX induces mTORC1-independent senescence.....	66
3.4 Apoptosis induction by CPX.....	68
3.5 CPX cooperates with RT and CT	71
3.6 Clinical implications.....	72
3.7 Conclusions	73
4. Material and Methods	77
4.1 Buffers and solutions.....	77
4.2 Chemicals	78
4.3 Cell-based assays.....	78
4.3.1. Cell culture.....	78
4.3.1. Cryopreservation and thawing of cells	80
4.3.2. Treatment of cells	80
4.3.3. Irradiation of cells.....	80
4.3.4. Transfection of pSUPER constructs	81
4.3.5. Senescence Assay	81
4.3.6. Colony formation assay (CFA).....	81
4.3.7. Cell cycle analysis	82
4.3.1. EdU assay	82
4.3.1. Proliferation assay	83
4.3.2. Caspase-3/7 assay	83
4.3.3. TUNEL assay.....	83
4.3.4. γ -H2AX staining.....	84
4.3.5. Annexin V apoptosis detection.....	84
4.3.6. Generation of spheroids.....	84
4.3.7. Histological staining of spheroids	85
4.4 Protein-based assays.....	86
4.4.1. Protein extraction.....	86
4.4.2. Protein concentration determination and preparation of samples.....	86
4.4.3. SDS-PAGE, western blot and immunodetection of proteins.....	86
4.4.4. Proteome analysis (TMT10plex method)	88
4.5 RNA-based assays.....	90
4.5.1. RNA isolation	90

4.5.2. Reverse transcription (RT) and quantitative real-time PCR (qRT-PCR).....	90
4.6 Statistical analyses	91
5. Appendix	95
Supplementary figure.....	95
List of Figures	96
List of Tables	97
Abbreviations.....	98
Units and prefixes	102
References.....	103

Summary

Oncogenic human papillomavirus (HPV) types are major human carcinogens. Sustained expression of the viral *E6* and *E7* oncogenes is essential for the malignant growth of HPV-positive cancer cells. Moreover, cancer cells typically exhibit metabolic alterations. Surprisingly little is known about the relation between the HPV oncogenes and the cellular iron metabolism although it is increasingly recognised to be linked to tumourigenesis. Thus, the overall aim of the presented studies was to investigate the crosstalk between oncogenic HPVs and the iron metabolism of their tumourigenic host cells.

Interestingly, treatment of HPV-positive cervical cancer cells with the iron chelators deferoxamine (DFO) or ciclopirox (CPX) strongly suppresses expression of the viral *E6/E7* oncogenes, suggesting therapeutic potential for these agents. Further detailed work was focused on CPX since (in contrast to DFO) this drug can be applied topically and thus could be suitable for the treatment of HPV-induced (pre)neoplasias. It was found that CPX efficiently blocks cellular proliferation in both 2D and 3D cell culture, induces cell cycle arrest in the G1 and S phase and ultimately leads to cellular senescence. Both *E6/E7* repression and senescence are a consequence of iron deprivation since they can be prevented by excess iron. Notably, although mTORC1 signalling is widely believed to be required for senescence induction, the pro-senescent activity of CPX is independent of mTORC1 signalling. Proteome analyses revealed candidate proteins which might be involved in the CPX-induced growth arrest and senescence. Moreover, prolonged treatment of HPV-positive cervical cancer cells with CPX results in apoptosis which is observable under both normoxic and hypoxic conditions. Since CPX exerts pro-apoptotic effects also under hypoxia, it could be used in combination with radio- and chemotherapy which both are typically less active against hypoxic tumour cells.

Taken together, these results reveal that HPV oncogene expression is very sensitive to iron deprivation. CPX could be a particularly promising agent for the treatment of HPV-positive cancers since it represses *E6/E7*, induces senescence and apoptosis under normoxic conditions and can also eliminate hypoxic cells which pose a major problem for the efficacy of anti-cancer drugs in the clinic.

Zusammenfassung

Onkogene Typen humaner Papillomviren (HPVs) sind Hauptkarzinogene für den Menschen. Die kontinuierliche Expression der viralen *E6*- und *E7*-Onkogene ist essentiell für das maligne Wachstum HPV-positiver Tumore. Krebszellen besitzen zudem typischerweise metabolische Veränderungen. Überraschend wenig ist über eine mögliche Verbindung zwischen den HPV-Onkogenen und dem zellulären Eisenmetabolismus bekannt, obwohl dieser zunehmend mit der Krebsentstehung in Verbindung gebracht wird. Als übergeordnetes Ziel untersuchte die vorliegende Arbeit daher die Interaktion zwischen onkogenen HPVs und dem Eisenmetabolismus ihrer tumorigenen Wirtszellen.

Interessanterweise führt die Behandlung HPV-positiver Zervixkarzinomzellen mit den Eisenchelatoren Deferoxamin (DFO) oder Ciclopirox (CPX) zu einer starken Hemmung der viralen *E6/E7*-Onkogenexpression, was auf ein therapeutisches Potenzial für diese angewandten Wirkstoffe hinweist. Weitere, detaillierte Untersuchungen waren auf CPX fokussiert, da dieses Medikament (im Gegensatz zu DFO) topisch angewandt werden kann und daher für die Behandlung HPV-induzierter (Prä-)neoplasien geeignet sein könnte. Es konnte gezeigt werden, dass CPX das Zellwachstum unter 2D- und 3D-Zellkulturbedingungen effizient hemmt, die Zellen in der G1- und S-Phase arretiert und letztendlich zu zellulärer Seneszenz führt. Sowohl die *E6/E7*-Hemmung als auch die Seneszenz werden durch Eisenentzug verursacht, da sie durch einen Überschuss an Eisen verhindert werden können. Obwohl im Allgemeinen angenommen wird, dass ein aktiver mTORC1-Signalweg für die Seneszenz-Induktion notwendig ist, kann gezeigt werden, dass die pro-seneszente Wirkung von CPX unabhängig von mTORC1 erfolgt. Proteomanalysen ergaben Hinweise auf Proteine, die im Wachstumsarrestes und der Seneszenz durch CPX beteiligt sein könnten. Des Weiteren wird gezeigt, dass eine länger andauernde Behandlung mit CPX in HPV-positiven Zervixkarzinomzellen sowohl unter normoxischen als auch unter hypoxischen Bedingungen in Apoptose resultiert. Da CPX auch unter Hypoxie pro-apoptotisch wirkt, könnte CPX in Kombination mit Radio- und Chemotherapie eingesetzt werden, welche gegen hypoxische Zellen typischerweise weniger wirksam sind.

Zusammenfassend zeigen die Ergebnisse, dass die HPV-Onkogenexpression sehr sensitiv auf Eisenentzug reagiert. CPX könnte ein besonders vielversprechender Wirkstoff für die Behandlung HPV-positiver Tumore sein, da es *E6/E7* reprimiert, Seneszenz und Apoptose

unter normoxischen Bedingungen induziert und außerdem hypoxische Zellen eliminiert, die ein großes Problem für die Effizienz der Krebstherapie in der Klinik darstellen.

Acknowledgements

First of all I would like to thank Prof. Dr. Felix Hoppe-Seyler for giving me the opportunity to conduct this dissertation in his lab and to start this project from scratch. Thank you for the constant guidance, support and input you gave me throughout the whole time. I also want to thank Prof. Dr. Karin Hoppe-Seyler for the many inspiring discussions about the project and many aspects beyond the lab. I could have not wished for better supervisors.

I would also like to acknowledge Prof. Dr. Walter Nickel for being my first referee and a member of my TAC. Thank you for the fruitful discussions and new ideas during the TAC meetings. I am also very grateful for the opportunity to test the IncuCyte® in your lab and the assistance of Menna Ahmed. I would like to thank Dr. Marco Binder and Dr. Steeve Boulant for being members of my Thesis Committee. Furthermore I want to thank Prof. Dr. Frank Rösl for being a valuable TAC member and giving me a lot of helpful recommendations.

I want to thank Bianca Kuhn, who is not only a former colleague and now collaborator but also a close friend. Thank you for your support throughout my PhD life as a friend and co-worker. I especially want to express my gratitude for performing the proteome analyses and helping me with the data analysis. In this regard I also want to thank Prof. Dr. Jeroen Krijgsveld for the collaboration.

Furthermore, I would like to thank Dr. Joschka Willemsen and Dr. Marco Binder for generating HeLa mCherry H2B and SiHa mCherry H2B cell lines and providing us with the protocol and plasmids to generate other mCherry H2B labelled cell lines. I want to express my gratitude also to Jenny Hetzer, Danijela Heide and Prof. Dr. Mathias Heikenwälder who helped me to establish and optimise a protocol for the embedding, sectioning and staining of spheroids. Many thanks go to Dr. Damir Kronic from the light microscopy core facility for the support with the microscope and patience during the macro generation for the analyses.

I especially wanted to thank Dr. Bruno Galy for the many fruitful discussions on iron metabolism and the inspiring input you gave me.

Importantly, I want to express my gratitude to two former Master's students Johanna Ira Blase and Anja Herrmann. It was a pleasure to have someone to share the project with, including all ups and downs. I appreciated the close collaboration and the discussions with you a lot. Thank you so much for contributing to this dissertation. Furthermore, I want to thank the whole F065 lab. Especially Julia Bulkescher, Claudia Lohrey and Angela Holzer who not only patiently

answered the countless questions regarding protocols and where to find what, but also supported me a lot with their expertise especially towards the end of the PhD time. I also want to thank all current and former members of the F065 lab: Svenja Adrian, Johanna Ira Blase, Felicitas Boßler, Julia Botta, Julia Bulkescher, Antonia Däschle, Anja Herrmann, Angela Holzer, Sofie Knoll, Bianca Kuhn, Claudia Lohrey, Julia Mändl, Tobias Strobel and Dongyun Yang. You all have contributed to the familiar atmosphere that I appreciate most and which I will deeply miss. Furthermore, I would like to thank Thomas Holz for the constant help with all computer-related problems. I also want to acknowledge Diana Schalk for the help in all administrative matters. Thank you, Ulrike Ackermann, Natalie Erbe-Hofmann and Claudia Tessmer for the pleasant company during breakfasts and lunches.

Finally, I want to thank my family, especially my mother and Sarah for the support and love throughout the whole time. Thank you for encouraging me to achieve my goals and for always being there for me. I am also deeply grateful for Till. Your support especially during the stressful times is beyond comparison. Thanks for cheering me up or motivating me when I needed it. You're the best partner I could wish for.

Publications, patents and presentations

Publications

Hoppe-Seyler K, Bossler F, Braun JA, Herrmann AL, Hoppe-Seyler F. The HPV E6/E7 Oncogenes: Key Factors for Viral Carcinogenesis and Therapeutic Targets. Trends in Microbiology, 2018. 26(2): p.158-168.

Braun JA, Herrmann AL, Bulkescher J, Kuhn BJ, Holzer A, Lohrey C, Krijgsveld J, Heikenwalder M, Hoppe-Seyler K, Hoppe-Seyler F. Inhibition of the HPV *E6/E7* oncogenes by the iron chelator ciclopirox. Manuscript in preparation.

Patent application

Iron Chelators in Tumor Therapy, European Patent Application 17203391.2 (23.11.2017)

Presentations

Braun JA, Herrmann AL, Hoppe-Seyler K, Hoppe-Seyler F. Inhibition of Viral E6/E7 Oncogene Expression and Induction of Senescence in HPV-positive Cancer Cells. 28th Annual Meeting of the Society for Virology, Gesellschaft fur Virologie e.V. (GfV) und Deutsche Vereinigung zur Bekampfung der Viruskrankheiten e.V. (DVV). 14.-17.03.2018, Wurzburg, Germany. Oral presentation.

Braun JA, Bossler F, Hoppe-Seyler K, Hoppe-Seyler F. Crosstalk between Oncogenic HPVs and the Host Cell Metabolism. POF review. 29.-31.01.2018 Heidelberg, Germany. Poster presentation.

Braun JA, Herrmann AL, Hoppe-Seyler K, Hoppe-Seyler F. The effect of iron chelators on HPV-positive cancer cells. Helmholtz International Graduate School for Cancer Research PhD Poster Presentation. 24.11.2017, Heidelberg, Germany. Poster presentation.

Braun JA, Blase JI, Hoppe-Seyler K, Hoppe-Seyler F. The effect of iron chelators on the phenotype of HPV-positive cancer cells. Helmholtz International Graduate School for Cancer Research Retreat. 03.-05.07.2017, Weil der Stadt, Germany. Oral presentation.

Braun JA, Blase JI, Hoppe-Seyler K, Hoppe-Seyler F. The effect of iron chelators on the phenotype of HPV-positive cancer cells. Retreat of the DFKZ research programme infection, inflammation and cancer. 22.-24.05.2017, Rastatt, Germany. Oral presentation.

Braun JA, Hoppe-Seyler K, Hoppe-Seyler F. Iron Chelators Block HPV Oncogene Expression and Induce Senescence. Retreat of the DFKZ research programme infection, inflammation and cancer. 30.05.-01.06.2016, Schontal, Germany. Oral presentation.

CHAPTER 1

INTRODUCTION

1. Introduction

1.1 Human Papillomavirus (HPV) and cancer

Human papillomaviruses (HPVs) are non-enveloped, double-stranded DNA viruses belonging to the family of papillomaviridae. More than 180 different HPV types are known [1]. Depending on their potential to induce cancer, HPVs can be grouped into high-risk and low-risk HPVs. Mucosal infection with low-risk HPVs (e.g. type 6 and 11) can cause benign genital warts and condylomas whereas lesions infected with high-risk HPVs (type 16, 18, 31, 33, 35, 39, 45, 51, 52, 56, 58 and 59) may progress to cancer [2]. The causal role of HPV in carcinogenesis is best described in cervical cancer [3]. In the 19th century, the Italian physician Rigoni-Stern noticed a high frequency of cervical cancer in married women, widows and prostitutes, whereas virgins and nuns very rarely showed signs of it; concluding that the incidence of this cancer is linked to sexual contact [4]. In the 1970s, zur Hausen and co-workers proposed that cervical cancer could be associated with HPV infection [5] and in 1983, Dürst et al. were able to isolate HPV16 DNA from a cervical cancer specimen [6]. Today, it is known that virtually all cervical cancers are HPV-positive with the high-risk types HPV16 and HPV18 accounting for approximately 70% of all cases [7]. HPV16 alone causes 40-60% of all cervical cancers [8]. In total, 4.5% of all human cancers worldwide are associated with HPV infections, among them are additional cancers of the anogenital region (vulva, vagina, penis, anus), head and neck cancers [9] and non-melanoma skin cancer [10].

Because of the important role of high-risk HPV types as human carcinogens, prophylactic vaccines have been developed. Gardasil®9 is a nonavalent vaccine which protects against HPV6, 11, 16, 18, 21, 33, 45, 52 and 58 and thus against 90% of all cervical cancer cases in women and 80-95% of other HPV-related cancers in both men and women [11]. However, despite the efficiency and success of these vaccines, only 1.7% of all females worldwide received at least one shot of HPV vaccines with developing countries having the lowest vaccination rates [12]. Thus, cervical cancer will remain a major health care problem in the future.

1.2 Pathogenesis of HPV-linked cancer

HPVs infect keratinocytes in the basal layer of squamous epithelia, i.e. skin and mucosal surfaces, and their replication is tightly linked to the host cell's differentiation status [13]. During cell division, keratinocytes differentiate and progress to the surface of the epithelium where the viral particles can be released. Infections with HPV types are often cleared by the

immune system without manifestation of clinical symptoms [14]. However, if oncogenic HPV types persist in the infected cell, cancer can arise [15]. Transformation is associated with the expression of the viral oncogenes *E6* and *E7* which are able to deregulate the host's cell cycle and to interfere with senescence and apoptosis (further discussed below). Both the *E6* and *E7* oncoproteins have shown transforming potential in various experimental systems [16, 17] and their continuous expression is necessary to sustain the malignant phenotype of HPV-positive cancer cells [18]. Typically, *E6/E7* can give rise to precursor lesions named cervical intraepithelial neoplasias (CINs) [19], which are classified from CIN1 to CIN3 depending on an increasing grade of cellular dysplasia. In many cases, they can spontaneously regress, but a fraction of CIN3 lesions can progress to invasive cancer (Figure 1) [20].

During progression from CIN1 to CIN3 and cervical cancer, *E6* and *E7* expression often increases [21]. HPV *E6/E7* expression is usually repressed by the viral *E2* protein [22]. Oncogenic HPVs can evade this repression through integration of the viral DNA in the host genome which typically results in the loss of the *E2* open reading frame (ORF). As a consequence, the expression of *E6/E7* increases. Most cervical cancers contain one or more copies of HPV integrated in the host genome. In HPV18-positive cervical cancers, HPV18 DNA is almost always integrated. HPV16 integrates in 76% of HPV16-positive cervical cancer cases [23]. Interestingly, premalignant lesions usually contain episomal viral DNA, whereas in malignant tumours most often integrated HPV DNA is found [24, 25]. This suggests that viral integration occurs in cells that transit from non-malignant to malignant tumour cells.

It should be noted, however, that the percentage of women infected with high-risk HPVs which eventually develop cancer is low [26]. Furthermore, the prevalence of infected women is greatest between the age of 25 and 35 years, whereas cervical cancer is more common in women older than 45 years, indicating that the progression from initial infection to cancer usually is a process over decades [27]. This suggests that there are additional events involved in carcinogenesis than HPV infection alone [28]. *E6/E7* may support oncogenesis, for example by inducing genetic instability [29] and the accumulation of these genetic errors may then facilitate cancer progression.

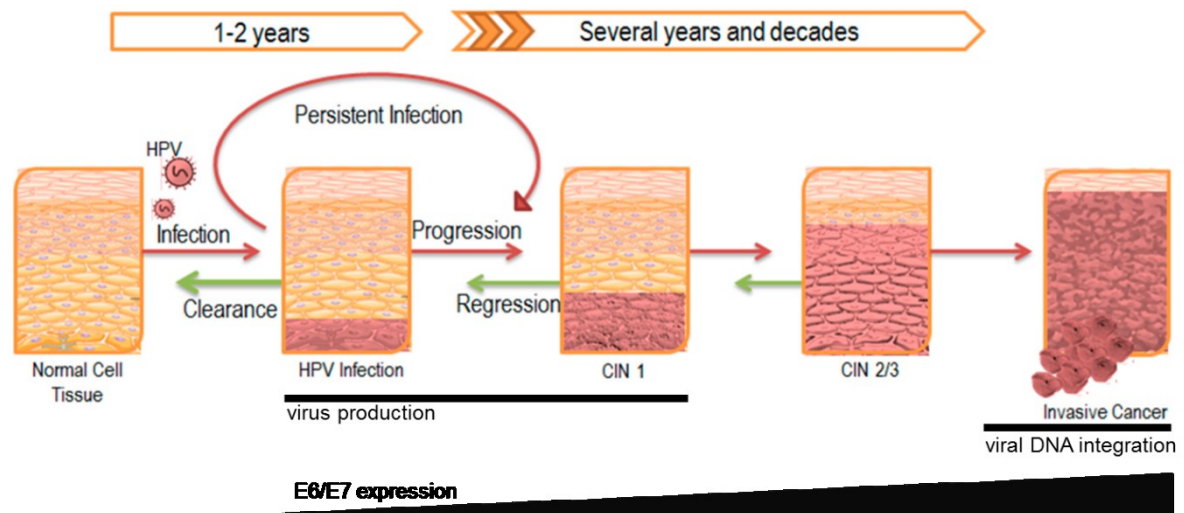


Figure 1: HPV-induced carcinogenesis. Persistent infection with HPV can lead to the formation of premalignant precursor lesions. E6/E7 expression is increased during progression from CIN1 to invasive cancer. Malignant tumours often contain integrated HPV DNA. Image modified from [30].

1.3 HPV oncogenes *E6* and *E7*

The E6 and E7 oncoproteins are essential for HPV-linked oncogenesis and interfere with crucial cellular tumour suppressor pathways. Among other targets, E7 is able to bind to the retinoblastoma protein (pRb) and thereby deregulates the cell cycle [31]. pRb is a tumour suppressor involved in the negative regulation of cell cycle transition from G1 to S phase. It binds to the transcription factor E2F and thereby prevents the induction of E2F-stimulated genes which can promote cell cycle progression into S phase [32]. Usually, cells under an abnormal growth stimulus, as exerted by an oncogene, are predisposed to undergo apoptosis [33], which has also been observed in cells overexpressing E7 alone (Figure 2) [34]. However, apoptosis is blocked by E6 as it mediates the degradation of the pro-apoptotic p53 protein [35, 36]. In specific, E6 forms a complex with the cellular ubiquitin ligase E6-associated protein (E6AP) and subsequently undergoes conformational changes rendering it competent to bind p53. The complex E6/E6AP then recruits p53 and induces its proteasomal degradation.

These considerations indicate that the HPV *E6* and *E7* oncogenes can cooperate during carcinogenesis and, in line with this, it has been found that the transforming capacities of E6 and E7 are enhanced when they are expressed together, compared to the expression of E6 or E7 alone [37, 38]. Moreover, silencing *E6* and *E7* rapidly induces senescence, an irreversible growth arrest, in HPV-positive cells [39]. This indicates that not only the transformation but also the maintenance of the malignant phenotype of HPV-positive cancer cells depends on

E6/E7 expression, i.e. the cells are “oncogene-addicted” [40]. Thus, E6 and E7 should be promising therapeutic targets for both immunotherapeutic approaches and for the generation of specific E6/E7 inhibitors.

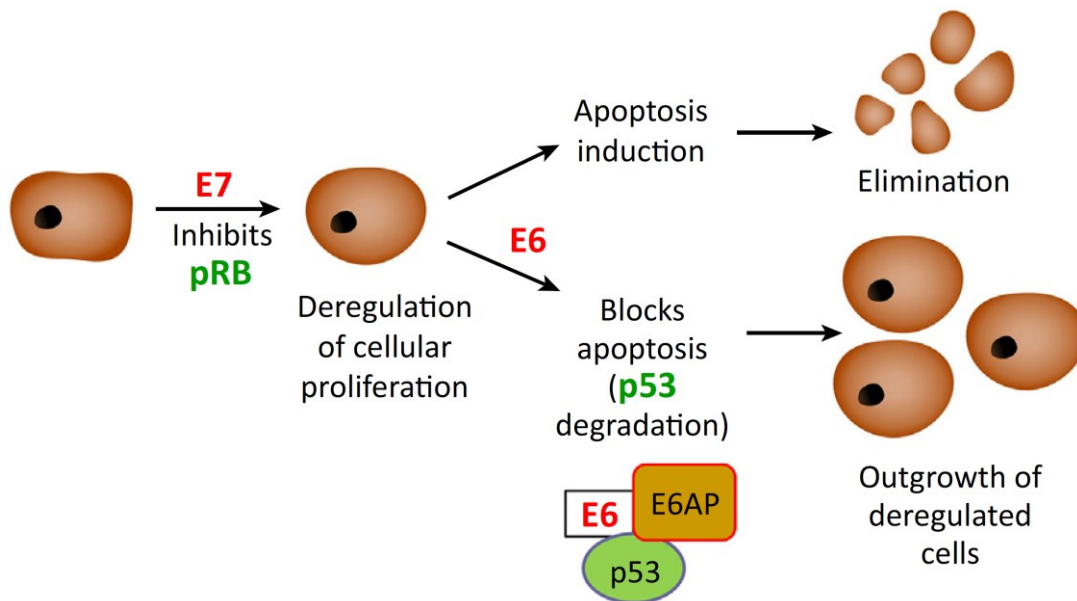


Figure 2: Cooperation of HPV E6 and E7 oncoproteins during oncogenesis. E7 deregulates the cell cycle through inhibition of pRb. Reactive apoptosis is prevented by E6, which forms a complex with E6AP and p53 and subsequently induces p53 degradation. Adapted from [40].

1.4 Therapy of HPV-positive cervical cancer

Precancerous lesions and cervical cancers are usually removed surgically. In more advanced cancers the concomitant treatment with cisplatin-based chemoradiotherapy can be indicated [41]. However, given the role of E6/E7 in the transformation and growth, HPV-positive cancers could be particularly vulnerable to therapeutic strategies that target E6 and E7. These approaches should in principle be highly specific treatments, since the viral proteins are only expressed in HPV-positive preneoplastic and neoplastic lesions whereas uninfected, healthy tissue would not be affected. Immunotherapeutic approaches have been developed that deliver immunogenic epitopes of E6/E7 to the immune cells [42]. Such vaccines were promising in animal models and were also able to generate an HPV-specific cytotoxic T-cell response in some patients. However, the tumour regression is minimal and the clinical outcome does not correlate with T-cell response [43]. An explanation for the thus limited success of immunotherapy of HPV-positive cancers might be that oncogenic HPVs have developed sophisticated mechanisms to evade the immune system, such as generating an immunosuppressive environment [42] or interfering with the antigen-presenting machinery [44].

Several approaches are currently pursued which aim to inactivate E6/E7 expression or function, for example via siRNA [45] or molecules that impair the interaction of E6 with E6AP [46, 47]. Structural analyses of HPV16 E6 and the E6/E6AP/p53 complex revealed an E6AP binding pocket in the E6 protein [35]. Interestingly, this binding pocket can be targeted with molecules that inhibit the formation of the E6/E6AP/p53 complex and thus p53 is reconstituted [48]. p53 then initiates apoptosis.

Collectively, these findings suggest that HPV E6 and E7 are promising targets for the treatment of HPV-positive cancer cells [40]. However, such therapies might be complicated by the fact, that many cervical cancers, similar to other tumours entities, contain hypoxic regions [49]. It is known that tumour hypoxia is correlated with higher resistance towards therapy [50].

1.5 Tumour hypoxia

Hypoxia is characterised by a median oxygen concentration below 2% in comparison to 4-9% oxygen (“physoxia”) in most normal tissues [51]. Two major forms of hypoxia can be distinguished: chronic hypoxia due to diffusion limitations and cycling hypoxia due to perfusion limitations. Chronic hypoxia is caused by an enlarged distance of a cell from the blood vessel. Diffusion of oxygen in tissues can only reach as far as 100-200 μm [52], meaning that a tumour cell which is further than 200 μm away from a blood vessel is inadequately supplied with oxygen. Tumours that suffer from chronic hypoxia respond by enhancing the generation of new blood vessels (angiogenesis). However, in comparison to normal vasculature, the architecture of tumour blood vessels is both structurally and functionally abnormal [52]. This can lead to an inadequate perfusion of the microvessels (e.g. through temporary partial or total occlusions by blood cells) which exposes neighbouring tumour cells to repeated cycles of hypoxia and reoxygenation, called cycling hypoxia [53].

Hypoxic tumours usually have a poor clinical prognosis which might be explained by processes that are altered under hypoxic conditions [53]: (1) increased genetic instability due to elevated reactive oxygen species (ROS) levels [54] and downregulated DNA repair mechanisms [55], (2) metabolic switch to increased glycolysis [56], (3) suppression of apoptosis [57] and senescence [58], (4) activation of autophagy [59], (5) induction of angiogenesis [60] and (6) the induction of invasion and migration [61]. These mechanisms can support the evolution of more aggressive and resistant tumour cells which constitutes a major obstacle for the treatment of hypoxic tumours [53].

Furthermore, cells under hypoxic conditions are more resistant to radiotherapy (RT) and chemotherapy (CT) [50]. On the one hand resistance to RT can be caused by the lack of molecular oxygen which is needed to manifest the irradiation-induced DNA damage [62]. On the other hand resistance to CT can be related to the lack of blood vessels that are needed to transport chemotherapeutic drugs [63] or to the upregulation of drug efflux proteins in hypoxic cells [64]. Furthermore, chemotherapeutic drugs often act by targeting dividing cells but tumour cell proliferation can be inhibited under hypoxic conditions [64]. Therapeutic strategies have been developed in which radiotherapy is combined with inhalation of hyperoxic gas and the vasodilator nicotinamide in order to increase the oxygen availability in the tissue [65, 66]. However, although promising, these approaches have eventually been discontinued due to the complex technical requirements and poor patient compliance [67]. Thus, there is a great need for therapies that can target hypoxic tumour cells and cooperate with radio- and chemotherapy.

1.6 Hypoxia in cervical cancer

Cervical cancers typically show a heterogeneous distribution of better and less ventilated regions. More than 60% of the tumours contain hypoxic and/or anoxic (0% oxygen) regions. The median oxygen concentration in cervical cancer is around 1.2% in comparison to 5.6% in the normal cervix [68]. A major weakness of many functional studies on HPV-linked carcinogenesis is that they are conducted under standard cell culture conditions at 20% oxygen which does not reflect the conditions in a tumour.

Previous work of our lab has shown that HPV-positive cancer cells strongly downregulate E6 and E7 under hypoxic conditions [39]. Interestingly, other than under normoxia, repression of E6/E7 under hypoxic conditions does not result in senescence, but in a reversible state of dormancy and the cells resume proliferation upon reoxygenation. This could render therapy of hypoxic HPV-positive tumours even more difficult, since not only RT and CT are less efficient in hypoxic tumour regions, but also treatment with prospective E6/E7 inhibitors or E6/E7 targeting immunotherapeutics may fail, since the viral target proteins are no longer expressed in hypoxic tumour cells. Moreover, the hypoxia-induced dormancy of HPV-positive cancer cells is reversible, suggesting that upon reoxygenation (e.g. through neovascularisation or therapy-induced shrinkage of the tumour) these cells could serve as a reservoir for tumour recurrence.

1.7 Senescence

The induction of senescence in tumour cells is considered to be a promising strategy for tumour therapy [69]. Cellular senescence can be categorised into replicative and premature senescence. Replicative senescence was first described by Hayflick and Moorhead in human fibroblasts [70]. They noticed an irreversible loss of the proliferative potential of cells after a certain number of cell doublings. Today it is known that replicative cellular senescence is caused by the shortening of telomeres which occurs during each cell cycle [71]. When telomeres reach a critical length (referred to as the Hayflick limit), cells undergo senescence. On the contrary, premature senescence happens without the loss of telomeres and can be induced by a plethora of intrinsic and extrinsic factors, including oxidative stress, DNA damage, mitochondrial dysfunction, oncogene activation, loss of tumour suppressors and also treatment with radio- and chemotherapy [72]. In general, senescence is characterised by a stable growth arrest accompanied by certain phenotypic alterations, such as senescence-associated β -galactosidase (SA- β -gal) activity, a large, flattened and sometimes multinucleated morphology of the cells, chromatin remodelling and a complex pro-inflammatory secretome [72].

Senescence can be induced and maintained by the p16/pRb and p53/p21 tumour suppressor pathways [73]. p53 is induced by telomeric attrition, oncogenic and oxidative stress. As a response to DNA damage a kinase cascade involving ATM, ATR, CHK1 and CHK2 is initiated which eventually activates p53. p53 subsequently induces the transcription of the cyclin-dependent kinase inhibitor p21 [74], which in turn blocks the cell cycle [75]. In comparison to a transient increase of p53 which results in a transient G1 arrest to allow DNA repair, senescence is characterised by sustained induction of p53 [76, 77]. Other proteins involved in senescence induction are encoded by the *INK4/ARF* locus. p16 (INK4a) and p15 (INK4b) are cyclin-dependent kinase inhibitors similar to p21 [78]. ARF is able to sequester MDM2, a ubiquitin ligase involved in the degradation of p53 [79, 80]. Thus, ARF activation stabilises p53. In young, normal cells the *INK4/ARF* locus is not transcribed due to epigenetic silencing [81]. During senescence, the repressive mark is removed leading to the induction of *INK4/ARF* transcription [81]. p16 expression correlates with both aging and senescence and is therefore one of the most widely used senescence marker [82].

Notably, in HPV-positive cancer cells, the MDM2-mediated degradation of p53 is not active and p53 is uniquely degraded via the E6/E6AP complex [83]. Moreover, p16 expression is upregulated in HPV-positive cancer cells, since E7 inhibits pRb which results in p16

overexpression [84]. Hence, upregulated p16 is actually used as a surrogate marker for the presence of HPV DNA [85] and cannot be employed as a senescence marker in HPV-positive cells.

Blagosklonny et al. [86] proposed a model which explains senescence as a two-step process. First, cells reversibly arrest due to a proliferative halt in the presence of conflicting pro-and anti-proliferative signals. Second, the cells undergo “geroconversion” into an irreversible growth arrest (senescence). This latter step is dependent on mTOR (mechanistic target of rapamycin) signalling. This scenario is mirrored in HPV-positive cancer cells [40]. E6 and E7 repression leads to a proliferative halt due to the reconstitution of p53 (leading to p21 activation) and pRb. However, in these cells mTOR signalling is maintained which represents a conflicting pro-proliferative stimulus (first step) and also allows geroconversion of the cells (second step). Importantly, mTOR signalling is impaired under hypoxia which allows hypoxic HPV-positive cells to evade senescence and to induce a reversible state of dormancy [39, 40].

These results also suggest that by circumventing the mTOR-dependency of senescence, hypoxic tumour cells could be sensitised to senescence-inducing therapies. This could be achieved by identifying agents that restore mTOR signalling under hypoxia, or agents that can induce senescence in an mTOR-independent manner (Figure 3).

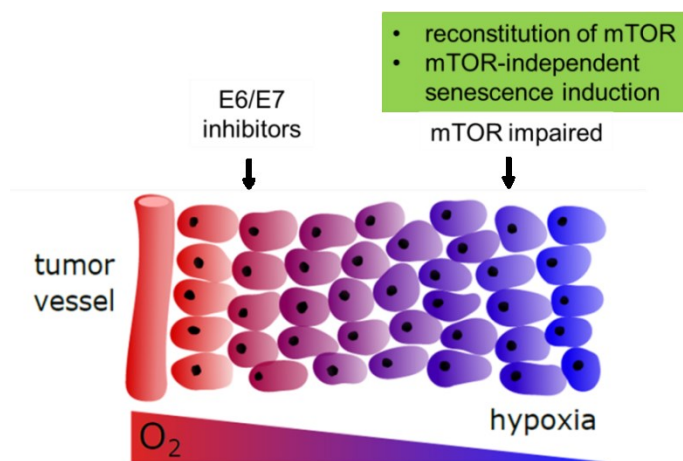


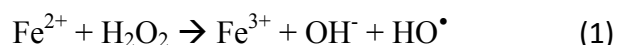
Figure 3: Possible strategies to target normoxic and hypoxic HPV-positive cancer cells. HPV-positive cancer cells could be targeted with prospective E6/E7 inhibitors which results in senescence induction in oxygenised cells. Under hypoxic conditions, where mTOR signalling is impaired, therapeutic approaches to induce senescence would need to restore mTOR signalling or induce senescence independent of mTOR. Image modified from [40].

mTOR-independent induction of senescence could have an additional benefit. Senescent cells secrete a plethora of pro-inflammatory factors that together account for the senescence-associated secretory phenotype (SASP) [87]. The composition of the SASP strongly depends on the cellular background of the senescent cell and the senescence-inducing stimulus. The function of the SASP is double-edged. Senescent cells secrete factors that reinforce senescence by an autocrine positive-feedback loop. Interestingly, also surrounding

cells then could undergo senescence as a response to the SASP [88]. Both would support the anti-tumourigenic effect of senescence-inducing therapies. Furthermore, the SASP has a pro-inflammatory nature. On the one hand this can be anti-tumourigenic due the recruitment of cells that remove the senescent cell. On the other hand sustained inflammation can be pro-tumourigenic. Further studies have also shown that senescent fibroblasts can promote the proliferation of tumour cells [89]. Interestingly, the mTOR pathway, more specific the mTOR complex 1 (mTORC1), is responsible for the induction of this pro-tumourigenic SASP [90]. Thus, agents that are able to induce mTOR-independent senescence could be particularly attractive for anti-cancer therapy, since they may not only target hypoxic tumour cells, but also prevent secretion of a pro-tumourigenic SASP by stromal fibroblasts.

1.8 Iron metabolism

Iron is an essential element needed for multiple processes in the cell. It is used as a co-factor in proteins that are responsible for oxidative phosphorylation (iron-sulphur clusters), DNA synthesis (ribonucleotide reductase) and oxygen binding and transport (haemoglobin) to name a few. Its biological significance mainly relies on the fact that iron is a transition metal which fluctuates between two oxidation states: ferrous iron (Fe^{2+}) and ferric iron (Fe^{3+}). However, this characteristic can also be toxic to the body since the oxidation-reduction processes generate ROS through the Fenton reaction [91]:



In the presence of hydrogen peroxide, ferrous iron can be oxidised to ferric iron which results in the generation of a hydroxide ion and a hydroxyl radical (1). In the next step (2) ferric iron is reduced back to ferrous iron and generates a proton and a hydroperoxyl radical. The net effect is the generation of water ($\text{OH}^- + \text{H}^+$) and two different oxygen radicals. These free radicals can cause damage to lipid membranes, proteins and nucleic acids of a cell. Since iron can be both beneficial and detrimental its levels need to be tightly regulated.

Each day, 25 mg of iron are needed for erythropoiesis, but only 1-2 mg are absorbed through the intestine [92]. The remaining iron is recycled from cells through macrophages and released from iron storage tissues such as the liver. In enterocytes dietary iron is absorbed via divalent metal transporter 1 (DMT1) and transported to the blood by ferroportin 1 (FPN1), a transmembrane protein that is the only known iron exporter to date [93]. Iron efflux from cells is tightly regulated by hepcidin, which is synthesised in the liver and promotes the

internalisation and degradation of ferroportin [93]. Ferroportin is coupled to ferroxidases which oxidise Fe^{2+} to Fe^{3+} . This oxidation step is necessary since the iron carrier transferrin (TF) in the plasma can only bind ferric iron (Fe^{3+}) [94].

Two ions of ferric iron bind to apo-transferrin to generate holo-transferrin (Figure 4). Iron uptake then occurs via receptor-mediated endocytosis in which two holo-transferrins bind to the homodimeric transferrin receptor (TFR, also known as TFRC or CD71) [95]. Two types of TFRs are known: TFR1 and TFR2. The expression of TFR2 is mainly limited to hepatocytes and iron-absorbing cells of the duodenum. After endocytosis and acidification of the endosome iron is released from transferrin due to the pH-dependent binding capacity of transferrin [96]. Ferric iron is subsequently reduced to Fe^{2+} by the metalloreductase STEAP3 (six-transmembrane epithelial antigen of prostate 3) [97] and transported into the cytosol via DMT1 where it can reach different destinations (see 1.9). The iron-free TF remains bound to TFR in the endosome and is recycled back to the cell membrane. There it is released from TFR and can sequester more iron [95, 98].

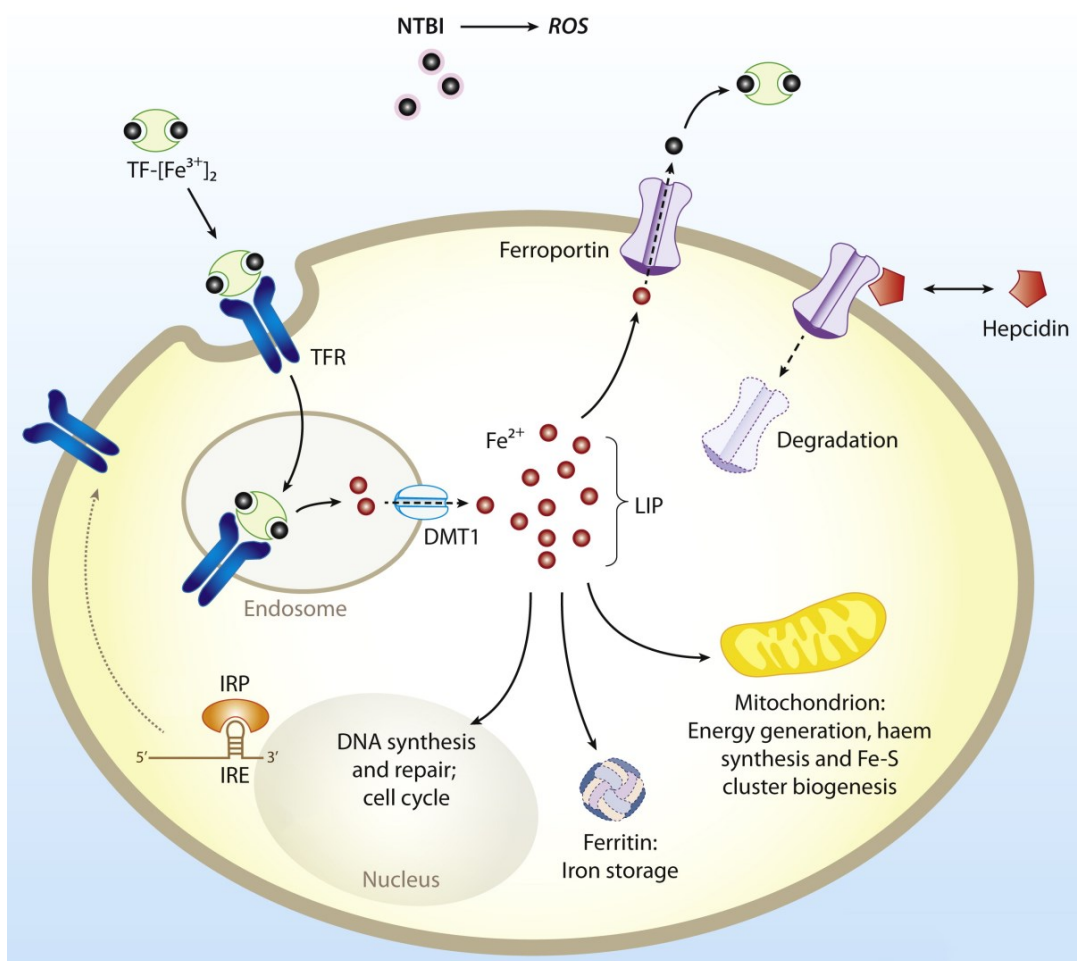


Figure 4: Cellular iron metabolism. Non-transferrin bound iron generates cytotoxic ROS and thus needs to be bound by transferrin. After receptor-mediated endocytosis, release and reduction of ferric

iron, iron is transported as ferrous into the cytoplasm where it feeds into the labile iron pool. From there it can be used in diverse biological processes, stored in ferritin or exported via ferroportin. Iron efflux is regulated by hepcidin which regulates the degradation of ferroportin. (Abbreviations: NTBI, non-transferrin bound iron; ROS, reactive oxygen species; TF, transferrin; TFR, transferrin receptor; DMT1, divalent metal transporter 1; LIP, labile iron pool; IRP, iron regulatory protein; IRE, iron responsive element). Image modified from [99].

1.9 Intracellular iron

The absorbed iron feeds into the so called “labile iron pool” (LIP). It consists of Fe^{2+} which can be directly incorporated into iron-dependent enzymes or used to control transcription of iron-regulated genes. Many attempts have been made to characterise the labile iron pool, but this has proven difficult due to its nature of being an intermediate or transitory pool between extracellular iron and iron that is associated with intracellular proteins [100]. In the broadest definition the labile iron pool comprises iron that can potentially participate in redox-reactions and can be scavenged by iron chelators. This portion is only 5% of a cell’s total iron content, which is between 50 μM and 100 μM [100].

In order to keep the labile iron pool relatively low, iron can either be exported via ferroportin or stored in ferritin which is the key player to detoxify excess intracellular iron and is therefore expressed in almost all tissues [92]. It consists of tissue-dependent ratios of 24 heavy (H) and light (L) ferritin subunits encoded by *FTH* and *FTL*, respectively. Ferritin can sequester up to 4500 atoms of ferric iron [101, 102]. The H subunit oxidises Fe^{2+} from the labile iron pool to Fe^{3+} [103] and the L subunit is responsible for the stabilisation of the ferritin complex and it facilitates the uptake of iron into the ferritin protein [104, 105].

The levels of iron in the labile iron pool are tightly regulated by the IRE/IRP (iron responsive element / iron regulatory protein) system (reviewed in [106-108]). IREs are highly conserved sequences (25-30 nucleotides) in the untranslated regions (UTRs) of mRNAs that encode for iron-dependent proteins such as ferritin and transferrin receptor 1. They represent binding sites for the two iron regulatory proteins: IRP1 and IRP2, encoded by *ACO1* and *IREB2*, respectively. When iron is decreased, IRP1 and IRP2 bind to IREs with high affinity. Depending on the location of IREs at the mRNAs, IRP binding inhibits translation or degradation of the mRNAs (Figure 5). In the case of ferritin (encoded by *FTH* and *FTL*) the IRE is located at the 5’ UTR [109]. In the absence of iron, IRP binds to the IRE and impedes translation initiation, resulting in reduced expression of the iron storage protein. In the mRNA of *TFR1* multiple IREs are located at the 3’ UTR of the mRNA [110] close to a recognition site for endonucleases [111]. Bound IRPs at the IREs of *TFR1* prevent endonucleolytic

cleavage of the mRNA and thus stabilise the mRNA and elevate expression of *TFRI* in order to increase iron uptake. Vice versa, in iron-replete conditions, iron binds to IRPs and prevents IRE binding. Thus, translation of ferritin is initiated whereas *TFRI* mRNA is degraded.

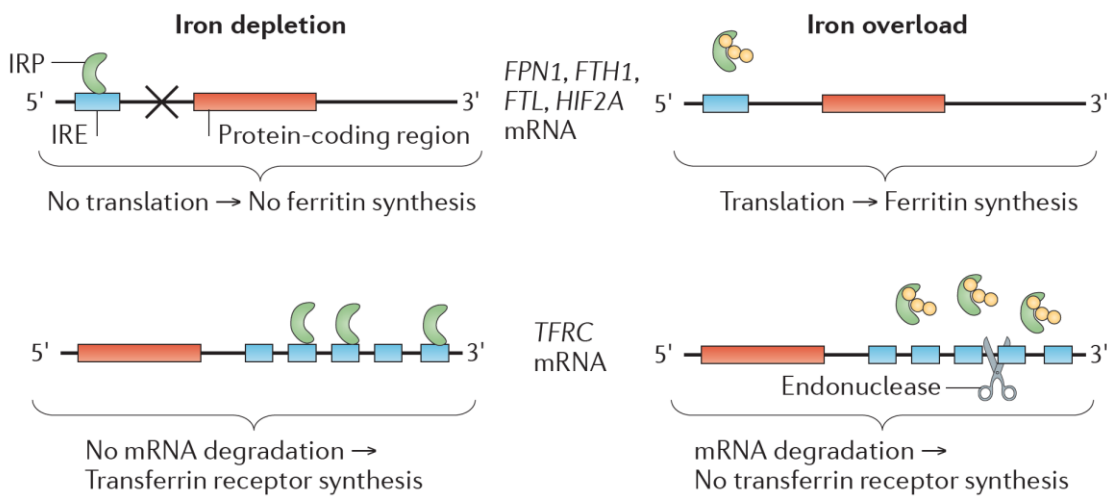


Figure 5: The IRE/IRP system. In iron-deficient cells, IRPs bind IREs. While binding of IREs at the 5' UTR inhibits translation, binding of IREs at the 3' UTR stabilises the target mRNA. In the presence of iron IRPs dissociate from IREs. (Abbreviations: IRP, iron regulatory protein; IRE, iron responsive element; FPN1, ferroportin-1; FTH1, ferritin, heavy polypeptide 1; FTL, ferritin light polypeptide 1; HIF2A, hypoxia-inducible factor 2 α ; TFRC, transferrin receptor). Image from [112].

Interestingly, the assembly of IRP1 with an iron-sulphur cluster converts IRP1 into an isoform of the cytosolic aconitase which is responsible for the isomerisation of citrate to isocitrate in the citric acid cycle [113]. These two functions of IRP1 are mutually exclusive and depend on the iron status of the cell. Both IRP1 and IRP2 RNA-binding capacities are regulated by iron. For IRP1, iron dictates the change in its function from binding IRE to aconitase without changing the expression of IRP1 protein, whereas IRP2 RNA-binding decreases in iron-replete cells due to iron-dependent proteasomal degradation of IRP2 [114]. Other IRE/IRP regulated mRNAs are among others *ferroportin-1* (*FPN1*) and *hypoxia-inducible factor-2 α* (*HIF-2 α*) with a single IRE in the 5' UTR (analogous to ferritin) and *DMT1* with an IRE in the 3' UTR (analogous to *TFRI*) [108]. Thus, upon iron deprivation *FPN1* and *HIF-2 α* are downregulated, whereas *DMT1* expression is increased.

In summary, to maintain the iron homeostasis, the cell has developed a sophisticated system of iron-dependent enzymes that regulate the appropriate expression of proteins necessary for iron import, export and storage.

1.10 Iron and oxygen homeostasis

An important role of iron is the binding and transportation of oxygen in haemoglobin. Thus, it is not surprising that both iron and oxygen metabolism are coordinated. Hypoxia-inducible factors (HIFs) are the key mediators in these processes since they are regulated by both iron and oxygen levels [115]. HIF consists of two subunits, HIF- α and HIF- β (also known as aryl-hydrocarbon-nuclear transporter, ARNT). Whereas HIF- β is constitutively expressed, HIF- α expression is altered in response to changes in oxygen tension [116]. When oxygen is available, prolyl hydroxylases (PHDs) hydroxylate proline residues of HIF- α , which recruits the von Hippel-Lindau factor (VHL) leading to ubiquitination and proteasomal degradation of HIF- α [117]. Since hydroxylation is impaired under hypoxic conditions, HIF- α accumulates and initiates the transcription of target genes in order to adapt to hypoxia. PHDs are not only oxygen, but also iron-dependent. Thus, upon iron deprivation HIF- α is also stabilised.

HIF-2 α plays an important role in the crosstalk between iron metabolism and hypoxia. Upon hypoxia *HIF-2 α* expression is increased due to stabilisation of the protein. However, in the absence of iron *HIF-2 α* mRNA is not translated due to an IRE in its 5' UTR [118]. Since *HIF-2 α* is involved in the stimulation of erythropoietin synthesis for erythropoiesis this could be a mechanism to avoid erythrocyte production when iron is not available. Thus, on the one hand, iron levels are crucial for the cell's response towards hypoxia.

On the other hand, hypoxia can also alter the cell's iron metabolism. Upon hypoxia the body induces erythropoiesis. To satisfy the demand of iron for this process, hepcidin expression is suppressed upon hypoxia and anaemia [119, 120]. The decrease of hepcidin stabilises ferroportin to elevate the efflux of iron from cells into the blood stream; for instance from duodenal enterocytes which absorb dietary iron and from macrophages which recycle and store iron from phagocytosed erythrocytes. Furthermore, HIF upregulates the expression of iron regulated genes such as *TFR1* and *DMT1* [121]. All together the plasma levels of iron increase, which then can be utilised by erythroid precursor cells during erythropoiesis.

1.11 Iron and cancer

As discussed above, iron generates reactive oxygen species that are able to cause DNA mutations. Furthermore, iron is required by ribonucleotide reductase (see 1.14), an essential enzyme in DNA synthesis and cell proliferation. Consequently, iron can not only accelerate tumour initiation but it is also needed to support tumour growth. Various studies have linked increased iron levels to greater susceptibility to develop tumours (reviewed by Torti and Torti

[122]). Given the role of iron in proliferation it is not surprising that tumour cells have developed mechanisms to increase their iron uptake. TFR1 expression is upregulated in many cancers including lymphomas [123], gliomas [124], lung cancer [125], breast cancer [126] and others. *DMT1* is upregulated to increase iron influx and *HAMP* (encoding hepcidin) expression is increased to decrease iron efflux through repression of ferroportin [127, 128]. Additionally, the expression of ferroportin is downregulated [128]. Furthermore, IRP1 and IRP2 overexpression not only enhances tumour growth in xenograft models [129, 130], but has also been observed in breast cancer [131]. IRP overexpression elevates TFR1 expression but also decreases ferritin expression. The coordinated increase of iron influx together with the reduction of the iron storage protein has been suggested to increase the availability of intracellular iron for metabolic processes in cancer cells [132]. Taken together cancer cells have altered the iron metabolism to increase their labile iron pool in order to satisfy their demand for iron. Given the cancer cells' avidity for iron the question arises whether iron chelators could serve as anti-tumour agents.

1.12 Iron chelators

Iron chelators are small molecules which bind iron with high affinity. Iron ions have six coordination sites that can be bound by iron chelators. An iron chelator that occupies all six coordination sites is called a hexadentate iron chelator (ratio chelator:iron = 1:1, Figure 6). A tridentate chelator occupies three coordination sites (ratio = 2:1) and a bidentate chelator occupies two coordination sites which results in a ratio of 3:1.

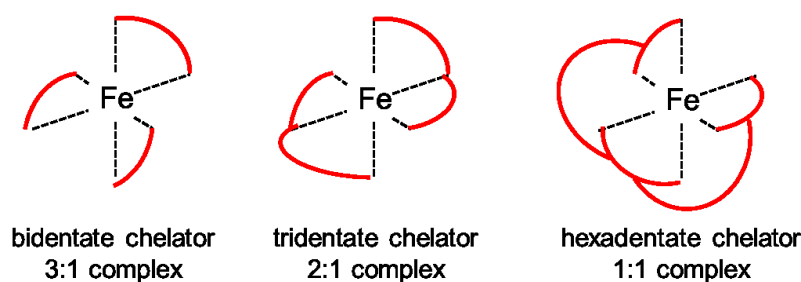


Figure 6: Complexes of iron chelators and iron ions. Depending on the number of occupied coordination sites at the iron ion, iron chelators (red) can be classified as bidentate, tridentate or hexadentate iron chelators.

Iron chelators are used in the clinic to treat iron overload diseases such as hereditary haemochromatosis and beta-thalassemia, or iron intoxication due to abuse consumption of iron. Currently three iron chelators are used in the clinic for iron chelation therapy: deferoxamine (DFO), deferiprone and deferasirox. DFO is a hexadentate Fe^{3+} chelator [133],

approved by the FDA for long-term iron chelation therapy. Since it is a hydrophilic molecule it cannot penetrate the cell membrane and depends on endocytosis [134, 135]. Unfortunately it has a short plasma half-life and needs to be administered by frequent and lengthy injections which leads to suboptimal patient compliance [136]. Deferiprone and deferasirox are both orally available. Despite the improved acceptance from patients, deferiprone is not used as standard therapy for β -thalassemia, since its efficiency is lower than DFO [137]. Deferasirox, however, seems to have similar efficacies in comparison to DFO and due to the oral application it could become a preferable choice for iron chelation therapy [138]. Systemic or oral gavage of iron chelators leads to the reduction of serum iron levels which causes side effects like gastrointestinal toxicities, kidney and liver damage [139]. Thus, to treat diseases of the skin and mucosa, the use of topical iron chelators could allow the application of high doses without side effects at the systemic level as observed after systemic or oral application. Notably, a topically applicable antimycotic drug, called ciclopirox, has recently been identified as an iron chelator [140].

1.13 Ciclopirox (CPX)

Ciclopirox (6-cyclohexyl-1-hydroxy-4-methyl-2(1H)-pyridone) is an antifungal agent to treat mycoses of the skin, nails and also mucosa. It has been used in the clinic for decades and shows a very good safety profile [141]. The antimycotic activity of CPX differs from other fungicides which primarily target the cell membrane by binding to the membrane component ergosterol or by interfering with its biosynthesis [142]. CPX has been shown to not only disrupt the cell membrane [143], but also to target different metabolic processes (e.g. respiration) [144] and intracellular pathways regulating DNA repair and cell division in yeast [145]. These activities are presumably attributed to the ability of CPX to chelate intracellular iron. However, the exact mechanism of action still remains to be elucidated.

CPX is a bidentate, lipophilic iron chelator [146]. It preferentially complexes ferric iron (Fe^{3+}) [144] and semiquantitative analyses show that CPX has an even higher binding capacity of ferric iron than DFO [146]. CPX is often used in the form of its olamine salt. The olamine entity improves the solubility in water but does not modify the pharmacological properties of CPX in any respect [141]. Thus, the term CPX will be used for both forms in the following. CPX can be applied as lacquer, shampoo, gel and vaginal suppository [141].

Notably, CPX has recently gained considerable interest in cancer research since it may also possess anti-tumourigenic potential. In multiple cell lines, CPX can induce cell cycle arrest in G0/G1 phase and apoptosis. Although the underlying mechanisms are not well understood,

some candidate molecular targets that may mediate these effects have been identified. For instance, CPX has been described to inhibit ribonucleotide reductase (RR), which catalyses the rate-limiting step in DNA synthesis and depends on iron (further discussed in 1.14) [147]. Another target is the deoxyhypusine hydroxylase (DOHH) [148]. Similar to RR, DOOH is also iron-dependent. DOHH is essential for the maturation of the eukaryotic translation initiation factor 5A (eIF5A). CPX blocks DOHH and thereby induces cell cycle arrest [148]. Furthermore, CPX downregulates a plethora of cyclins and cyclin-dependent kinases and induces p21 expression which results in a cell cycle arrest [149]. In addition, apoptosis-inducing properties of CPX have been reported which are associated to the downregulation of the anti-apoptotic proteins survivin and BCL-XL and enhanced cleavage of BCL-2 [149]. Other pathways described to be suppressed by CPX are Wnt/ β -catenin [150, 151], VEGF [152], mTOR [153] and myc [154].

Taken together CPX appear to have a broad spectrum of potential targets that are involved in carcinogenesis. Since CPX may have anti-tumourigenic potential it has been subjected to *in vivo* studies. It was revealed that CPX is competent to inhibit tumour growth in various xenograft models [149, 151, 155, 156]. After these promising studies, CPX has further been promoted to clinical phase I studies. The very first phase I study was conducted in patients with relapsed or refractory haematologic malignancies [157]. CPX was given orally and two out of 24 patients showed haematological improvements, although neither complete nor partial remission could be achieved. Serum concentrations of CPX could not be further elevated due to gastrointestinal toxicities which could explain the limited clinical benefit. In January 2018, a second clinical trial started in order to evaluate the safety and efficacy of a ciclopirox prodrug given intravenously to patients with solid tumours (ClinicalTrials.gov identifier: NCT003348514).

Upon topical application, about 7% of the applied dose can be detected in the skin of rats during an 8 h exposure of CPX with the maximum concentration after 2 h. Notably, only 0.15% of the applied dose actually reaches the systemic circulation with highest concentrations 3 h after application [158]. Thus, it is very unlikely to reach high systemic concentrations of CPX upon topical application. Although the absorption in the mucosa of the vagina of female patients is higher with up to 9% [141], the absorption rate is in general relatively low. Nonetheless, CPX has a high penetration capacity [159], since it can reach deep layers of the skin where it still has concentrations that are high enough to efficiently kill fungi. Thus, if CPX also exerts anti-tumourigenic effects on HPV-transformed cells, it might

serve as a promising new drug for the topical treatment of HPV-positive (pre)neoplastic lesions of the cervix.

1.14 Ribonucleotide reductase (RR)

Particularly interesting are reports suggesting that CPX can block the enzyme ribonucleotide reductase (RR), more specifically its iron-containing subunit M2 [147, 160]. RR has been suggested to be a promising target for anti-cancer therapy, since RR inhibitors possess anti-tumour activities both *in vitro* and *in vivo* [161] by inducing therapeutically desired phenotypes, including cell cycle arrest [162], senescence [163, 164] and apoptosis [165]. Notably, inhibition of RRM2 induces a DNA damage response [163] and interferes with DNA repair [166]. Interestingly, RR inhibition has also been investigated in cervical cancer cell lines and animal models [167] resulting in G1 cell cycle arrest and apoptosis *in vitro* and inhibition of tumour formation in xenograft models [167].

At the biochemical level, RR is responsible for the conversion of ribonucleoside di- or triphosphates (rNDPs/rNTPs) into deoxyribonucleoside di- or triphosphates (dNDPs/dNTPs) that are needed for DNA synthesis [168, 169]. It consists of two subunits RRM1 (also known as R1 or M1) and two M2 subunits (also known as R2), forming a heterotetramer (Figure 7). RRM1 contains the substrate binding site for rNDPs/rNTPs. Furthermore, it contains two allosteric sites - one regulates the specificity towards any of the four possible nucleosides, the other regulates the overall activity of RRM1 [170, 171]. The conversion of nucleoside to deoxynucleoside occurs via a free radical reaction for which a tyrosyl radical at M2 is essential. A diferric iron centre stabilises the tyrosyl radical [172].

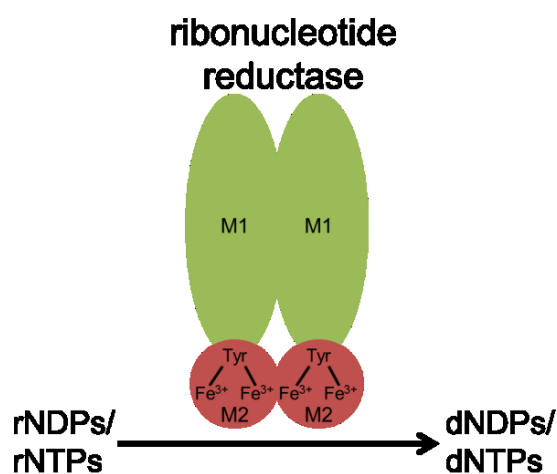


Figure 7: Ribonucleotide reductase. Ribonucleotide reductase (RR) consists of two RRM1 and two M2 subunits. M2 contains a tyrosyl radical which is essential for its catalytic activity and which is stabilised by a diferric centre. Two isoforms of M2 exist: RRM2 and p53R2.

Interestingly, M2 exists in two forms: RRM2 and p53R2 (also known as RRM2B) [173]. Both possess the diferric iron and tyrosyl radical centre and substitute for each other during dNDP/dNTP synthesis [174]. However, while RRM2 is cell cycle-dependent and maximally expressed during S phase, p53R2 expression can be induced by p53. RRM2 is thus needed for DNA synthesis during cell cycle progression and p53R2 provides dNDPs/dNTPs for normal DNA repair [175, 176] and mitochondrial DNA synthesis [177] in non-proliferating cells.

Given their role in cell proliferation it is not surprising that RRM1, RRM2 and p53R2 overexpression is observed in various cancers and that expression correlates with tumour grade [178]. Several inhibitors of RR have therefore been developed into anti-cancer drugs (reviewed in [179]). They can be classified in two groups: RRM1 inhibitors and RRM2/p53R2 inhibitors [179]. RRM1 inhibitors are often nucleoside analogues (e.g. gemcitabine) and thereby allosterically inhibit RR activity. RRM2/p53R2 can be targeted with iron chelators since the iron centre is essential for the enzymatic activity. Another approach is to scavenge the tyrosyl radical, for example by hydroxyurea (HU) [180]. HU was one of the first agents to treat cancer and has therefore been evaluated in many clinical studies (reviewed in [179]). Interestingly, the majority of these studies were performed in cervical cancer, especially in combinatorial treatments with radiotherapy. HU was able to sensitise cancers to RT and for some time it was used as standard of care to treat locally advanced cervical cancer. However, HU was replaced by cisplatin due to increased clinical benefit and less toxicities [181].

These considerations suggest that CPX, as an iron chelator, could exert anti-tumourigenic activities by means of RRM2/p53R2 inhibition. Furthermore, it might be possible that CPX could serve as a radiotherapy sensitiser, similar to HU.

1.15 Research objectives

Iron is essential for the proliferation of cells. Consequently, in order to facilitate tumour growth, cancer cells alter their iron metabolism to elevate intracellular iron levels. To date, it is not known whether the availability of iron affects cervical cancer, in specific the crosstalk between cellular iron metabolism and oncogenic HPVs is unknown. Hence, this work will examine the phenotypic consequences of iron chelators on HPV-positive cervical cancer cells. A focus will be put on the antimycotic drug ciclopirox which is a topically applicable iron chelator and may therefore be particularly suitable for the treatment of cervical (pre)neoplasias of the mucosa.

The following questions will be addressed in this dissertation:

- What are the effects of iron chelators on the expression of the viral oncogenes *E6* and *E7*?

Time and dose kinetics of different iron chelators will be performed and expression of *E6* and *E7* will be analysed on protein and mRNA level.

- What are the phenotypic consequences of iron deprivation?

Proliferation assays, cell cycle analyses, senescence and apoptosis assays will be performed to examine the cellular response to CPX treatment. The dependence of the observed effects on iron deprivation will be tested. Since standard 2D cell culture does not reflect the heterogeneity of a tumour, also 3D cell spheroids will be established and analysed.

- Do hypoxic cervical cancer cells respond to CPX?

Many cervical cancers are known to harbour hypoxic regions which can lead to increased resistance towards anti-tumour therapy. Hence, an emphasis will be placed on comparative analyses of CPX treatment under normoxic or hypoxic conditions. Furthermore, it will be investigated whether CPX can cooperate with radio- and chemotherapy.

- What are the cellular mechanisms that mediate the anti-tumourigenic effects of CPX?

Proteome analyses will be performed in order to identify signalling pathways that are affected by CPX treatment.

The overall aims of this work are to gain new insights into virus/host cell crosstalk during HPV-linked carcinogenesis and to investigate whether iron chelators, most notably CPX, could serve as prospective therapeutic agents against HPV-positive cervical cancers.

CHAPTER 2

RESULTS

2. Results

2.1 Iron chelators repress E6 and E7

To analyse the effect of iron chelators on HPV-positive cells, the expression of the viral oncogenes *E6* and *E7* was determined on mRNA and protein level upon treatment with the iron chelator deferoxamine (DFO). Furthermore, protein levels of the iron storage protein ferritin (more specific its heavy subunit) and *TFRI* mRNA levels were assessed as indirect measurements of intracellular iron levels. Upon iron depletion it is expected that ferritin protein levels decrease and *TFRI* mRNA amounts increase through the regulation by the IRE/IRP system (see Figure 5).

HPV18-positive HeLa and HPV16-positive SiHa cells were treated with 100 μ M DFO for 24-72 h (Figure 8A, B). Interestingly, DFO strongly decreases viral oncoprotein expression in a time-dependent manner. Ferritin protein levels are reduced after DFO treatment, indicating that DFO depletes intracellular iron levels under treatment conditions. E6/E7 repression by DFO is independent of the HPV type, since it can be observed in both HeLa and SiHa cells.

Furthermore, E6/E7 repression by DFO is also detectable on mRNA level as demonstrated by qRT-PCR analyses (Figure 8C, D). Relative *E6/E7* mRNA levels were assessed with primers that recognise all three transcripts classes coding for HPV E6/E7 in HeLa and SiHa cells (see 4.5.2) and the untreated control was set to 1.0 for each point of time. After 24 h HPV *E6/E7* mRNA levels moderately increase upon DFO treatment, although this is not reflected on protein level (Figure 8A, B). However, after 48 h treatment, a strong repression of *E6/E7* mRNA expression is detectable in both HeLa and SiHa cells, concomitantly with the strong downregulation of E6/E7 protein levels. *TFRI* mRNA levels increase during the first 24 h. In line with the reduction of ferritin protein levels after 24 h, this indicates that iron chelation by DFO precedes E6/E7 repression.

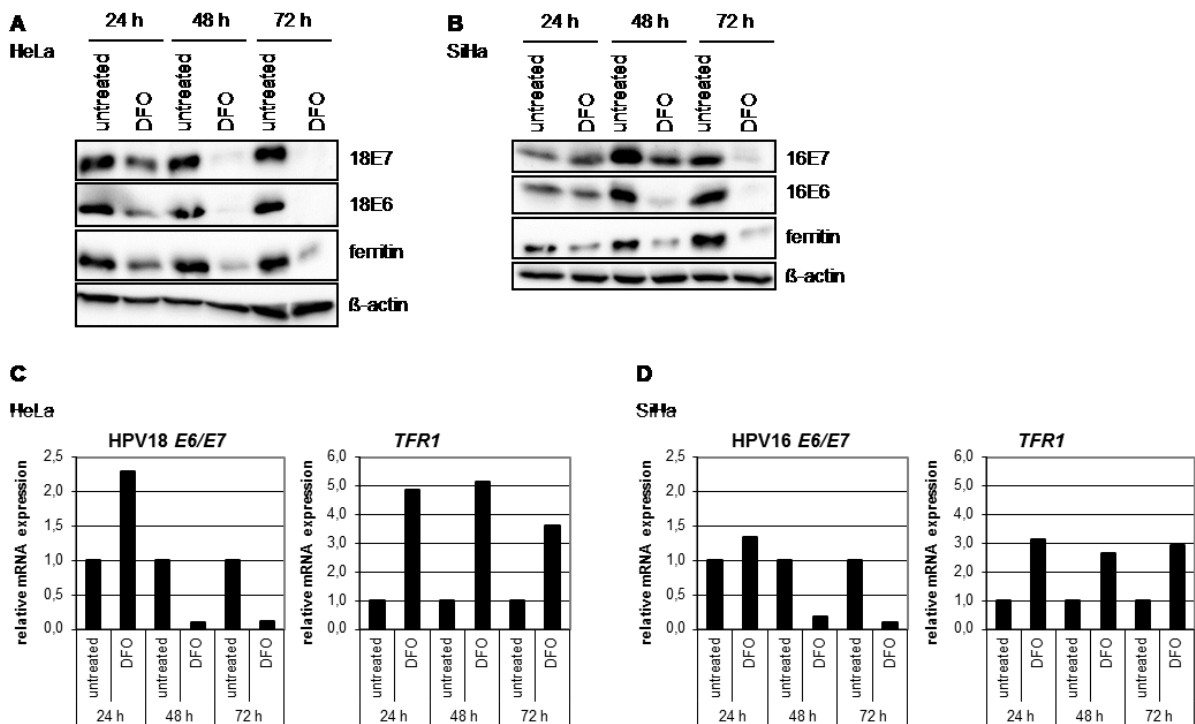


Figure 8: Iron chelators repress HPV16 and HPV18 E6 and E7 expression. (A), (B) HeLa (A) and SiHa (B) cells were treated with 100 μ M DFO for the indicated time periods. β -actin served as loading control. (C), (D) Relative mRNA expression of HPV18 *E6/E7* and *TFR1* in HeLa (C) and HPV16 *E6/E7* and *TFR1* in SiHa (D) cells upon 100 μ M DFO treatment. Controls of the respective points of time were set to 1.0. One exemplary experiment is depicted.

The results reveal that iron chelators possess the potential to strongly block HPV oncogene expression. To further corroborate this notion we analysed CPX, which - in contrast to DFO - can be applied topically and thus may be suitable for the treatment of HPV-induced (pre)neoplasias of the mucosa.

HeLa and SiHa cells were treated with different concentrations of CPX for up to 48 h. Figure 9A and B show that, alike DFO, CPX strongly represses HPV16 and HPV18 E6 and E7 proteins in a dose- and time-dependent manner. In HeLa cells, a strong repression of E6 and E7 occurs after 48 h with all tested concentrations and in SiHa cells, E6/E7 protein levels are strongly decreased after 24 h and 48 h exposure with CPX concentrations above 10 μ M. E6 repression appears to precede E7 repression in HeLa cells since a slight downregulation of E6 can already be seen after 12 h and 24 h with 10 μ M and 20 μ M CPX whereas E7 protein levels are not affected at these points of time. Ferritin is downregulated by CPX in both cell lines, indicating that CPX indeed decreases intracellular iron levels under treatment conditions.

Relative *E6/E7* mRNA levels were assessed in HeLa and SiHa cells and one representative experiment is shown for each cell line (Figure 9C and D, respectively) to depict the time-dependent regulation of *E6/E7* and *TFRI* transcription upon 10 μ M CPX treatment. Similar as observed for DFO, *E6/E7* mRNA levels increase after 24 h in HeLa and SiHa cells upon CPX treatment which, however, is not reflected on protein level (Figure 9A, B). After 48 h and 72 h, the *E6/E7* mRNA levels are strongly repressed in both cell lines. As expected, *TFRI* mRNA levels increase with CPX treatment, except in SiHa cells after 72 h CPX treatment which might be related to the observation that cells undergo apoptosis at this point of time. Alike DFO treatment, iron deprivation by CPX precedes *E6/E7* repression.

For statistical analyses of the extent of *E6/E7* mRNA repression, HeLa and SiHa cells were treated for 48 h with 10 μ M CPX. Figure 9E illustrates the \log_2 fold change of HPV18 *E6/E7* and *TFRI* expression of HeLa cells relative to solvent (EtOH)-treated cells. The mRNA levels of the solvent control were set to 1.0 (resulting in a \log_2 of 0). In HeLa *E6/E7* mRNA is significantly repressed to a \log_2 of -2.9 with $p < 0.001$; showing that CPX induces an almost 90% reduction of HPV18 *E6/E7* levels. A similar repression is induced by CPX in SiHa cells (Figure 9F) with a \log_2 fold change of -2.8 ($p = 0.003$). *TFRI* mRNA is significantly upregulated upon CPX treatment in both cell lines.

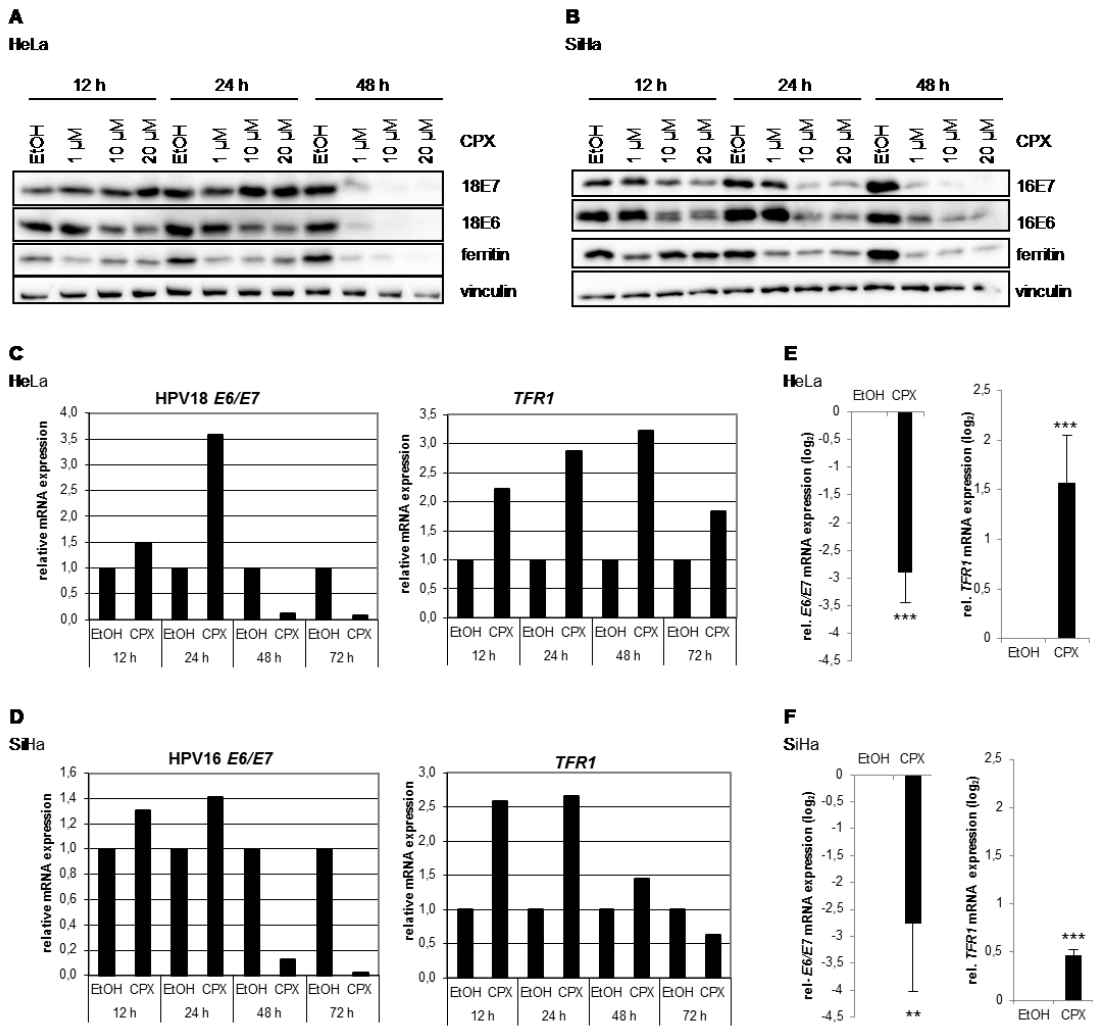


Figure 9: CPX represses HPV oncogene expression. (A), (B) Western blot analyses of HeLa (A) and SiHa (B) cells after CPX treatment. Cells were treated with 1-20 μM CPX for 12 h, 24 h or 48 h. Vinculin was used as loading control. (C), (D) Relative mRNA expression of *TFR1* and HPV18 *E6/E7* (HeLa, C) or HPV16 *E6/E7* (SiHa, D) after treatment with 10 μM CPX for the indicated time periods. One representative experiment is shown. (E), (F) For the point of time at 48 h the log₂ fold change was calculated from 3-5 independent experiments treating HeLa (E) or SiHa (F) cells with 10 μM CPX. *E6/E7* and *TFR1* mRNA levels relative to the EtOH control (set to 1.0) are depicted after logarithmic transformation. Standard deviations are indicated, ***=*p*<0.001, **=*p*<0.01.

To further corroborate that CPX-induced *E6/E7* repression is caused by deprivation of iron, *E7* protein expression was measured after treatment with CPX which has previously been complexed with iron or zinc (Figure 10A). Notably, when CPX was saturated with excess of two different iron donors - FeSO_4 as a ferrous iron (Fe^{2+}) donor or FAC as a ferric iron (Fe^{3+}) donor - *E7* repression is abrogated in HeLa cells. On the contrary, zinc is not able to impede the *E7* repression. The treatment of cells with iron (as either Fe^{2+} or Fe^{3+}) *per se* does not alter the expression of *E7* (Figure 10B). Concomitant results were obtained in SiHa cells. Collectively, these observations support the notion that *E6/E7* is repressed by iron deprivation

and the inhibition of viral oncogene expression through CPX is caused by its ability to chelate intracellular iron.

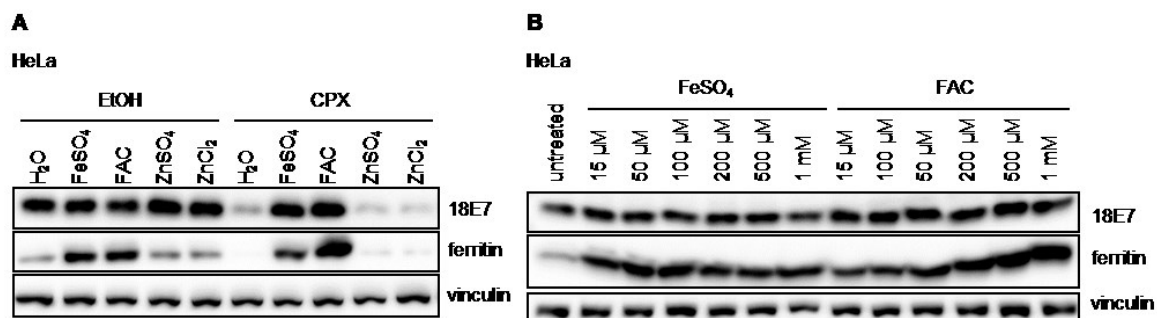


Figure 10: Excess iron prevents CPX-induced E7 repression. (A) Western blot analyses of HPV18 E7 and ferritin after 48 h treatment with 10 μM CPX in HeLa cells. Before treatment, CPX was complexed with 6.67 μM iron (FeSO₄, FAC) or zinc (ZnSO₄, ZnCl₂). CPX binds iron at a ratio of 3:1 [146]. 6.67 μM iron or zinc is equivalent to a twofold excess. (B) HeLa cells were treated with increasing concentrations of iron (FeSO₄ and FAC) for 24 h and analysed for the E7 and ferritin expression. Vinculin was used as loading control.

2.2 CPX inhibits cell proliferation

Next, the phenotypic consequences of CPX treatment were investigated. Since E6 and E7 are essential for the growth of HPV-positive cancer cells [182], the effect of CPX treatment on the proliferation of HeLa and SiHa cells was investigated. Cell proliferation in 2D cell culture was assessed by determining the increase of cell nuclei count with the IncuCyte® system, using cells that express the fusion protein mCherry H2B. In comparison to untreated or EtOH (solvent control)-treated cells, CPX causes a dose-dependent inhibition of cell growth in both HeLa and SiHa cells (Figure 11A and B, respectively). Importantly, CPX not only inhibited cell growth in 2D cell culture, but also in 3D cell culture. For the generation of spheroids a protocol was established which includes seeding cells in an ultra-low attachment microplate and supplementing the medium with methylcellulose. The size of spheroids upon treatment with different concentrations of CPX was measured with the IncuCyte® system using the acquisition and analysis tool for spheroids. Figure 11C and D depict the increase of spheroid size upon CPX treatment. Representative brightfield images of HeLa and SiHa spheroids that were treated with 10 μM CPX are shown in Figure 11E and F. It can be observed that the spheroids not only do not increase in size but especially in SiHa spheroids a decrease is visible, suggesting that besides inhibition of proliferation there might also be a component of cell death. After 3 d of CPX treatment, spheroids were sectioned and stained for the proliferation marker Ki-67 (Figure 11G) which indicates that CPX strongly inhibits proliferation. Furthermore, ferritin was analysed and at least in the outer cell layers of the

Results

spheroid there is a strong reduction of expression, indicating that CPX depletes these cells of iron. Corresponding results were obtained with SiHa spheroids.

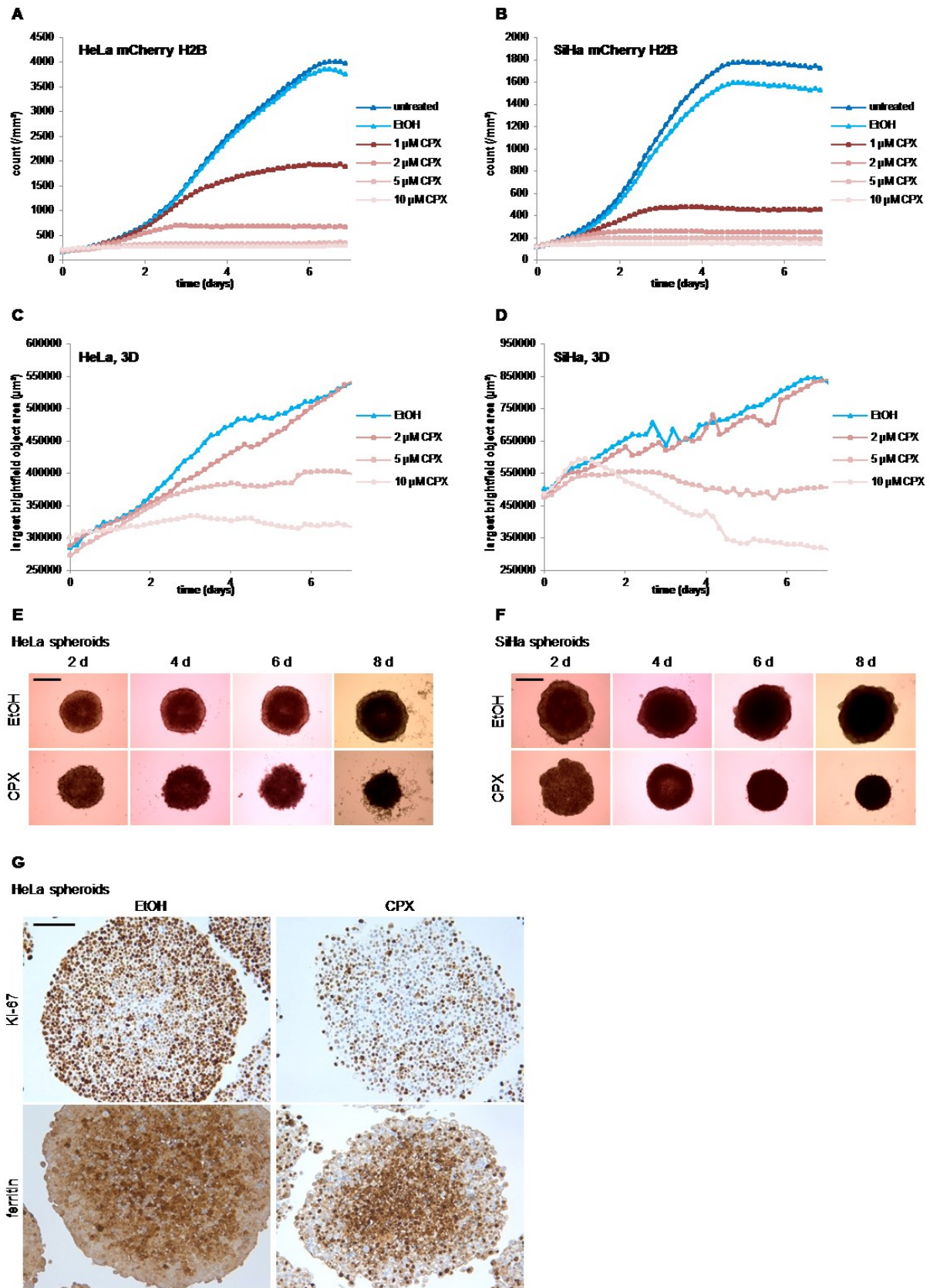


Figure 11: CPX inhibits proliferation. (A), (B) Cell proliferation of HeLa mCherry H2B (A) and SiHa mCherry H2B (B) cells under 2D cell culture conditions upon treatment with 1-10 μ M CPX. One representative experiment is shown. (C), (D) Size of HeLa (C) and SiHa (D) spheroids as assessed with the IncuCyte® system upon treatment with 2-10 μ M CPX. On representative experiment is depicted. (E), (F) Brightfield images of HeLa (E) and SiHa (F) spheroids after treatment with 10 μ M CPX for 2-8 days. Scale bar: 500 μ m. (G) Immunohistochemical stainings of HeLa spheroids that were treated with 10 μ M CPX for 72 h. A 10x magnification is shown, scale bar: 100 μ m.

2.3 CPX induces cell cycle arrest and senescence

The observed inhibition of cell growth by CPX could be explained by a reduced rate of cell proliferation (i.e. through induction of cell cycle arrest) or by an increase of cell death - or by a combination of both. To address this question, first, the cell cycle distribution upon CPX treatment was assessed with flow cytometry. Analyses of HeLa cells treated with CPX and stained with propidium iodide (PI) indicate that CPX induces a cell cycle arrest in G1 phase, as seen by the increase of the cells in G1 phase from about 60% to 80% after 24 h (Figure 12A). To analyse the cell cycle progression in more detail, EdU incorporation assays were performed in HeLa cells. EdU as a thymidine analogue is incorporated in the DNA during S phase and can be detected using flow cytometry [183]. One representative experiment is shown in Figure 12B. Upon EtOH treatment, 24.1% of the cells are in S phase as indicated by the positivity for EdU. G0/G1 and G2/M phase can be distinguished by the PI content of the cells. CPX treatment strongly decreases the percentage of cells incorporating EdU to virtually 0%, suggesting that the cells do no longer synthesise DNA. In comparison to the cell cycle analyses with PI alone, it can now be specified that CPX-treated cells are not only arrested in G1 phase but also in S phase. Cells with medium PI content (between G1 and G2) but negative for EdU represent S phase arrested cells. The reduction of EdU incorporation is significant with a p-value below 0.0001 (Figure 12B).

In order to test whether the cell cycle arrested cells undergo senescence, senescence-associated β -galactosidase assays (SA- β -gal assays) were performed. With this assay senescent cells are stained blue due to senescence-associated β -galactosidase activity [184]. Figure 12C shows that both HeLa and SiHa cells undergo senescence after treatment with CPX for 48 h. SA- β -gal assays were performed 4 days after release from CPX. The concomitant colony formation assays (CFAs) further support the induction of senescence (i.e. the induction of an irreversible growth arrest) since substantially fewer colonies grow out after release from CPX treatment (Figure 12D).

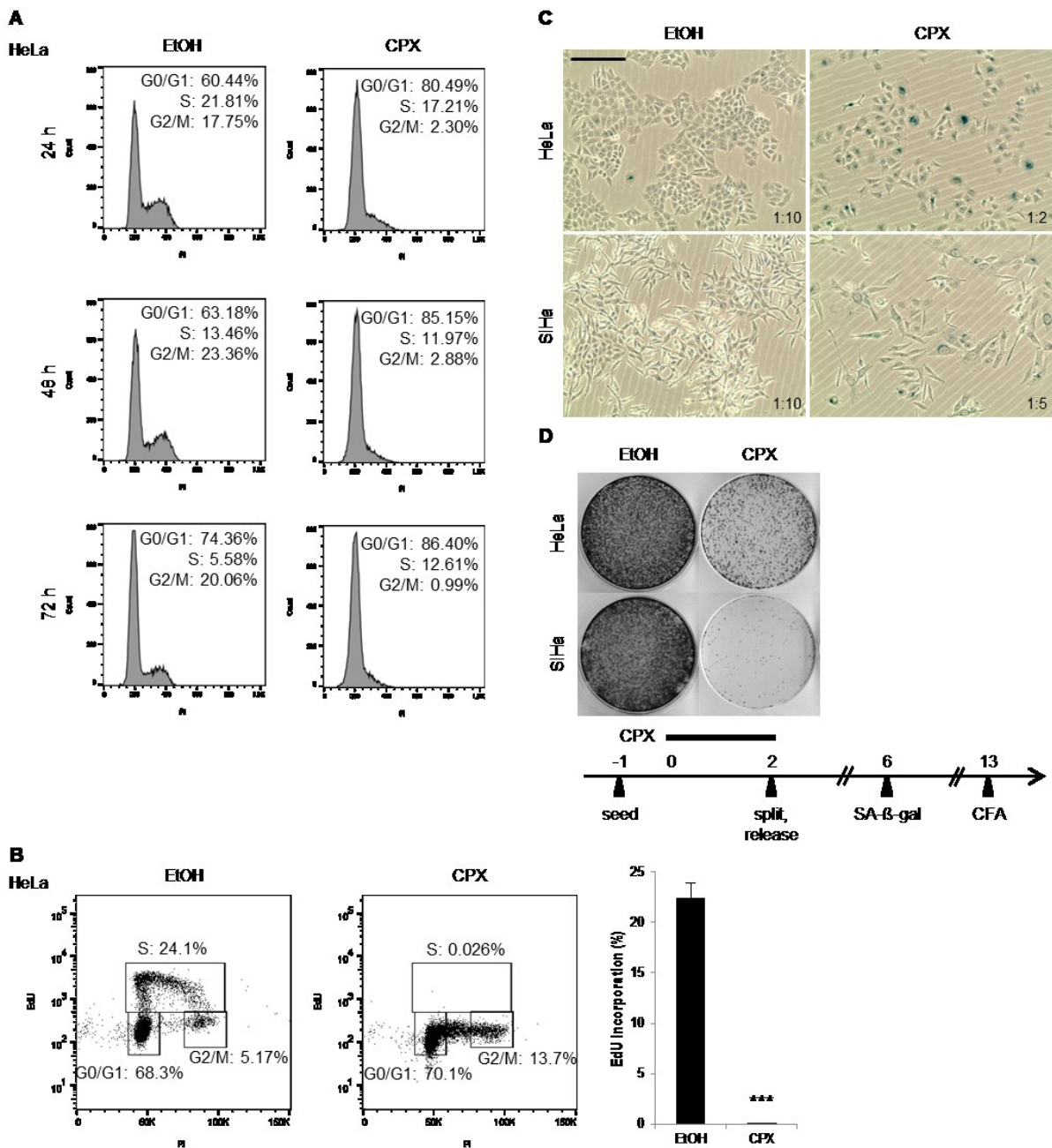


Figure 12: CPX induces cell cycle arrest and senescence. (A) Cell cycle analyses of HeLa cells treated with EtOH or 10 μ M CPX for the indicated time periods. Fraction of cells in G0/G1, S and G2/M are indicated (data for this subfigure was obtained in collaboration with Johanna Ira Blase). (B) EdU incorporation in HeLa cells upon EtOH or 10 μ M CPX treatment for 48 h. One representative image is shown. Statistical analysis of three independent experiments is depicted on the right. ***=p<0.001. (C) HeLa and SiHa cells were treated with 10 μ M CPX for 48 h. After treatment, cells were split and cultured in CPX-free medium. The split ratio is indicated for each image. 4 days after release SA- β -gal assays were performed (scale bar: 200 μ m). (D) Concomitant CFAs to (C) fixed 11 days after splitting and release. Scheme of experimental setup below.

A key regulator of senescence is p53 which induces the expression of p21, an inhibitor of cell cycle progression [74, 185]. Since CPX represses E6, which is involved in the degradation of

p53 [36], it was of great interest to investigate whether p53 is reconstituted upon CPX treatment and whether increase of p53 is the cause for the induction of senescence. Surprisingly, however, total p53 protein levels are not reconstituted upon CPX treatment, but decrease after 48 h and 72 h in HeLa (Figure 13A) and SiHa (Figure 13B) cells.

Since the activity of p53 can be altered through post-translational modifications, phosphorylation of p53 at serine 15 was analysed. On the one hand, phosphorylation of p53 at serine 15 stabilises p53 since it impedes interaction with and thus degradation through MDM2 [186]. On the other hand P-Ser15 of p53 is necessary for the transactivation of p53-responsive promoters including the *CDKN1A* promoter (encoding p21) [187]. Interestingly, CPX induces a strong phosphorylation of p53 at serine 15. In HeLa cells (Figure 13A) p53 is continuously phosphorylated upon CPX exposure from 24 h to 72 h, whereas in SiHa cells (Figure 13B) p53 phosphorylation appears to be transient in that it is detectable after 24 h treatment with CPX but not at later points of time. Furthermore, p21 protein levels were analysed in HeLa (Figure 13A) and SiHa (Figure 13B) cells and an increase is visible after 24 h CPX exposure in both cell lines. After 48 h and 72 h p21 protein levels are decreased. Notably, p21 downregulation was observed in HeLa despite p53 phosphorylation at serine 15.

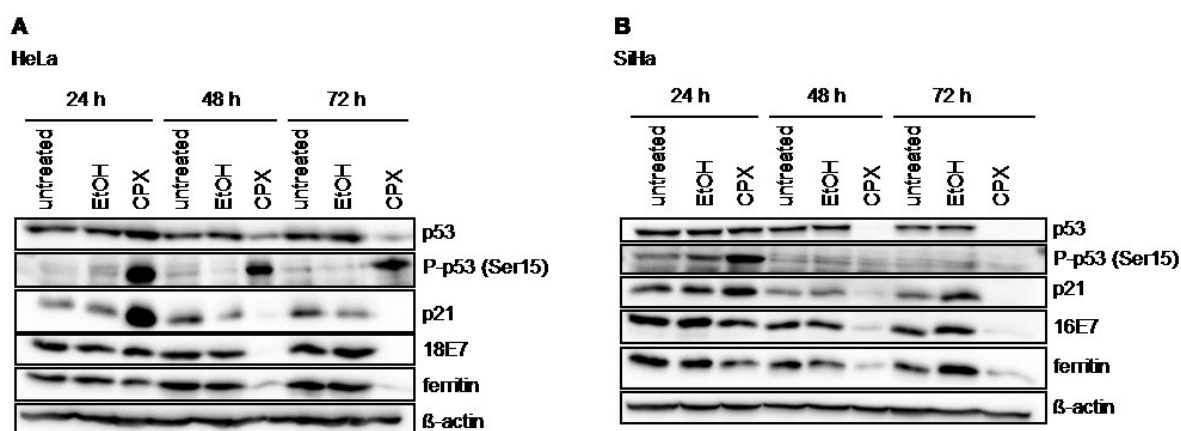


Figure 13: CPX induces phosphorylation of p53 at Ser15. (A), (B) HeLa (A) and SiHa (B) cells were treated with 10 μ M CPX for 24-72 h. P-p53 (Ser15), total p53, p21, E7 and ferritin were detected. β -actin was used as loading control.

Phosphorylation of serine 15 of p53 can occur as a response to DNA damage. To investigate whether the CPX-induced increase of P-p53 (Ser15) is linked to DNA damage, CPX-treated cells were analysed for histone H2AX phosphorylation (γ -H2AX) - a marker for DNA damage [188]. In both HeLa (Figure 14A) and SiHa (Figure 14B) cells a clear increase of γ -H2AX can be observed upon CPX treatment, indicating that CPX can induce DNA damage.

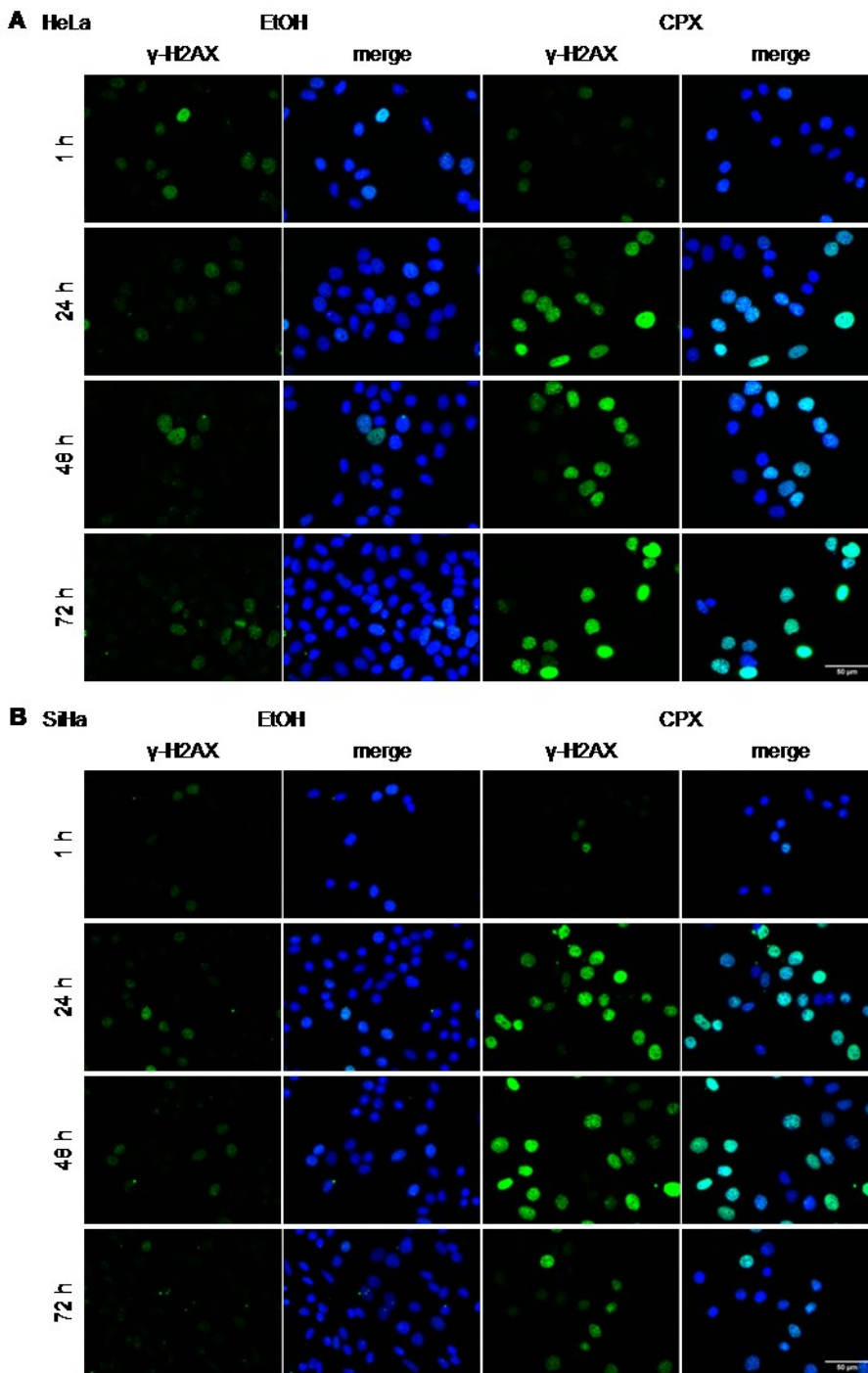


Figure 14: CPX causes DNA damage. (A), (B) HeLa (A) and SiHa (B) cells were treated with 10 μ M CPX for the indicated time periods. γ -H2AX expression was assessed by immunofluorescence (scale bar: 50 μ m).

To investigate whether p53 is necessary for the induction of senescence we took advantage of a HeLa cell line (HeLa “p53 null”), in which p53 is constantly and efficiently repressed by the stable expression of an shRNA targeting *TP53* [189]. Notably, CPX can induce senescence in HeLa “p53 null” cells as shown by SA- β -gal assays (Figure 15A). The notion is corroborated

by the decreased colony forming capacity as seen in concomitant CFAs (Figure 15B). Alike HeLa cells expressing p53 (Figure 12), HeLa “p53 null” cells also arrest in G1 phase as indicated by the increase of cells in G1 phase (Figure 15C). Moreover, EdU incorporation in HeLa “p53 null” cells was comparably repressed as in HeLa expressing p53 (please compare Figure 15D with Figure 12B). Collectively, the data indicate that both cell cycle arrest and the induction of senescence by CPX can occur p53-independent.

Furthermore, the repression of E6 and E7 by CPX is also p53-independent since it can be also observed in HeLa “p53 null” cells (Figure 15E). Importantly, neither P-p53 nor p53 were detectable upon CPX treatment (Figure 15F) indicating that knockdown of p53 remains efficient in HeLa “p53 null” cells under these experimental conditions.

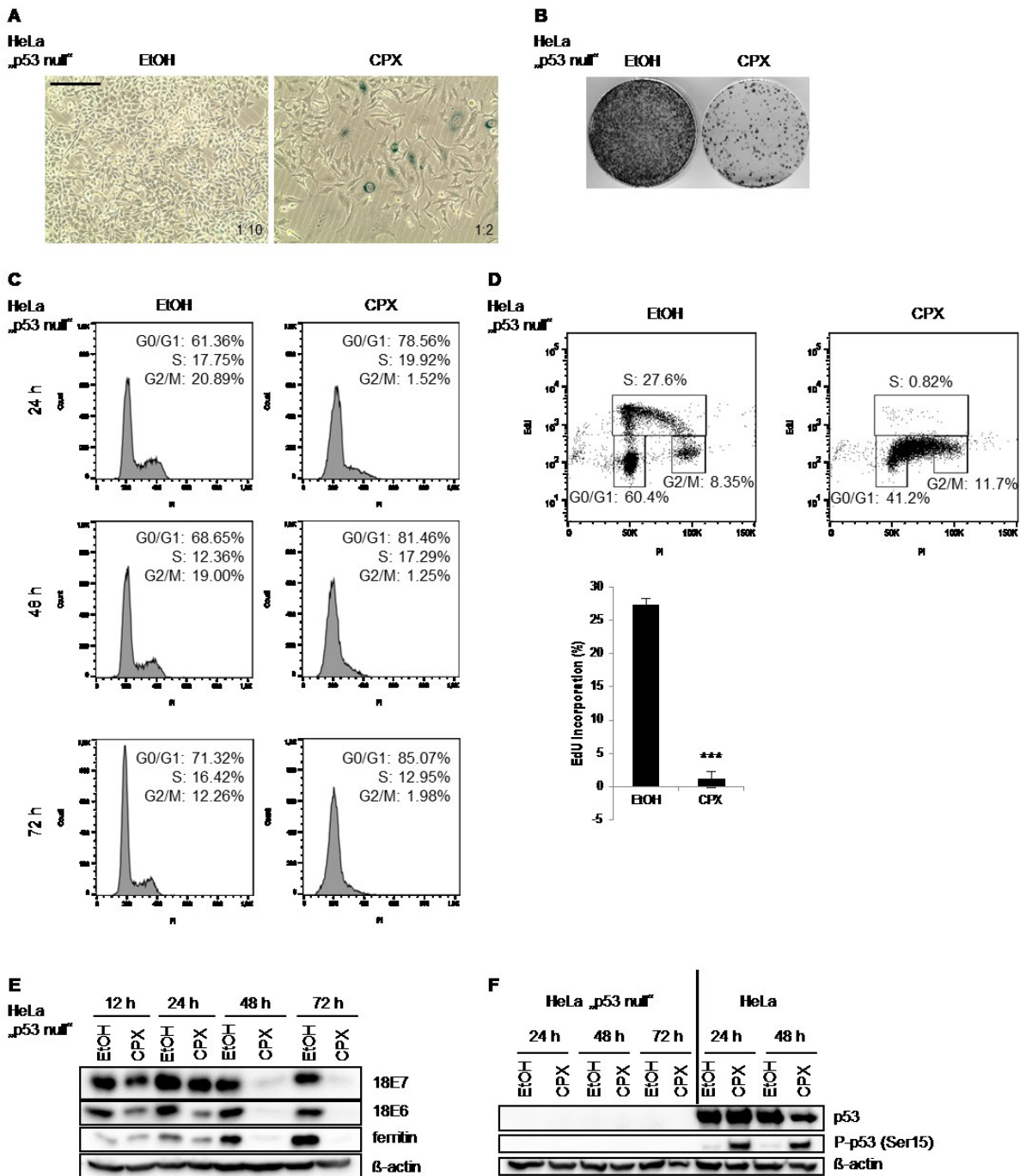


Figure 15: Senescence and cell cycle arrest induced by CPX are p53-independent. (A) Senescence assays in HeLa “p53 null” cells concomitant to Figure 12. Cells were treated with 10 μ M CPX for 48 h, released and subjected to SA- β -gal staining 6 days after splitting (scale bar: 200 μ m). (B) Concomitant CFAs to (A) fixed 11 days after splitting. (C) Cell cycle distribution after 10 μ M CPX treatment in HeLa “p53 null” cells (the data was obtained in collaboration with Johanna Ira Blase and is also depicted in [190]). (D) EdU incorporation after 48 h 10 μ M CPX treatment. One exemplary experiment is shown. Statistical analyses of three independent experiments are shown at the bottom. ***= $p < 0.001$. (E) Western blot analyses of HeLa “p53 null” cells treated with 10 μ M CPX for 12-72 h. (F) HeLa “p53 null” and HeLa cells were treated with 10 μ M CPX for the indicated time periods. Western blot analyses of p53 and P-p53 (Ser15) are depicted. β -actin served as loading control.

It was furthermore tested whether HIF-1 α is involved in CPX-induced E6/E7 repression, since HIF-1 α is known to be upregulated by CPX [146]. However, knockdown experiments indicate that E6/E7 repression by CPX is independent of HIF-1 α , since it can be observed in cells efficiently depleted of HIF-1 α (Figure 16). HIF-2 α would not be expected to be involved in E6/E7 repression since it is not expressed under normoxic conditions [39] and iron chelators additionally inhibit HIF-2 α protein translation due to an IRE in the 5' UTR of the *HIF-2 α* mRNA [118].

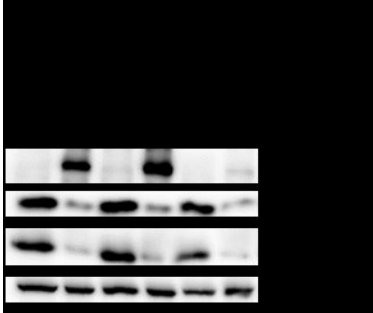


Figure 16: E6/E7 repression by CPX is HIF-1 α -independent. HeLa cells were transfected with shRNA against *HIF-1 α* or control vectors shcontr-1 and empty vector (EV). Then cells were treated with 10 μ M CPX for 48 h. Western blot analyses illustrate HIF-1 α , E6/E7 and ferritin expression.

To investigate whether the senescence induction by CPX is caused by iron deprivation, CPX was saturated with either iron or zinc prior to applying it to the cells. Senescence assays in HeLa (Figure 17A) and SiHa (Figure 17B) cells revealed that senescence induction by CPX, alike CPX-induced repression of E7, can be abrogated by saturating CPX with iron. In contrast, zinc cannot prevent the senescence induction by CPX. Concomitant CFAs in HeLa (Figure 17C) and SiHa (Figure 17D) cells support the notion that CPX induces senescence which can be prevented by the addition of iron. Furthermore, treatment of HeLa cells with another iron chelator (DFO) also induced senescence (Figure 17E) and reduced colony forming capacity (Figure 17F). Collectively, these data indicate that the pro-senescent effects of CPX are a consequence of intracellular iron depletion and that senescence induction might be a feature of iron chelators in general.

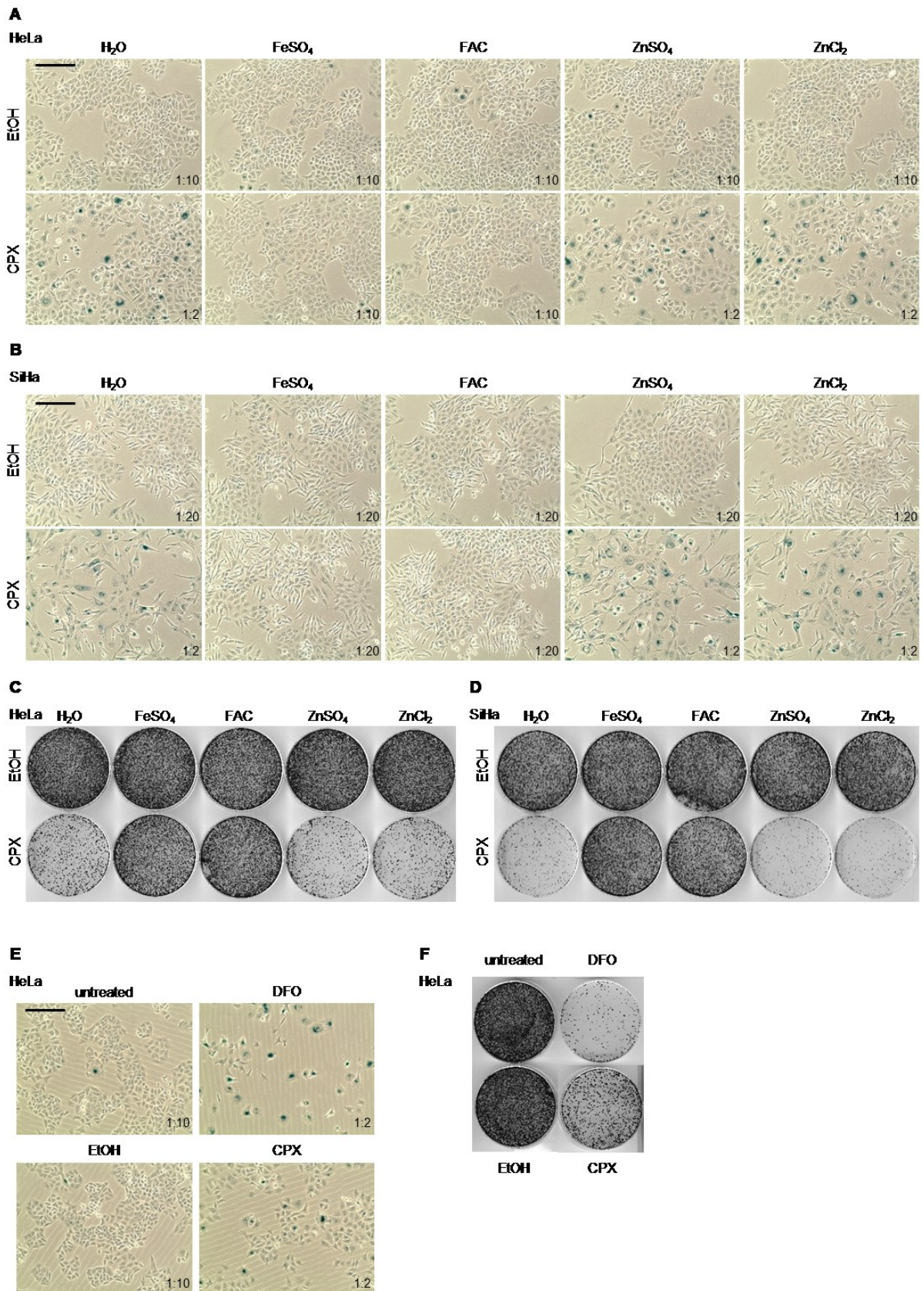


Figure 17: Senescence induction by CPX is caused by iron deprivation. (A), (B) HeLa (A) and SiHa (B) cells were treated with 10 μ M CPX for 48 h and subjected to SA- β -gal staining 5 days after splitting and release. CPX was complexed with 6.67 μ M iron (FeSO₄, FAC) or zinc (ZnSO₄, ZnCl₂) prior to treatment. Scale bar: 200 μ m. Split ratios are indicated in the image. (C), (D) Concomitant

CFAs to (A) and (B), respectively, stained 11 days after splitting. **(E)** Senescence assays of HeLa cells treated for 48 h with 100 μ M DFO or 10 μ M CPX. EtOH served as solvent control for CPX. After treatment, cells were split (ratio indicated in the image) and released in medium without iron chelators. Cells were stained 4 days after splitting (scale bar: 200 μ m). **(F)** Concomitant CFAs to (E) stained 12 days after splitting.

2.4 CPX induces apoptosis

Whereas anti-proliferative effects of CPX could clearly be demonstrated, some cells appear to escape senescence induction and continue to grow in CFAs after release from CPX treatment (Figure 12D). One explanation is that the cells that grow in CFAs are more resistant to CPX. To address this question HeLa and SiHa cells were treated with CPX. Then the cells that grew in CFAs were subjected to a second treatment with CPX. It could be observed that these cells are again growth-inhibited with CPX to a similar extent as cells that have not encountered CPX treatment before (data not shown). Moreover, several attempts to generate CPX-resistant cell lines have failed, suggesting that resistance mechanisms against CPX are very unlikely to develop.

Very interestingly, however, when the exposure of CPX was prolonged from two to five days the number of HeLa (Figure 18A) and SiHa (Figure 18B) cells that grow out in CFAs after CPX release was reduced to zero. Concomitant senescence assays were performed, but very few cells could be detected after CPX treatment and release. This suggests that the CPX-induced reduction of colony forming capacity in CFAs is not caused by an increase of the total number of senescent cells, but by cell death upon treatment and hence loss of cells. The induction of cell death by CPX is attributed to iron deprivation since this phenotype could be prevented by iron but not zinc (Figure 18A and B). To investigate whether cell death by CPX is mediated by apoptosis, several assays were performed (Figure 18C-F). In live cell imaging analyses the activation of caspase 3/7 upon CPX exposure was assessed in HeLa cells using the IncuCyte® Caspase-3/7 Green Reagent which couples a binding motif for activated caspase 3/7 to a DNA intercalating dye. Upon apoptosis induction, activated caspase 3/7 cleaves the non-fluorescent reagent and generates a fluorescent dye which binds to the DNA. Hence, apoptotic cells emit green fluorescence. The number of apoptotic (green) cells was normalised to the cell confluence. Upon CPX treatment, the activation of caspase 3/7 increases over time suggesting that cells start to undergo apoptosis after 2-3 days (Figure 18C). A plateau is reached after 4-5 days indicating that all cells are positive for activated caspase 3/7. Further, HeLa cells were stained for the apoptosis marker Annexin V

and PI upon 72 h treatment with CPX. In comparison to EtOH treatment, CPX increases the fraction of late apoptotic cells (Annexin V and PI positive) from 8.74% to 45.3% (Figure 18D). Moreover, also in TUNEL assays a time-dependent increase in apoptosis could be observed, as exemplified for SiHa cells (Figure 18E). After 48 h treatment with CPX, the cells are still negative for TUNEL, yet a reduction of the number of CPX-treated cells is visible in comparison to EtOH-treated cells, reflecting the growth inhibitory effect of CPX. After 3 and 4 days, however, the number of cells that undergo apoptosis increases as seen by the positive TUNEL staining. Notably, apoptosis induction by CPX is also dose-dependent since after 4 d treatment with 2 μ M CPX the cells are negative for TUNEL, whereas 10 μ M CPX induces apoptosis (Figure 18F). (As a side note: analogous results were obtained for HeLa cells, but SiHa cells were preferentially used for TUNEL assays since apoptotic HeLa cells tend to detach from the culture dish and the extent of apoptosis induction would be underestimated in HeLa cells).

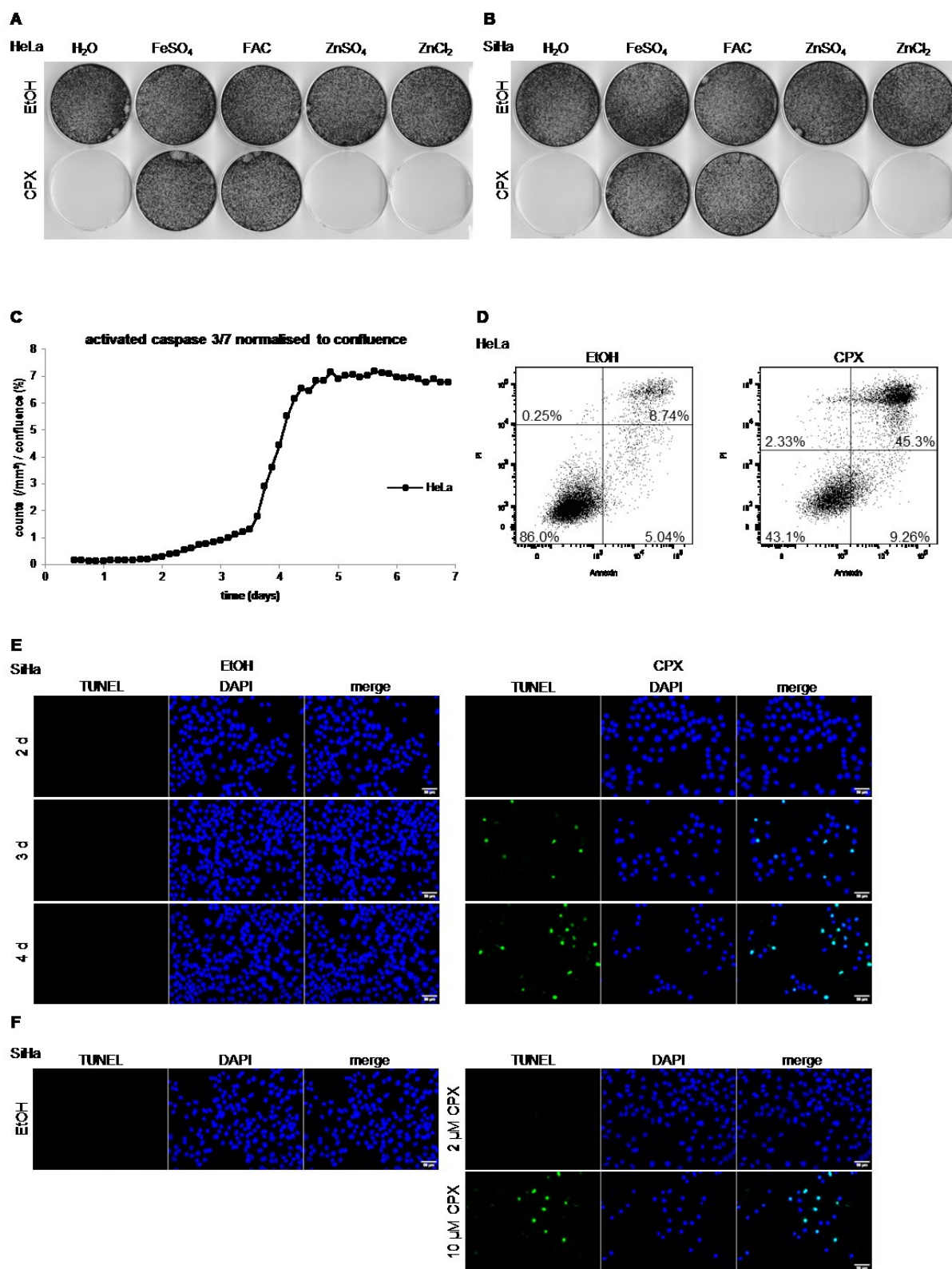


Figure 18: CPX induces apoptosis. (A), (B) CFAs in HeLa (A) and SiHa (B) cells exposed to 10 μ M CPX for 5 days. CPX was complexed with 6.67 μ M iron (FeSO₄, FAC) or zinc (ZnSO₄, ZnCl₂) prior to treatment of the cells. After treatment, cells were split and cultured in CPX-free medium. Cells were fixed 10 days after splitting. (C) HeLa cells were treated with 10 μ M CPX for 7 days in the presence of 5 μ M IncuCyte® Caspase-3/7 green reagent for apoptosis detection. Activated caspase 3/7 (green count/mm²) was assessed and normalised to the confluence (in percent) of the cells. (D) HeLa cells were treated with 10 μ M CPX for 72 h and stained with Annexin V and PI. Annexin V⁺/PI⁺ cells

represent early apoptotic cells, Annexin V⁺/PI⁺ cells represent late apoptotic cells. **(E)** TUNEL assays of SiHa cells after 10 μ M CPX treatment for up to 4 days (scale bar: 50 μ m). **(F)** SiHa cells were treated with 2 μ M or 10 μ M CPX for 4 days and subjected to TUNEL assays (scale bar: 50 μ m).

The time-dependent induction of apoptosis was also shown by analyses of PARP cleavage. In HeLa cells, PARP cleavage is detected after 24 h treatment with CPX and a strong increase is seen after 72 h (Figure 19A). In SiHa cells PARP cleavage is detectable after 72 h of CPX exposure (Figure 19B). DFO also induces PARP cleavage in HeLa (Figure 19C) and SiHa (Figure 19D) cells, suggesting that the apoptosis induction after prolonged treatment is a common feature of iron chelators. It should be noted that the concentration of CPX was ten times less than the concentration of DFO, indicating that CPX is more potent to induce apoptosis.

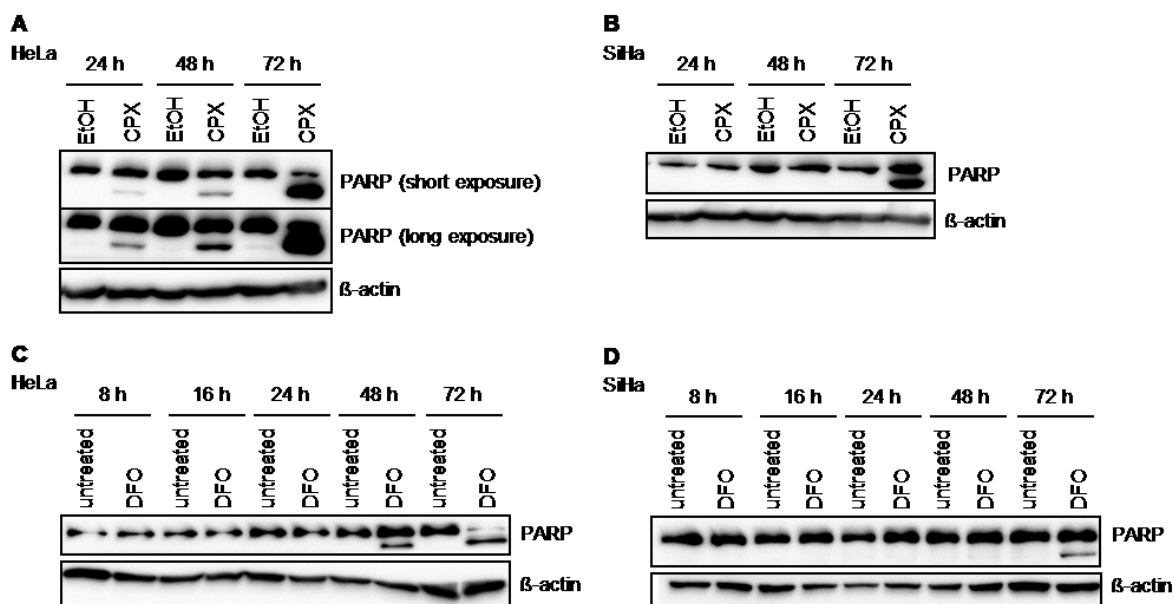


Figure 19: CPX induces PARP cleavage. (A), (B) HeLa (A) and SiHa (B) cells were treated with 10 μ M CPX for the indicated time periods. PARP cleavage was assessed using an antibody that recognises both full length (uncleaved) PARP (upper band) and the larger fragment (lower band) after cleavage. (C), (D) HeLa (C) and SiHa (D) cells were treated with 100 μ M DFO for the indicated time periods (for HeLa, same image of loading control was used in Figure 8A). β -actin served as loading control.

p53 not only plays a role in senescence but also in apoptosis induction [191]. Thus, HeLa “p53 null” and HeLa expressing p53 were analysed for caspase 3/7 activation upon CPX treatment. Interestingly, the lack of p53 remarkably delays apoptosis (Figure 20A), suggesting that p53 contributes to the regulation of apoptosis by CPX. Furthermore, the strong increase of PARP cleavage after 72 h exposure to CPX is not seen in HeLa “p53 null cells”

(Figure 20B, compare to Figure 19A), consistent with the finding that apoptosis is induced at later points of time. The observation that HeLa “p53 null” cells eventually undergo apoptosis upon prolonged CPX treatment (Figure 20A) indicates that CPX-induced apoptosis not necessarily depends on p53.

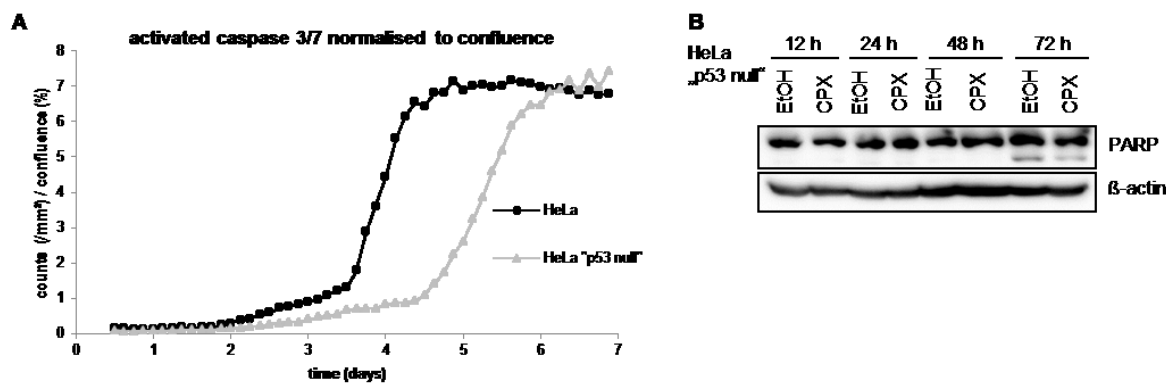


Figure 20: Apoptosis induction by CPX is delayed in HeLa "p53 null" cells. (A) HeLa and HeLa “p53 null” cells were treated with 10 μ M CPX and 5 μ M IncuCyte® Caspase-3/7 green reagent for apoptosis detection. Activated caspase 3/7 (green count/mm²) was assessed and normalised to the confluence (in percent) of the cells (the data for HeLa cells is also shown in Figure 18C). (B) HeLa “p53 null” cells were treated with 10 μ M CPX for 12-72 h and analysed for (cleaved) PARP expression. β -actin was used as loading control.

To further corroborate that the delay of CPX-induced apoptosis is caused by the lack of p53, the experiment was repeated in a different cellular background using HCT116 colon cancer cells. HCT116 p53^{-/-} and HCT116 p21^{-/-} cells were supplied by the lab of Bert Vogelstein [192, 193] and, together with parental HCT116 cells, subjected to activated caspase 3/7 measurement upon CPX treatment. A delay in apoptosis can also be observed in HCT116 p53^{-/-} cells compared to parental HCT116 cells (Figure 21). In specific, about 50% of parental HCT116 cells were killed after 3 days of CPX treatment, whereas 50% of HCT116 p53^{-/-} cells were dead after 4 days CPX treatment. Notably, the lack of p21 renders HCT116 cells more vulnerable to CPX treatment since HCT116 p21^{-/-} cells already start to induce apoptosis after only 1 day (Figure 21), suggesting that a lack of p21 accelerates apoptosis induction by CPX. Collectively, the data comparing HCT116 and HCT116 p53^{-/-} cells also indicate that a lack of p53 delays the apoptotic response towards CPX treatment, yet, apoptosis induction by CPX can be p53-independent.

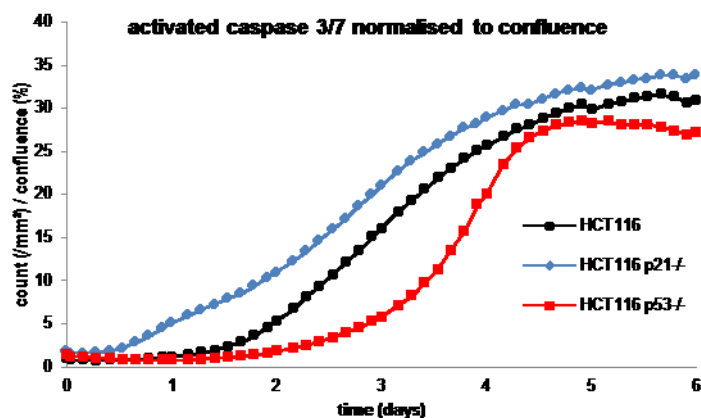


Figure 21: The lack of p53 delays CPX-induced apoptosis in HCT116 cells. HCT116, HCT116 p53^{-/-} and HCT116 p21^{-/-} cells were treated with 10 μ M CPX and 5 μ M IncuCyte® Caspase-3/7 green reagent for apoptosis detection. Activated caspase 3/7 (green counts/mm²) was measured with the IncuCyte® system and normalised to the confluence (in percent) of the cells.

2.5 CPX induces mTORC1-independent senescence

According to Blagosklonny et al. a major player in senescence induction is active mTOR signalling ([86], please also refer to 1.7 and to Figure 3). In line with this, senescence induction upon E6/E7 inhibition was prevented with the mTOR inhibitor rapamycin [39]. To investigate whether mTOR signalling is also necessary for CPX-induced senescence, HeLa and SiHa cells were pre-treated with the mTOR inhibitor rapamycin and then treated with CPX. After treatment, cells were released from CPX and rapamycin, and subjected to senescence assays (Figure 22A, B) and CFAs (Figure 22C, D). As indicated by the induction of SA- β -gal activity (blue cells), CPX is able to induce senescence in the presence of rapamycin, suggesting that mTOR signalling might not be required for senescence induction by CPX. Concomitant CFAs support that notion, since a comparable amount of colonies grow out after CPX treatment in the presence and absence of rapamycin. Rapamycin is considered to be a specific inhibitor of mTOR complex 1 (mTORC1) [194], although some studies indicate that mTORC2 can be inhibited by prolonged treatment with rapamycin [195]. Treatment with rapamycin induced effects on mTORC1 downstream targets S6K and 4E-BP1 as anticipated from studies by Choo et al. [196] and as previously published by our lab [39]. In specific, rapamycin decreases the phosphorylation of S6K, but barely affects 4E-BP1 phosphorylation (Figure 22E, F). The results indicate that under the experimental conditions, mTORC1 signalling is downregulated after 24 h rapamycin treatment and hence mTORC1 signalling through P-S6K appears to be dispensable for CPX-induced senescence. This is remarkable since the anti-senescent activity of rapamycin in HPV-positive cancer cells was linked to inhibition of S6K phosphorylation [39]. Interestingly, CPX not only is capable of inducing senescence under these conditions, but acts as an mTORC1 inhibitor itself since P-S6K is downregulated upon CPX treatment in both cell lines (Figure 22G, H). In contrast to rapamycin, CPX additionally strongly decreases the phosphorylation of E4-BP1.

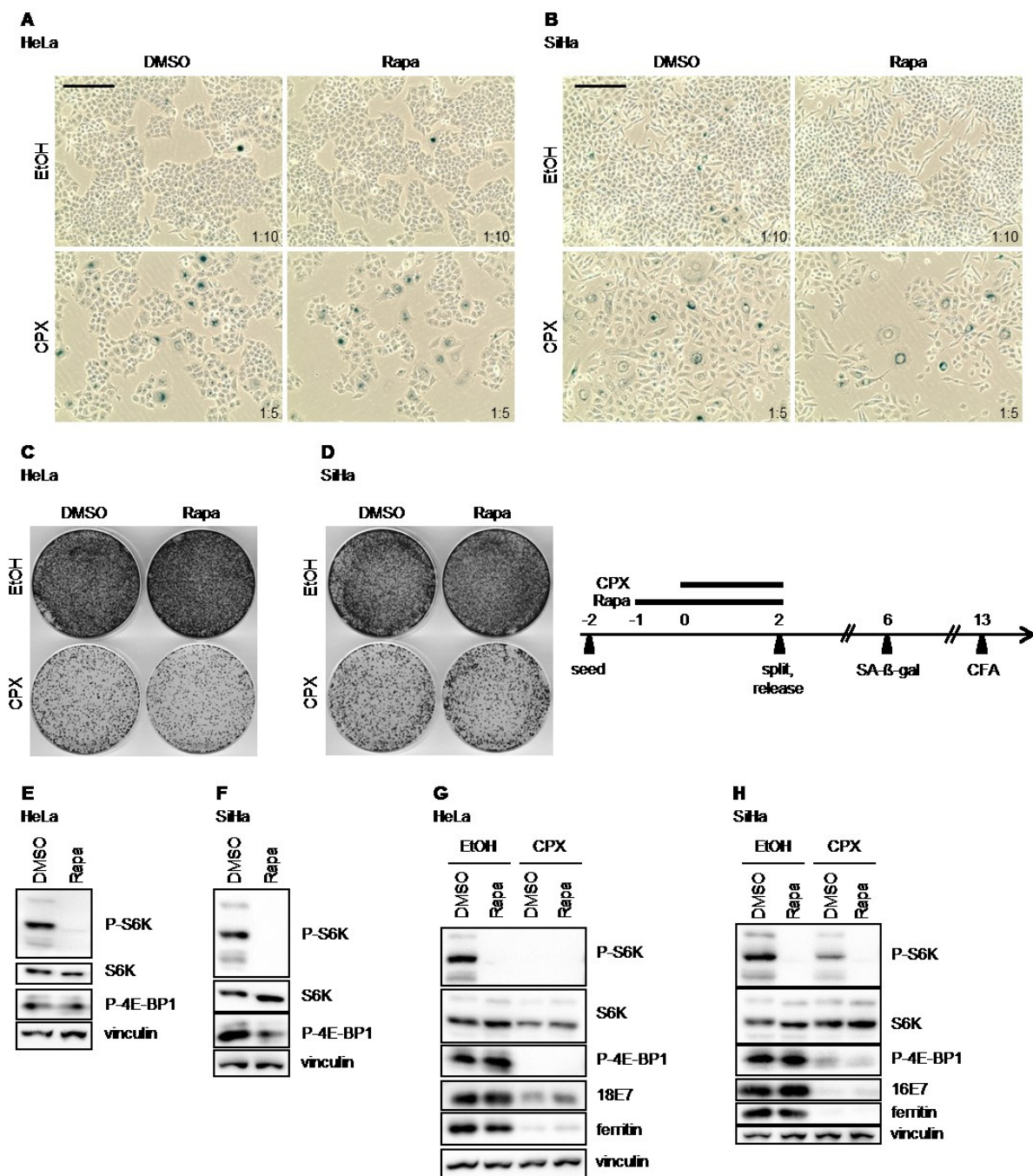


Figure 22: CPX induces mTORC1-independent senescence. (A), (B) Senescence assays of CPX-treated HeLa (A) and SiHa (B) cells in the presence or absence of rapamycin (Rapa). DMSO was used as solvent control for rapamycin. Scale bar: 200 μ m, split ratios are displayed in the images. (C), (D) Concomitant CFAs to (A) and (B). Right side: scheme of experimental setup for (A)-(D): Cells were pre-treated with 50 nM rapamycin for 24 h, then 10 μ M CPX was added for another 48 h. After treatment, cells were split and cultured in medium without CPX and without rapamycin. (E), (F) HeLa (E) and SiHa (F) cells were treated with 50 nM rapamycin for 24 h. (G), (H) Western blot analyses of HeLa (G) and SiHa (H) cells that were treated according to (A)-(D). Substrates indicating active mTORC1 signalling: P-S6K and P-4E-BP1. Vinculin served as loading control.

The repression of mTORC1 by CPX was subsequently investigated in more detail. HeLa (Figure 23A) and SiHa (Figure 23B) cells were treated with CPX for different periods of time

and mTORC1 signalling was analysed by western blot. P-S6K and P-4E-BP1 are strongly downregulated in both HeLa and SiHa cells after 48 h. Total levels of S6K in SiHa also slightly decrease after CPX treatment for 48 h and 72 h. Furthermore, protein levels of REDD1 (regulated in development and DNA damage responses 1) were analysed. REDD1 is a negative regulator of mTORC1 [197] and is upregulated after 12 h and 24 h CPX treatment in HeLa and SiHa cells (Figure 23C and D). After 48 h and 72 h, it is strongly repressed.

Next, it was investigated whether mTOR repression is a specific feature of CPX or whether it can be also achieved upon treatment with another iron chelator. Interestingly, DFO represses mTORC1 signalling similar to CPX (Figure 23E, F), suggesting that the repression is a feature of iron chelators in general. In both cell lines the strongest repression of P-S6K and P-4E-BP1 can be observed after 48 h and 72 h. Alike CPX, DFO reduces the levels of S6K in SiHa cells. Furthermore, a slight reduction of S6K is seen in HeLa cells after 72 h. REDD1 is upregulated by DFO after 8-24 h and decreased after 48-72 h which mirrors the data obtained by CPX. Collectively, these results suggest that iron chelators repress mTORC1 signalling which may be linked to the induction of the negative regulator REDD1. However, since mTORC1 signalling is not restored upon REDD1 repression it is possible that additional factors are involved or that the initial induction of REDD1 expression is sufficient to inhibit mTORC1 signalling at later points of time.

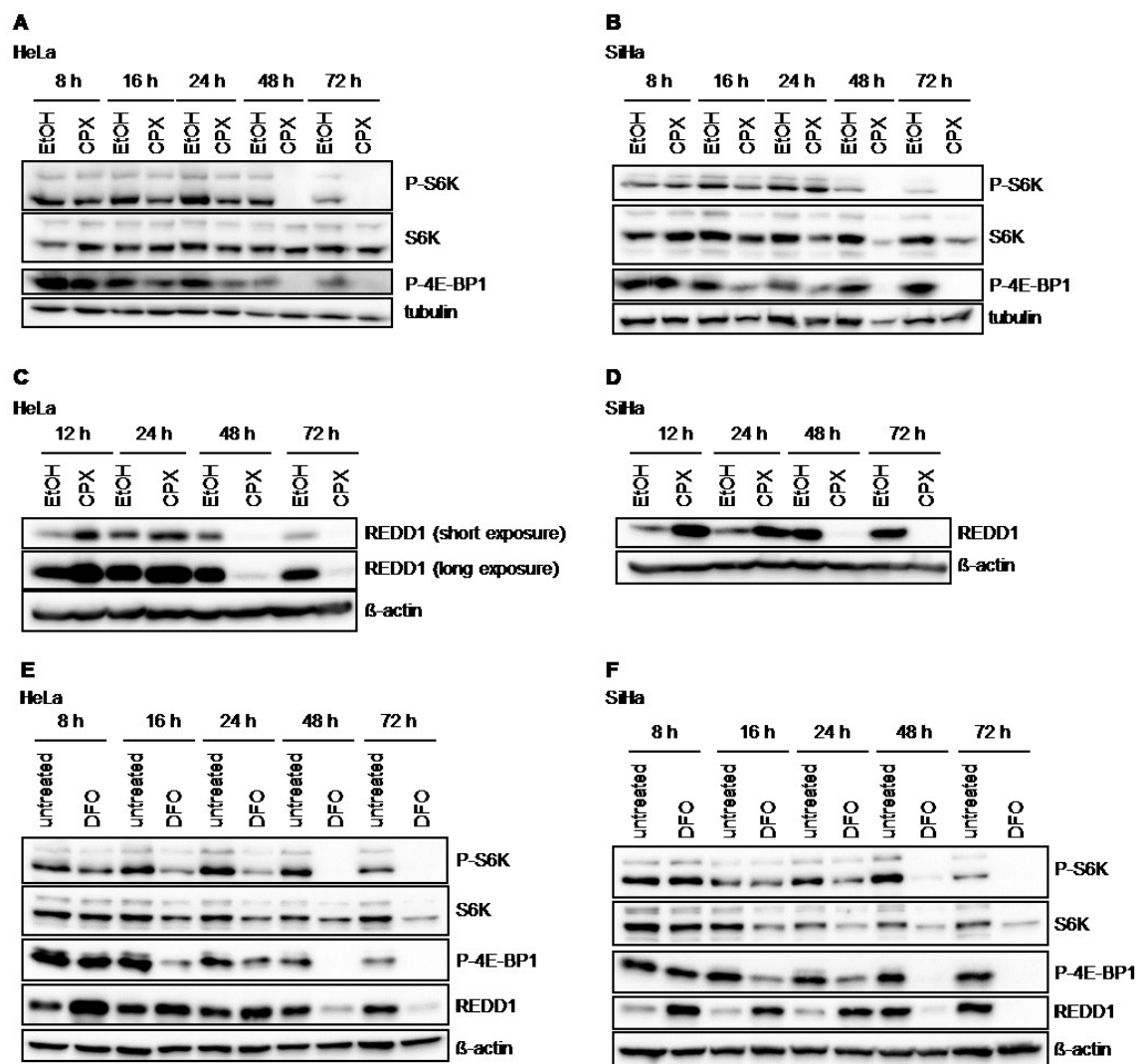


Figure 23: Iron chelators repress mTORC1 signalling. (A), (B) HeLa (A) and SiHa (B) cells were treated with 10 μM CPX for 8-72 h and analysed for the expression of P-S6K and P-4E-BP1. Tubulin served as loading control. (C), (D) HeLa (C) and SiHa (D) cells were treated with 10 μM CPX for 12-72 h and analysed for REDD1 expression (same image of loading control as in Figure 19A and B). (E), (F) HeLa (E) and SiHa (F) cells were treated with 100 μM DFO for the indicated time periods. Substrates of the mTORC1 pathway and REDD1 were analysed. β-actin served as loading controls.

2.6 CPX exhibits growth inhibitory effects under hypoxic conditions

The fact that CPX induces senescence in an mTORC1-independent manner suggests the possibility that it could also induce senescence under hypoxic conditions, where mTORC1 signalling is impaired ([198], see also Figure 3). To this end, HeLa and SiHa cells were cultured under hypoxic conditions (1% O₂) for 24 h, then CPX was added for another 72 h. Western blot analyses of SiHa cells (Figure 24A) show that CPX is active under hypoxic conditions since CPX can repress E7 further - in addition to the repression of E7 by hypoxia itself. E6 is repressed to the detection limit by hypoxia and thus, it could not be assessed

whether CPX represses E6 under hypoxic conditions any further. Ferritin is also repressed by CPX at 1% oxygen proving that CPX is active under hypoxia. Furthermore, CFAs of HeLa and SiHa cells (Figure 24B) show that upon CPX treatment under hypoxic conditions, there is a reduced colony forming capacity after release from CPX treatment and hypoxia (see scheme in Figure 24C). However, senescence assays do not show an obvious increase in the absolute number of senescent cells after CPX treatment in comparison to EtOH suggesting that the growth inhibitory effect seen in CFAs is more likely due to the apoptotic component resulting from CPX treatment. In line, SiHa cells subjected to TUNEL assays under hypoxic conditions indicate that after 3 days of CPX exposure there is a clear increase in apoptosis and after 5 and 6 days basically all cells are TUNEL positive (Figure 24D).

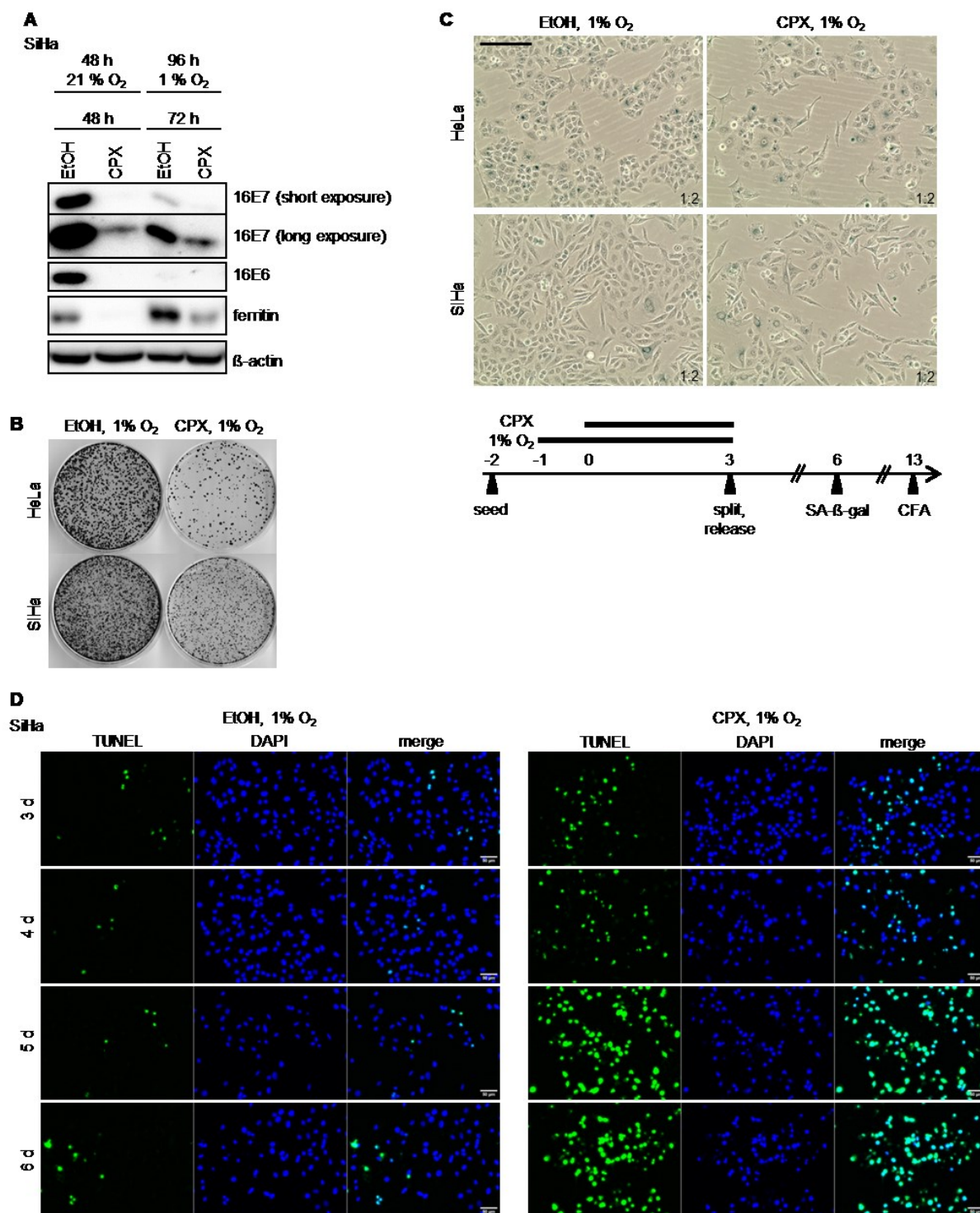


Figure 24: CPX treatment under hypoxic conditions. (A) SiHa cells were treated with 10 μM CPX either for 48 h under normoxic conditions (21% O₂) or 72 h under hypoxic conditions (1% O₂) after 24 h pre-incubation at 1% O₂. Western blot analyses show HPV16 E6/E7 and ferritin expression. β-actin was used as loading control. (B) CFAs of HeLa and SiHa cells after 10 μM CPX treatment for 72 h under hypoxic conditions. After treatment, cells were split and released, CFAs were stained 11 days after splitting. (C) Senescence assays of HeLa and SiHa cells treated as in (B), stained 3 days after splitting (ratios are indicated, scale bar: 200 μm). Experimental setup is depicted in the scheme below. (D) TUNEL assays of SiHa cells treated with EtOH or 10 μM CPX under hypoxic conditions after 3-6 days (scale bar: 50 μm).

To summarise, CPX treatment under normoxic conditions results in senescence and apoptosis, depending on the duration of the treatment. Under hypoxic conditions, cells do not undergo senescence upon CPX exposure but primarily react with induction of apoptosis.

2.7 CPX cooperates with RT and CT

Many treatment options in the clinic such as radio- and chemotherapy have limited efficiencies in targeting hypoxic regions of the tumour [199]. Since CPX exhibits anti-tumourigenic effects under hypoxic conditions it was of great interest to test CPX in combination with RT and CT. Figure 25 shows the cooperative effect of CPX with RT and CT. HeLa and SiHa cells were irradiated and subsequently treated with CPX for 4 days (top panels). In the case of hypoxia, cells were incubated at 1% O₂ for 24 h prior to irradiation and treatment. CFAs show that γ -irradiation is efficient in inhibiting cell growth under normoxic conditions in both HeLa (left upper panels) and SiHa (right upper panels) cells since very few colonies grew out after release in comparison to non-irradiated controls. Growth inhibition by irradiation was less efficient under hypoxic conditions than under normoxia (in SiHa cells the effect is only minor). Notably, however, the combinatorial treatment of RT with CPX reduced the number of colonies under both normoxic and, importantly, also under hypoxic conditions, indicating that CPX can cooperate with RT at normoxia and hypoxia.

In the case of CT, two compounds were tested: cisplatin (CDDP, middle panels) and etoposide (Eto, bottom panels) which were combined with CPX for 3 and 4 days, respectively. The efficiency of CDDP was comparable under 21% and 1% oxygen in HeLa cells and the concomitant treatment with CPX reduced colony numbers further under both conditions. In SiHa cells, the treatment with CDDP alone was much less efficient under hypoxic conditions in comparison to normoxia but a combinatorial treatment with CDDP and CPX under hypoxic conditions reduced the number of colonies growing in CFAs. The same holds true for etoposide in both HeLa and SiHa cells. Efficient growth inhibition by etoposide alone is limited to oxygenated cells. Under hypoxic conditions CPX cooperates with etoposide and reduces the colony forming capacity. Concomitant senescence assays show that under normoxic conditions CDDP and etoposide induce senescence, whereas irradiation and CPX mainly induce apoptosis under the tested conditions since very few cells were present after treatment. Furthermore, they show the outgrowth of colonies under hypoxic conditions which could be prevented by the combinatorial treatment with CPX. The results of the senescence assays are depicted in the master's thesis of Anja Herrmann [200]. Collectively,

the results provide strong evidence that CPX can cooperate with both RT and CT under normoxic and hypoxic conditions.

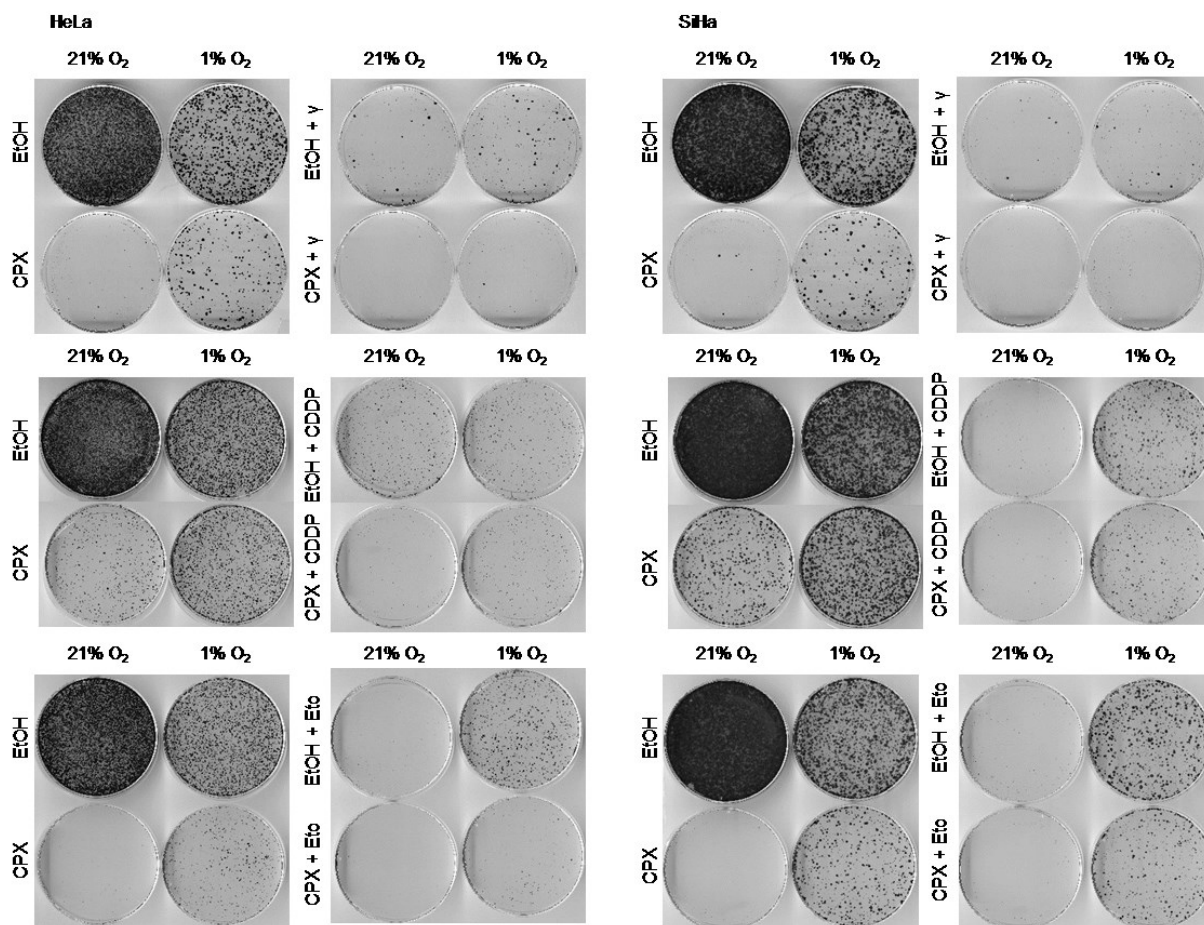


Figure 25: CPX cooperates with RT and CT. HeLa (left panels) and SiHa (right panels) cells were treated with 10 μ M CPX for 4 days after γ -irradiation with 10 Gy (upper panels). Combinatorial treatments of 10 μ M CPX with 5 μ M CDDP (middle panels) for 3 days and 5 μ M etoposide (lower panels) for 4 days are shown. All cells were split and released after treatment. CFAs were stained 11 days after release (data obtained in collaboration with Anja Herrmann and also contained in her master's thesis [200]).

2.8 Proteome analyses after CPX treatment

To further elucidate the mechanisms behind the anti-proliferative effects of CPX, proteome analyses were performed, analysing SiHa cells treated with CPX for 48 h under normoxic conditions. Out of almost 6000 detected proteins, 377 proteins were differentially expressed according to a threshold defined as an at least two-fold increase or decrease (\log_2 fold change $\geq +1.0$ or ≤ -1.0) and adjusted p-value smaller than 0.05. Among the significantly regulated proteins, 85 proteins are upregulated and 292 proteins are downregulated upon CPX treatment. The volcano plot illustrates the distribution of all detected proteins according to the

\log_2 fold change and the adjusted p-value (Figure 26A). It can be noticed that among the detected proteins the majority is downregulated upon CPX treatment.

The significantly regulated proteins were ranked according to their \log_2 fold change and subjected to gene set enrichment analyses (GSEA). Among the top ranked gene sets that are positively enriched by CPX treatment, gene sets that are also positively regulated by hypoxia were detected (Figure 26B shows one exemplary gene set). GSEA further revealed that gene sets related to aging and apoptosis are enriched by CPX treatment, corroborating the experimental findings obtained in the present work. Among the gene sets that are negatively regulated by CPX is the iron sulphur cluster binding gene set (Figure 26B). Another gene set is related to cell cycle transition from G1 into S phase. Interestingly, a gene set which is involved in the metabolism of nucleotides was found to be negatively regulated by CPX (although with a false discovery rate of 0.308). In this context, it is noteworthy that the RR has been described as a target of CPX (please refer to 1.14) and hence, it was aimed to investigate the role of RR in senescence and apoptosis induction by CPX under normoxic and hypoxic conditions.

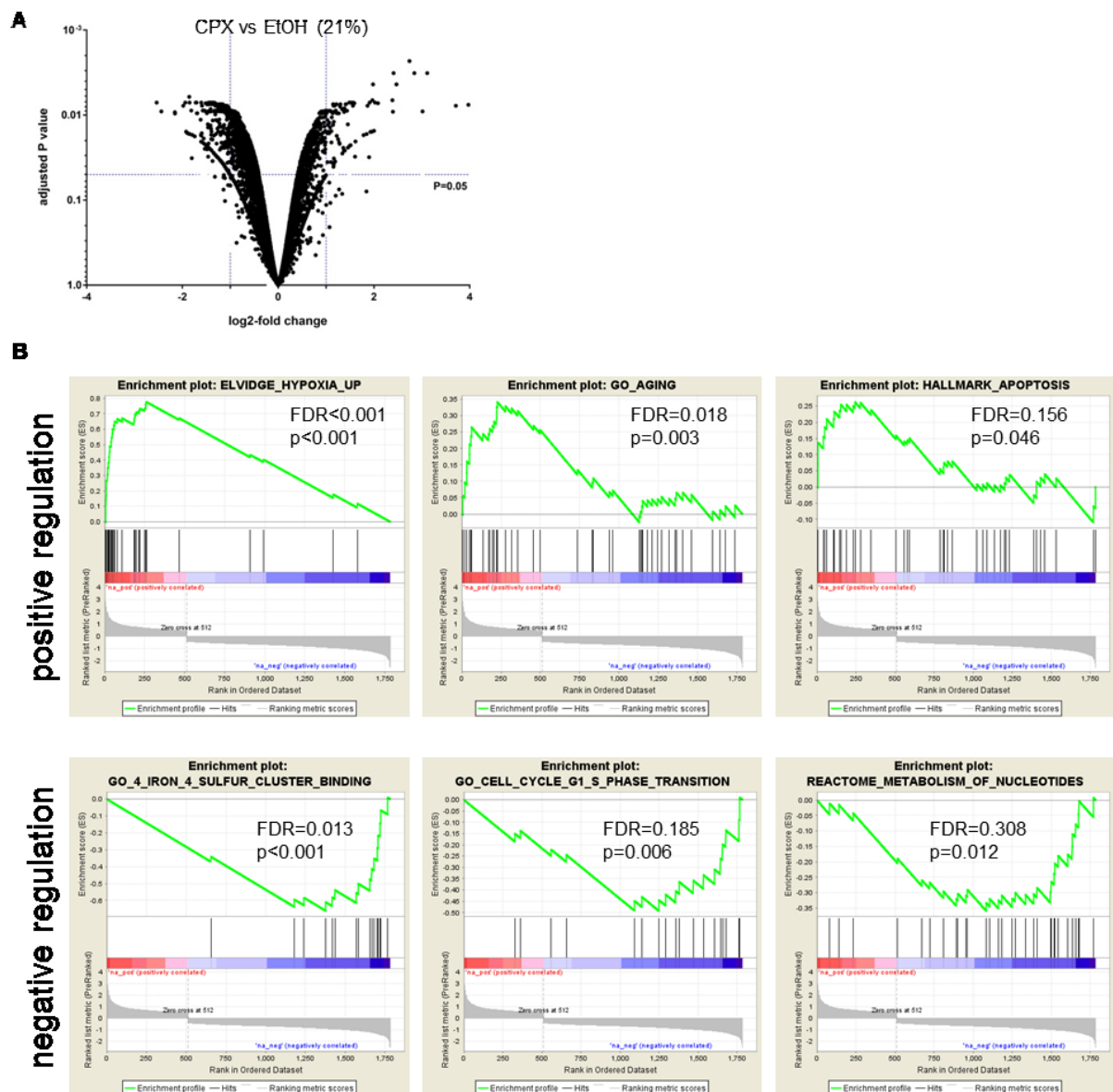


Figure 26: Proteome analyses of CPX treatment. (A) Proteins differentially regulated in SiHa cells after 10 μ M CPX treatment for 48 h. Volcano plots were obtained in collaboration with Bianca Kuhn. **(B)** GSEA of data obtained with proteome analysis. Selection of gene sets positively (upper panels) or negatively (lower panels) enriched by CPX treatment in SiHa cells. FDR, false discovery rate.

2.9 HU induces senescence, but not apoptosis

Inhibition of RRM2 is known to induce senescence [163]. This iron-containing subunit of RR can be inhibited either by iron chelators or HU which destabilises the tyrosyl radical. To investigate whether CPX acts via inhibition of RR, cells were treated with the RR inhibitor HU under normoxic and hypoxic conditions and results of senescence and apoptosis assays were compared to the results obtained with CPX treatment. Figure 27A-D show that HU induces senescence both under normoxic (A) and hypoxic (C) conditions as indicated by the increase of SA- β -gal positive cells (blue staining). Consistently, HU reduces the colony

forming capacity in HeLa cells under normoxic (B) and hypoxic (D) conditions supporting the notion that HU induces senescence. Furthermore, the senescence induction by HU is (alike CPX-induced senescence) mTORC1 independent, since cells undergo senescence in the presence of the mTORC1 inhibitor rapamycin as indicated by the positive SA- β -gal staining and the reduction of colonies that grow out after HU treatment (Figure 27E, F). Concomitant results were obtained in SiHa cells treated with HU under normoxic and hypoxic conditions (Supplementary Figure 1).

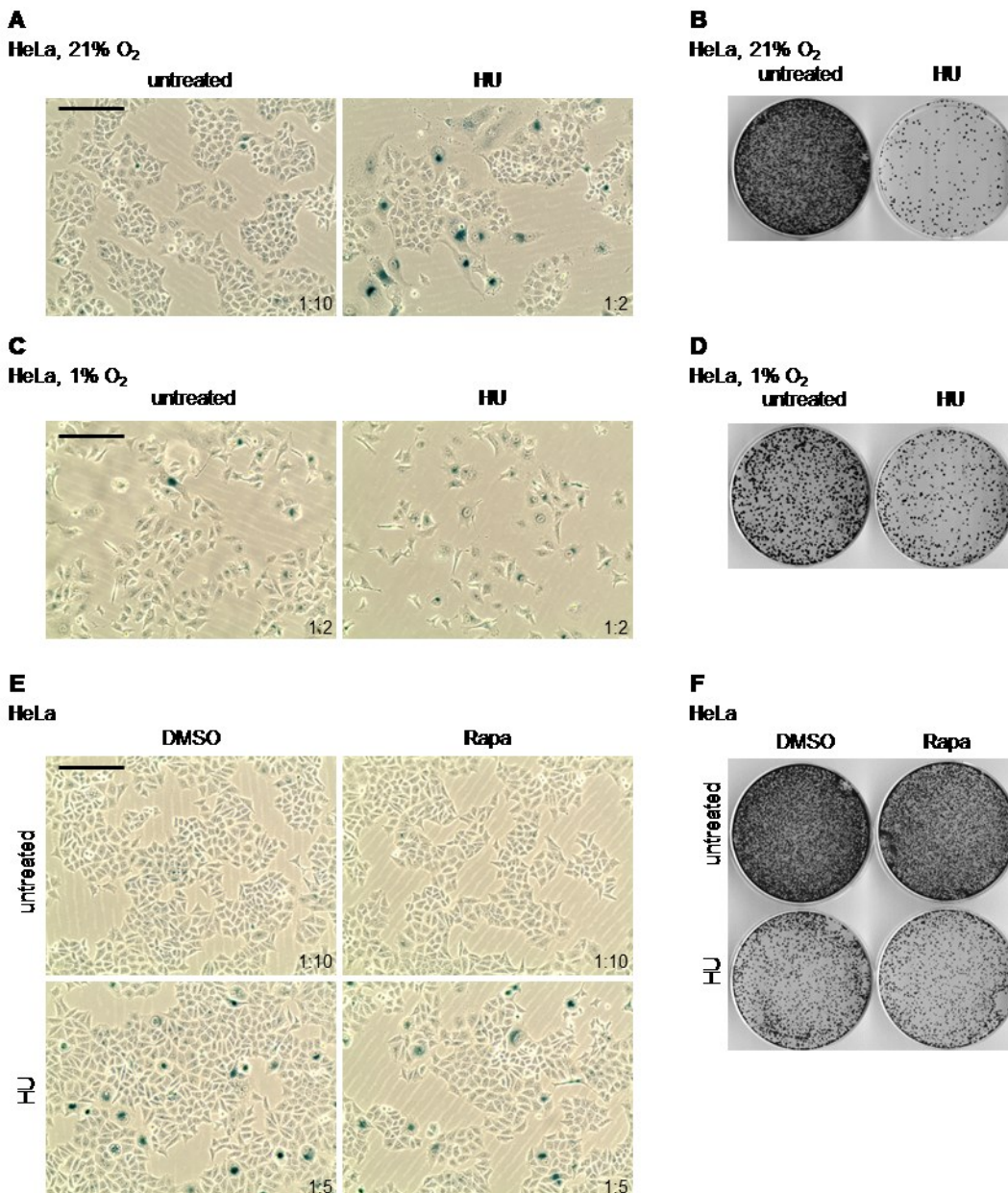


Figure 27: HU induces senescence. (A) Senescence assays of HeLa cells after 1 mM HU treatment for 48 h under normoxic conditions. After splitting at the indicated ratios, cells were released and stained for SA- β -gal 4 days after splitting (scale bar: 200 μ m). (B) Concomitant CFAs to (A), fixed 11 days after splitting. (C) HeLa cells were cultured under hypoxic conditions for 24 h and then treated with 1 mM HU for 96 h. After treatment cells were cultured under normoxic conditions and in

medium without HU. SA- β -gal staining was performed 3 days after splitting (scale bar: 200 μ m, split ratios indicated). **(D)** Concomitant CFAs to **(C)** 13 days after splitting. **(E)** HeLa cells were treated with 50 nM rapamycin for 24 h. Then 1 mM HU was added for 48 h. After treatment, cells were split at the indicated ratios and cultured in HU- and rapamycin-free medium. Senescence assays were performed 4 days after splitting (scale bar: 200 μ m). **(F)** Concomitant CFAs to **(E)** were stained 10 days after splitting.

Furthermore, apoptosis was analysed under normoxic and hypoxic conditions in SiHa cells upon HU exposure (Figure 28). Treatment with 1 mM HU for up to 4 days under normoxic conditions results in a minor increase of apoptotic cells as indicated by TUNEL stainings (Figure 28A). Under hypoxic conditions apoptosis could not be detected with 1 mM HU and exposure of up to 6 days (Figure 28B). The data suggests that the growth inhibitory effect of HU under normoxic and hypoxic conditions is caused by the induction of senescence, but not apoptosis.

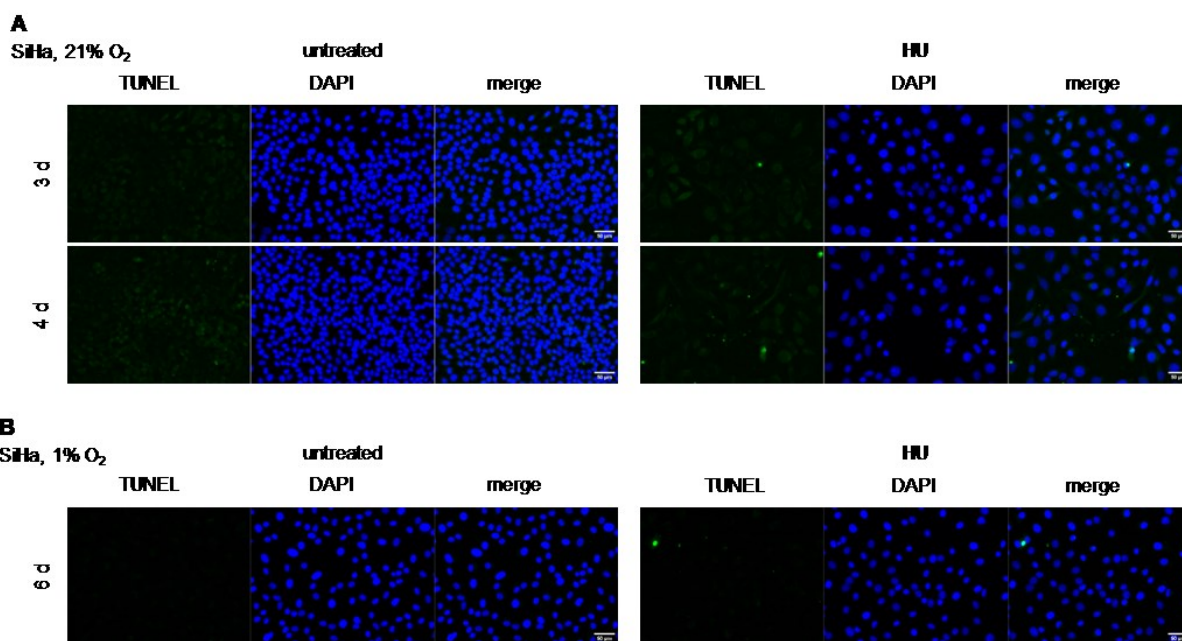


Figure 28: Apoptosis assays upon HU treatment. (A) SiHa cells were treated with 1 mM HU under normoxic conditions for 3 and 4 days and subjected to TUNEL assays (scale bar: 50 μ m). **(B)** SiHa cells were cultured at 1% O₂ for 24 h. Then 1 mM HU was added for another 6 days and cells were subjected to TUNEL assays (scale bar: 50 μ m).

Taken together, these results provide an indication that RR inhibition may be involved in CPX-induced senescence under normoxia. Both HU and CPX induce mTORC1-independent senescence. Furthermore, HU is a described RR inhibitor [180] and CPX as an iron chelator can also inhibit RR [147, 160]. However, experiments pinpointing the mechanism of senescence induction by CPX to reduced RR activity need to be performed in the future.

Preliminary experiments have been performed using shRNA to silence *RRM1*, *RRM2* and *RRM2B* (encoding for p53R2). No effects on senescence induction could be observed which, however, was explained by poor knockdown efficiencies. Furthermore, overexpression of *RRM2* did not prevent the CPX-induced senescence, as well as supplementing cells with deoxynucleosides or deoxynucleotides. Nonetheless, further work appears to be warranted, which could include a more efficient downregulation of RR subunits by the CRISPR/Cas technology or generation of an iron-independent RR in order to illuminate the role of RR as a potential target for mediating the pronounced pro-senescent and pro-apoptotic effects of CPX in HPV-positive cancer cells.

CHAPTER 3

DISCUSSION

3. Discussion

HPV-positive cancer cells are oncogene addicted meaning with respect to their malignant phenotype they rely on the constant expression of the two viral oncoproteins E6 and E7 [40]. Although E6/E7 are considered to be valuable targets for the treatment of HPV-positive cancers, therapeutic approaches directed against E6/E7 have not been promoted to the clinic, yet. Furthermore, since HPV-positive cancers reversibly shut down E6/E7 expression under hypoxic conditions, E6/E7 targeting therapies may only be effective in oxygenated areas where E6/E7 are expressed [39]. In addition, the hypoxic subregions of a tumour likely contribute to resistance towards radio- and chemotherapy [50] and may contain reservoir cells for tumour recurrence upon reoxygenation [39]. Thus, it is of great interest to find a therapy that is able to target both normoxic and hypoxic HPV-positive cancer cells.

In this dissertation iron chelators were studied on their potential to serve as prospective drugs against HPV-positive cancers. An emphasis was placed on the iron chelator CPX, since it originally has been developed as an antimycotic drug which can be applied topically on skin and mucosa. The study shows for the first time that iron chelators like CPX strongly inhibit E6/E7 expression. Moreover, CPX induces cellular senescence and apoptosis under normoxic conditions which both are desirable phenotypes for anti-cancer therapy. Importantly, CPX also exhibits growth inhibitory effects via the induction of apoptosis under hypoxic conditions. Since CPX is active under hypoxic conditions it may not only be promising as a single agent for cancer therapy but could also complement CT and RT which are usually less efficient under hypoxic conditions.

3.1 Repression of E6/E7 by iron chelators

All tested iron chelators (DFO and CPX) strongly reduce both *E6/E7* mRNA and E6/E7 proteins amounts. Hence, the repression of E6 and E7 could occur on several mechanistic levels, such as transcriptional control, mRNA stability, mRNA translation and/or protein stability.

E6 and E7 are transcribed from polycistronic mRNAs and transcription of *E6/E7* is controlled by cis-elements in the upstream regulatory region (URR) of the HPV genome. The URR harbours several known transcription factor binding sites (reviewed in [201]). Among these factors are some that have previously been associated with iron: AP-1 (activator protein-1) and NF-IL6 (nuclear factor for interleukin 6 expression, also known as C/EBP β , CCAAT/enhancer binding protein- β).

AP-1 was shown to increase its DNA binding activity upon treatment with DFO [202, 203]. It is a key activator of *E6/E7* transcription [204]. However, depending on the composition of the AP-1 complex, it can also act as a transcriptional repressor of HPV *E6/E7* [205]. The AP-1 complex is a dimer consisting of Jun (c-Jun, JunB, JunD) and Fos (c-Fos, FosB, Fra-1, Fra-2) proteins [206]. It was shown that an increase in c-Fos expression and the concomitant decrease in Fra-1 expression matches the progression of cervical lesions [207]. Furthermore, Fra-1 expression inversely correlates with malignancy of HPV-associated cervical carcinoma [208]. Treatment with an antioxidant can change the composition of the AP-1 complex which results in repression of HPV *E6/E7* [205]. In specific, c-Jun and JunB preferentially dimerise with Fra-1 instead of c-Fos upon treatment which results in the repression of HPV *E6/E7*. Further, it is known that Notch-1 expression in HPV-positive cells can also mediate the switch from c-Jun/c-Fos to c-Jun/Fra-1 [209] and, consequently, Notch-1 can repress HPV *E6/E7* transcription [210]. Interestingly, our proteome analyses have shown that Notch-1 expression is significantly elevated upon CPX treatment, suggesting that the repression of *E6/E7* may be regulated through alteration of the AP-1 complex to a repressive state. This possibility is currently under investigation.

NF-IL6 is a repressive transcription factor for HPV16 early gene expression [211]. Furthermore, its binding to the promoter of inducible nitric oxide synthase is increased upon DFO treatment [212]. Hence, repression of *E6/E7* transcription could also possibly be mediated by repressive binding of NF-IL6 to the URR which also warrants further investigation.

The reduction of *E6/E7* mRNA could also be caused by decreased mRNA stabilities. To this end, mRNA stability assays were performed by Anja Herrmann in HeLa cells [200]. It was shown that HPV18 *E6/E7* mRNA stability is not altered upon CPX treatment. Thus, the reduction of *E6/E7* mRNA upon iron deprivation is most likely caused by a lower transcription rate.

Translation of iron regulated genes can be mediated by the IRE/IRP system (see 1.9 and Figure 5). The repression of *E6/E7* was shown to be iron-dependent, since it could be observed upon treatment with different iron chelators and since it could be abrogated when CPX was complexed with iron prior to treatment. Hence, the question arises whether the *E6/E7* mRNA contains a 5' IRE similar to ferritin. However, the search for an IRE anywhere in the genome of HPV16 or HPV18 with the IRE search tool SIREs Web Server 2.0 [213] was negative, indicating that *E6/E7* expression might not be regulated by the IRE/IRP system.

Interestingly, E6 protein repression upon iron chelation in HeLa cells appears to occur earlier than E7 repression. Since the expression of E6 and E7 is regulated by alternative splicing and splicing can be affected e.g. by epidermal growth factor (EGF) [214], it might be possible that iron is involved in the switch from *E6* to *E7* transcripts. Another hypothesis is that E6 and E7 proteins exhibit different protein stabilities after CPX treatment. Experiments by Anja Herrmann demonstrate that CPX reduces the half-lives of 18E6 and 16E6 by a factor of two and three, respectively [200]. A reduction of the protein half-life could also be observed for 16E7 in SiHa but the protein stability of 18E7 in HeLa cells was not affected by CPX. Hence, the difference between E6 and E7 repression in HeLa cells could possibly be associated to the reduced protein stability of E6 but not E7, rendering E7 more stable than E7. The data also indicate that - besides downregulation of the mRNA - reduced protein stabilities contribute to the decrease of E6/E7 protein expression. The potential of CPX to affect protein stability is in line with a recent report describing that CPX can induce the proteasomal degradation of Cdc25A by a thus far uncharacterised mechanism [215].

Taken together it could be shown that iron chelators strongly repress HPV E6 and E7 expression. There are only two studies available which specifically investigate the effects of iron chelators on HPV-positive cancer cells *in vitro* [216] and *in vivo* [217]. Only one of them [216] assessed HPV oncogene expression, which, however, was restricted to the analysis of E6 expression only and showed no alteration upon DFO treatment. In view of the strong and robust E6/E7 repression which was detected in the present study in all investigated HPV-positive cancer cell lines, it can only be hypothesised that the exposure to DFO was not long enough to affect E6 expression in this previous report. Thus, the presented dissertation is the first study to reveal iron chelators as potent E6/E7 inhibitors. The repression likely occurs on several levels, including transcriptional repression and decreased protein stabilities.

3.2 Growth inhibition by CPX

Another major finding of this dissertation is that CPX exerts its growth inhibitory effects through different mechanisms. First, it induces cell cycle arrest in G1 and S phase leading to cellular senescence. Furthermore, after prolonged exposure to CPX, cells undergo apoptosis.

The observed capacity of CPX to inhibit proliferation and induce cell cycle arrest is corroborated by the finding that other iron chelators induce similar phenotypic effects in cells of other histological backgrounds (reviewed in [218]). Furthermore, the anti-proliferative effect of CPX in HPV-positive cells is supported by the previous finding that CPX can inhibit cell proliferation in HeLa cells [219]. The cell cycle analyses performed in the present

dissertation revealed that HeLa cells arrest in G1 phase after CPX treatment, which is supported by two other studies linking CPX-mediated growth inhibition to G1 arrest [220, 221]. The additional EdU incorporation assays performed in the present investigations further showed that cells also halt in the S phase, suggesting that CPX not only induces a G1 arrest, but also blocks S phase progression. Yoon et al. [222] performed BrdU assays (analogous to EdU) in Chang cells, which later were identified as HeLa cells. They demonstrated that DFO diminishes BrdU incorporation which corroborates our findings of CPX-induced decrease of EdU incorporation. Notably, the anti-proliferative properties of iron chelators observed *in vitro* are also detectable in experimental *in vivo* models (reviewed in [122]).

A possible mechanism why cells arrest and induce senescence upon CPX treatment is CPX-induced inhibition of RRM2, since RRM2 knockdown has previously been linked to senescence [163]. Since both HU and CPX induce senescence, the anti-proliferative effect of CPX could be mediated via RRM2-inhibition. RR activity is crucial for DNA synthesis during S phase. It is essential that the pool of dNTPs rises in S phase, since the nucleotides present in G1 phase only would be sufficient for the replication of a small fraction of the genome [223]. The expression of RRM2 is induced during S phase [224] in order to increase dNTP synthesis and satisfy the demand. Consequently, inhibition of RR with HU in mammalian cells decreases the pool of dNTPs. More specifically dATP, dCTP and dGTP are decreased while dTTP levels increase [225]. Hence, upon RR inhibition, DNA replication is limited by the pre-existing dNTPs from G1 phase. When the cell is depleted of dNTPs by HU, DNA synthesis can no longer be pursued and replication forks arrest which can eventually lead to DNA double strand breaks [226, 227]. DNA damage is sensed by a complex checkpoint cascade that includes ATM and ATR which eventually induce cell cycle arrest [228].

If CPX induces cell cycle arrest through the inhibition of RR, a decreased dNTP pool will be anticipated. To date it has not been investigated whether CPX diminishes the pool of dNTPs. However, other iron chelators were tested in one study [229], showing that roughly two-thirds of the tested iron chelators, among them DFO, reduce dATP levels and increase dTTP levels, which is similar to the findings for HU. Thus, it may be assumed that CPX as an iron chelator could also decrease dNTP levels. Consequences of dNTP depletion are (1) inhibition of DNA replication in S phase, (2) cell cycle arrest and (3) the introduction of DNA damage (discussed above). All these effects were found by this dissertation to be induced by CPX treatment in HPV-positive cancer cells. In specific, EdU incorporation assays indicate that replication is stalled, which is accompanied by a cell cycle arrest in G1 and S phase.

Furthermore, H2AX is phosphorylated indicating the induction of DNA damage response of HPV-positive cancer cells by CPX. This latter finding is corroborated by the response of other cell types towards CPX treatment [221] and was also observed for another iron chelator, mimosine, which activates the DNA damage response, as indicated by H2AX phosphorylation and CHK1 and CHK2 phosphorylation (downstream targets of ATR and ATM, respectively) [221]. Another link between CPX treatment and the induction of a DNA damage response is provided by a study which revealed that CPX exposure increases the phosphorylation of CHK1 as a response to active ATR signalling [230].

Collectively, these data suggest that CPX induces cell cycle arrest through the inhibition of DNA synthesis. Most likely, as a consequence of impaired replication, the DNA damage response pathway is activated which may be mediated via ATR and CHK1, and which eventually leads to cell cycle arrest.

Senescence is a response to a plethora of stressors, including replication stress and DNA damage [72]. It has been proposed that senescence can also be a consequence of oncogene-induced depletion of dNTPs levels which causes DNA damage and finally results in oncogene-induced senescence [231, 232]. Interestingly, oncogene-induced senescence could be prevented by the addition of exogenous nucleotides. Our results revealed that both CPX and DFO induce senescence. To investigate the hypothesis whether dNTP depletion is the cause for senescence induction by iron chelators, cells treated with CPX were supplemented with either deoxynucleosides or dNTPs. If CPX mediates senescence via RR inhibition and subsequent loss of dNTPs, restoration of dNTP levels will impede senescence induction. Restoration of dNTP levels can be achieved by the addition of dNTPs or deoxynucleosides, which can be converted to deoxynucleotides via scavenger pathways (reviewed in [233]). However, both approaches could not prevent senescence induction by CPX. Although intracellular dNTP levels were not measured, both deoxynucleosides and dNTPs appeared to reach the nucleus of the cells. EdU incorporation assays revealed that in the presence of deoxynucleosides or dNTPs, EdU is no longer incorporated. This latter finding suggests that both deoxynucleosides and dNTPs compete with EdU and hence are incorporated into the DNA rather than EdU due to the higher abundance in comparison to EdU. Furthermore, HU-induced senescence could also not be prevented by deoxynucleoside or dNTP supplementation. The obtained data suggest, that CPX- and HU-induced senescence might not be caused by dNTP depletion or that the addition of deoxynucleosides and dNTPs is not able to restore the dNTP pool to an extent that is sufficient to prevent senescence.

Interestingly, Aird et al. stated that the addition of exogenous nucleosides was only able to prevent oncogene-induced senescence, but not senescence induced by DNA damaging agents like etoposide and doxorubicin [232]. Hence, it alternatively could be speculated that CPX induces senescence as a consequence of DNA damage independent of the dNTP pool which thus cannot be prevented by the addition of nucleotides.

Nonetheless, the presented results demonstrate that senescence induction by CPX is iron-dependent, since it can be efficiently blocked by the addition of iron. As *E6/E7* repression by siRNA rapidly induces senescence [39] and CPX represses *E6/E7*, the most obvious explanation is that CPX induces senescence via the repression of *E6* and *E7*. Consistent with this, repression of *E6/E7* upon CPX treatment can also be prevented by the addition of iron. However, CPX also induces senescence in HPV-negative cells, indicating that the senescence induction by CPX can be independent of *E6/E7* repression. Intriguingly, these data also indicate that HPV-positive tumours may be more sensitive to CPX treatment, since CPX additionally represses *E6/E7* which is essential for the malignant phenotype of these cells.

A major pathway in senescence induction is the stimulation of p53 and its transcriptional target p21. Hence, p53 and p21 protein levels were investigated upon CPX treatment. Interestingly, after 48 h CPX exposure, leading to senescence, both p53 and p21 proteins are downregulated. The finding also argues against the possibility that CPX-induced senescence is primarily induced via *E6/E7* repression, since the senescence response in HPV-positive cancer cells is linked to the reconstitution of p53 and pRb [234, 235]. Moreover, the data suggests that p53 and p21 might not be relevant for CPX-induced senescence.

However, at earlier points of time (24 h) p21 expression is elevated. Furthermore, a drastic increase in the phosphorylation of serine 15 of p53 was observed which could increase p53-mediated activation of target genes [187] despite a reduction of total p53 levels. Serine 15 can be phosphorylated by ATM and ATR upon DNA damage [236, 237] and the phosphorylation prevents binding to and the degradation of phosphorylated p53 through MDM2 [186]. The expression of p21 is increased after 24 h, suggesting that the phosphorylation of serine 15 is sufficient to increase p21 transcription, although total p53 levels are not altered. However, the situation appears to be more complex, since in HeLa cells, p21 levels are decreased after 48 h and 72 h CPX treatment although P-p53 (Ser15) levels remain upregulated.

It might be possible, that the initial elevation of p21 after 24 h CPX treatment is sufficient to induce senescence, although p21 is downregulated at later points of time. It was shown that p21 expression correlates with the amount of DNA damage [238]. At sublethal doses of DNA damaging agents, expression is increased to arrest the cell cycle and allow DNA repair. Upon lethal doses, p21 is downregulated to allow apoptosis induction. Since both senescence and apoptosis induction was observed upon CPX treatment, depending on the duration, it may be possible that CPX mediates senescence and apoptosis through p21 induction. DNA damage-induced senescence can also be mediated by the p16-Rb pathway, also as a secondary pathway when p53/p21-mediated senescence induction failed [239]. Specifically, in the absence of p53, DNA damage leads to the induction of senescence through ROS-mediated p16 expression [240]. p16 can also be induced as a response to other stress stimuli which then involves the p38-MAPK pathway [241]. However, given the fact that p16 is overexpressed in HPV-positive cancer cells, but does not induce senescence, it is unlikely that CPX induces senescence through p16 in HPV-positive cancer cells.

Adding another level of complexity, several other pathways have been linked to CPX-induced cell cycle arrest and senescence. For instance repression of Wnt signalling is considered as a trigger for senescence induction in primary human cells which occurs independently of pRb and p53, but involves GSK3 β -mediated phosphorylation of histone chaperones [242]. CPX was shown to downregulate Wnt signalling as indicated by decreased expression of β -catenin [151] and Wnt target genes [243]. However, the proteome analyses performed in this dissertation revealed that β -catenin expression, a readout for canonical Wnt signalling, is not affected by CPX. Also gene set enrichment analyses remained inconclusive whether Wnt signalling is affected by CPX treatment. This issue could be further clarified in future studies, e.g. by performing luciferase reporter assays which can detect active Wnt signalling, such as the TOPflash/FOPflash [244] assay.

Another study links CPX-induced cell cycle arrest to the degradation of Cdc25A [230]. Cdc25A is a phosphatase involved in removing inhibitory phosphorylations from CDK4, CDK6, CDK2 and CDK1 [245-247] and hence regulates the transition from G1 to S and G2 to M phase. CPX induces phosphorylation and subsequent proteasomal degradation of Cdc25A, which then results in the accumulation of inhibitory phosphorylated G1-CDKs [230]. Consequently, CPX-treated cells arrest in G1 phase. Interestingly, degradation of Cdc25A upon CPX treatment is associated with the activation of ATR and CHK1 as a response to CPX-induced DNA damage [230], suggesting that it may be associated with RR

inhibition. Notably, expression of Cdc25A has also been linked to HPV E7. In reporter assays, expression of E7 induces the Cdc25A promoter [248, 249] whereas inhibition of E6/E7 represses the Cdc25A promoter in cervical cancer cells [250]. Thus, CPX-induced degradation of Cdc25A may additionally be enhanced by CPX-induced repression of E7 in HPV-positive cancer cells which downregulates Cdc25A expression.

Another candidate for contributing to CPX-induced cell cycle arrest is NDRG1 (N-Myc downstream regulated gene 1), since NDRG1 is upregulated upon treatment with CPX [150] or other iron chelators [251], and increased expression of NDRG1 induces cell cycle arrest [252]. Interestingly, the proteome analyses in SiHa cervical cancer cells performed in the present investigation also revealed that NDRG1 levels are elevated more than twofold upon CPX treatment. Notably, a previous study has reported that ectopic expression of NDRG1 in SiHa cells resulted in cell cycle arrest [253]. Thus, it will be highly interesting to further study the role of NDRG1 in the CPX-induced proliferation stop in HPV-positive cancer cells, an issue which is currently under investigation in the laboratory.

3.3 CPX induces mTORC1-independent senescence

Blagosklonny et al. described a model in which mTOR is indispensable for senescence induction [86]. In line with this model, treatment with the mTORC1 inhibitor rapamycin prevents the induction of an irreversible growth arrest [254]. More specifically, rapamycin renders cells competent to resume proliferation when the senescence-inducing stimulus is removed (reversible growth arrest). Despite the notion that mTOR signalling is essential for senescence induction, and despite the previous work of our lab showing that impairment of mTORC1 signalling is important for the evasion from senescence in HPV-positive cancer cells [39], the data obtained in the present investigations provide strong evidence that senescence can also be induced when mTORC1 signalling is inhibited.

Here, it is shown that CPX induces senescence in an mTORC1-independent manner since treatment with rapamycin does not prevent CPX-induced senescence. Actually, CPX itself also downregulates mTORC1 signalling in HPV-positive cells, a finding which is supported by the analyses of other cell models [153, 255]. The results of the present study indicate that the mTORC1 inhibition could occur via induction of REDD1 which inhibits mTORC1 through the TSC1/2 axis [197]. Since REDD1 is a direct target of HIF-1 α [256] the upregulation of REDD1 could be associated to the stabilisation of HIF-1 α which was shown to be upregulated upon CPX treatment (Figure 16). An additional mechanism by which CPX may mediate mTORC1 inhibition is AMPK, which is activated upon lack of ATP [257]. Since

CPX activates AMPK, and CPX-mediated mTORC1 inhibition can be prevented by inhibition of AMPK to some extent [255], CPX-induced mTORC1 inhibition could be a consequence of CPX-induced depletion of ATP levels. This notion is supported by the finding that iron chelators indeed reduce ATP levels [229].

Interestingly, CPX was reported to induce phosphorylation of AKT at serine 473 [153] - a target of mTORC2 signalling [258] - implicating that CPX activates the mTORC2 signalling pathway, possibly through the relief of the negative-feedback loop upon mTORC1 inhibition [153]. Preliminary data of our lab suggest that CPX slightly induces AKT phosphorylation at serine 473 in HPV-positive cells, supporting that notion. Indeed, mTORC2 has been linked to senescence induction, e.g. in endothelial cells where senescence was shown to be mediated via mTORC2 and could be inhibited by knockdown of *RICTOR* (a specific component of mTORC2) or treatment with an AKT inhibitor [259]. Consequently, CPX may also contribute to senescence induction in HPV-positive cancer cells via mTORC2 activation. In line with this finding are preliminary results in our laboratory, showing that KU-0063794 - which blocks both mTORC1 and mTORC2 [260] - inhibited CPX-induced AKT Ser473 phosphorylation and partially prevented CPX-induced senescence. To investigate the question whether mTORC2 is necessary for CPX-induced senescence in more detail, further studies on the involvement of mTORC1 and mTORC2 are warranted, including the application of specific inhibitors of mTORC1/2 or knockdowns of specific mTORC1 and mTORC2 components such as *RAPTOR* and *RICTOR*, respectively.

mTORC2 signalling is intact under hypoxic conditions as indicated by phosphorylation of AKT at serine 473 ([261-263] and Bossler et al., submitted for publication). It would be conceivable that if CPX mediates senescence via active mTORC2, senescence will also be induced under hypoxic conditions. However, no obvious increase in senescent cells could be observed upon CPX-treatment at 1% oxygen in comparison to EtOH-treated cells. The data indicate that besides mTORC2 additional mechanisms may be involved in CPX-mediated senescence which are impaired under hypoxic conditions. Comparative studies of signalling pathways that are associated with senescence but differentially regulated under normoxic and hypoxic conditions could give insights in the underlying mechanism of CPX-induced senescence which occurs under normoxic conditions but not under hypoxia.

In this context, it is noteworthy that although both HU and CPX induce mTORC1-independent senescence under normoxia, only HU is able to induce senescence also under hypoxic conditions. It would be of great interest to elucidate the pathway involved in

HU-induced senescence under hypoxia and to investigate whether this pathway is altered upon CPX treatment.

The finding that CPX induces mTORC1-independent senescence may have important implications for using it as an anti-cancer drug. Many therapies like RT and CT exert their anti-tumourigenic effects by inducing senescence. However, induction of senescence is accompanied by the establishment of a SASP in fibroblasts in the tumour (micro)environment which can promote tumour growth, invasion, migration and metastasis (reviewed in [264]). Importantly, mTORC1 signalling is responsible for the establishment of this pro-tumourigenic SASP, since it can be counteracted by rapamycin treatment [90]. In specific, the cited study shows that fibroblasts that were induced to senesce by irradiation promote tumour growth *in vitro* through secretion of pro-inflammatory SASP factors. Moreover, these fibroblasts also promoted tumour growth in xenografts, which could be substantially reduced by the treatment with rapamycin. The fact that CPX not only induces senescence but also inhibits mTORC1 suggests that CPX may have the advantage over other senescence-inducing therapies that it prevents the (mTORC1-dependent) pro-tumourigenic SASP. It thus will be of great interest to investigate the composition and biological activities of the CPX-induced SASP and to compare it with, for example, the irradiation-induced SASP. These studies would include comparative measurements of expression and secretion of typical SASP factors like IL-1a/b, IL-6 and IL-8 among others (a list of SASP factors can be found in [264]) and analyses of the biological effects of the SASP on the phenotype of HPV-positive cancer cells (e.g. by co-culture with senescent fibroblasts or by treatment with conditioned medium). If these studies reveal that CPX induces a more favourable SASP than other senescence-inducing therapies, CPX could be a very potent anti-tumour drug, not only as a monotherapy, but also in combinatorial treatments for example with RT and CT.

3.4 Apoptosis induction by CPX

Besides cell cycle inhibition and induction of senescence, CPX exerts anti-tumourigenic effects by the induction of apoptosis. The presented data indicate, that the cell death of HPV-positive cancer cells upon CPX treatment is mediated by apoptosis, since several hallmarks of apoptosis were observed: (1) caspase 3/7 is activated, (2) PARP cleavage occurs, (3) cells stain positive for Annexin V and PI and (4) cells stain positive for TUNEL. The general potential of CPX to induce apoptosis is further corroborated by several studies *in vitro* (selection: [265-268]) and *in vivo* [149, 269]. As a possible mechanism, CPX was shown to downregulate the anti-apoptotic proteins BCL-XL and survivin [149], which results in the

release of cytochrome c from the mitochondria and activation of the caspase cascade which initiates apoptosis. The results obtained in this dissertation also indicate that activation of the caspase cascade is involved in CPX-induced apoptosis, since caspase 3 and caspase 7 are activated upon CPX treatment (Figure 18C) and PARP cleavage occurs (Figure 19). To further corroborate the involvement of caspases in CPX-induced apoptosis it would be worthwhile to treat cells with CPX in the presence of the pan-caspase inhibitor z-VAD-FMK. Indeed, z-VAD-FMK is able to partially prevent CPX-induced apoptosis in human rhabdomyosarcoma cells [149].

However, since z-VAD-FMK could not completely abrogate apoptosis upon CPX treatment [149] it is possible that CPX mediates cell death also via additional, caspase-independent pathways. A possible scenario of cell death without the involvement of caspases is mitochondrial dysfunction, resulting in the loss of the mitochondrial transmembrane potential and the release of cytochrome c and components of the respiratory chain [270]. The effect of iron chelators on mitochondria is complex. On the one hand, CPX can prevent the depolarisation of the mitochondrial membrane upon H₂O₂ treatment [271]; most likely through the anti-oxidative properties of CPX [272]. On the other hand, DFO downregulates components of the iron-sulphur clusters of the respiratory chain and thereby inhibits complex II activity [273]. The proteome analyses performed in the present dissertation support the notion that CPX inhibits the respiratory chain complexes since gene sets of oxidative phosphorylation were negatively enriched by CPX treatment. It is further corroborated by the finding that CPX can induce a collapse of the mitochondrial membrane potential [274].

Mechanistically, CPX-mediated apoptosis might also be supported by the inhibition of the deoxyhypusine hydroxylase (DOHH). Several studies show that CPX can inhibit this iron-dependent enzyme and, subsequently, the maturation of the eukaryotic translation initiation factor eIF5A which is hypusinated by DOHH [148, 219, 275]. Unhypusinated eIF5A1 is a trigger for the induction of mitochondrial apoptosis in HeLa S3 cells and overexpression of (unhypusinated) eIF5A1 results in the loss of mitochondrial transmembrane potential, release of cytochrome c and caspase activation [276]. Consistently, Hanauske-Abel et al. have linked apoptosis induction by CPX to the inhibition of eIF5A1 hydroxylation [274]. They furthermore state that apoptosis induction by CPX is independent of p53 since it can also be observed in HPV-positive cells. The latter statement certainly is an overinterpretation of their data, since p53 is still detectable in HPV-positive cells. Yet, the present dissertation provides experimental evidence that CPX-induced apoptosis in HeLa cells

can occur independent of p53 since HeLa “p53 null” cells also undergo apoptosis upon CPX treatment, although the process is delayed. p53-independent apoptosis by CPX could furthermore be shown in HCT116 cells. The observation that the lack of p21 in HCT116 cells (expressing wildtype p53) actually renders these cells more vulnerable to the pro-apoptotic effects of CPX treatment is consistent with the notion that p21 is considered to be an inhibitor of p53-dependent apoptosis [277].

An interesting study was performed by Baar et al. [278] who demonstrated that senescent cells can be forced to undergo apoptosis. Usually, senescent cells are considered to be protected from apoptosis [279]. Baar et al. proposed a model where senescent cells are protected from apoptosis by the expression of FOXO4 which sequesters p53 [278]. Inhibition of FOXO4 results in the release of p53 from the nucleus and selectively induces apoptosis of senescent cells. CPX induces senescence after 48 h treatment (and release in CPX-free medium) but also apoptosis upon prolonged CPX treatment in HPV-positive cancer cells. Furthermore, in preliminary experiments it could be observed that CPX is able to induce apoptosis in irradiated, senescent fibroblasts. Hence, it is conceivable that CPX interferes with an anti-apoptotic pathway in senescent cells and thereby induces apoptosis in senescent cells. Likely, however, this does not involve FOXO4, since preliminary experiments indicate that FOXO4 silencing did not affect CPX-induced apoptosis in HPV-positive cells (not shown).

In contrast to senescence, apoptosis induction upon CPX treatment can also be observed under hypoxic conditions. To investigate whether apoptosis induction of CPX might be mediated via RR inhibition, apoptosis was measured upon treatment with the RR inhibitor HU. Although some studies demonstrate the apoptosis-inducing effect of HU [280-283], it was not observed in SiHa cells, suggesting that CPX-induced apoptosis might not be linked to RR inhibition.

Apoptosis as a consequence of hypoxia can be caused by inhibition of the electron transport chain of the mitochondria which leads to the decrease of the mitochondrial membrane potential, lack of ATP, activation of BAX/BAK and the release of cytochrome c [284]. Since CPX might inhibit the iron-sulphur clusters as observed for DFO [273] it is possible that CPX-mediated apoptosis under hypoxic conditions is mediated by targeting the mitochondria. Interestingly, the addition of glucose which maintains ATP levels under hypoxia was sufficient to prevent hypoxia-induced apoptosis, suggesting that not hypoxia *per se*, but the lack of ATP upon hypoxia triggers apoptosis [285]. Similar observations were made with CPX treatment. When cells under normoxia were cultured with excess glucose - for instance

in high glucose medium (25 mM instead of 5.5 mM), at low densities or with excess medium - CPX-induced apoptosis was remarkably delayed, suggesting that CPX-induced apoptosis could also be mediated by the depletion of ATP.

Another possible mechanism involves ROS, which are elevated under hypoxic conditions [54]. Apoptosis under hypoxic conditions is mediated by the activation of caspase 9 in a ROS-dependent manner [286]. In the presence of the radical scavenger N-acetylcysteine (NAC), hypoxia-induced elevation of ROS and apoptosis can be prevented. The effect of CPX on ROS levels is controversially debated.

Finally, apoptosis under hypoxic conditions can also be mediated via HIF-1 α , which can induce the expression of pro-apoptotic proteins of the BCL-2 family [287] or stabilise p53 [288] under hypoxic conditions. Since CPX induces HIF-1 α expression under normoxic conditions it is possible that apoptosis-induction by CPX is mediated by the upregulation of HIF-1 α .

Taken together, CPX is capable of inducing apoptosis independent of oxygen levels. Many therapies, such as radio- and chemotherapy, are more efficient in oxygenated than in hypoxic tumour regions. Hence, CPX could be used to complement RT and CT.

3.5 CPX cooperates with RT and CT

Depending on stage, cervical cancer is usually treated with surgery and/or radiotherapy, either alone or in combination with chemotherapy as radiochemotherapy (American Cancer Society). The rationale behind combining RT and CT is that the effects of both therapies can synergise and enhance the efficacy in comparison to either treatment alone. Furthermore, doses can be reduced which decreases toxicities and side effects. RR inhibitors have been described to sensitise cells to RT and CT. For instance the RR inhibitor gemcitabine synergises with etoposide *in vitro* [289]. Furthermore, HU treatment in combination with RT achieved almost 90% response (partial or complete) in cervical cancer patients in comparison to 65% upon RT monotherapy [290]. Since iron chelators can also inhibit RR, it is coherent that iron chelators synergise with RT and CT. Indeed, the iron chelator 3-AP is described to sensitise cervical cancer cells to RT [291], most likely through RR inhibition-mediated impairment of the DNA damage response [292].

The present data indicate that CPX also cooperates with RT and CT, since it sensitises cervical cancer cells to RT as well as etoposide- or CDDP-based CT. The conclusion is supported by a study in leukaemia cells, showing that CPX synergises with cytarabine and has

additive effects with daunorubicin [147]. The cooperative effect of CPX with RT and CT could be particularly pronounced in HPV-positive cancer cells, since CPX also represses E6/E7 which has been described to synergise with CDDP treatment [293, 294].

3.6 Clinical implications

The systemic application of iron chelators reduces serum iron levels and is hence associated with side effects including liver damage [139]. Topical application of CPX only locally depletes cells of iron and does not cause systemic toxicities. It is important to note that the CPX concentrations tested in this study (10 μM or less) can be achieved in the human skin. Kellner et al. show that application of 1% CPX cream on human cadaver skin results in concentrations in the millimolar range in the outermost layer of the skin [159]. CPX concentrations decrease with penetration depth, but at a depth of 2 cm concentrations above 7 μM could still be detected [159]. *In vivo* studies of healthy volunteers show that upon topical treatment with 1% CPX cream, concentrations between 340 μM and 8 μM could be achieved in the stratum corneum, depending on treatment duration and depth of the skin layer analysed [295].

Nonetheless, it would also be possible to administer CPX orally, since the concentrations used in this dissertation can also be achieved by oral gavage of CPX without reaching dose-limiting toxicities. For example, in humans up to 2 μM CPX could be reached as serum concentrations [157], which were shown by this dissertation to also inhibit tumour growth in 2D cell culture.

It should furthermore be noted that due to its widespread use as an antimycotic drug, the safety profile of CPX has extensively been studied. Topical administration to skin or vagina is devoid of systemic toxicities and mild local reactions only occur in less than 5% of the treated patients [141]. Hence, severe side effects of CPX as a topical anti-cancer agent are very unlikely.

A major problem of anti-cancer therapeutics is that cancer cells can develop several resistance mechanisms to evade therapy, including drug inactivation or efflux, alterations of drug targets and the inhibition of cell death [296]. However, since iron is essential for a plethora of biological processes, it is very unlikely that resistance mechanisms against iron chelators develop. The finding that it was impossible to generate CPX-resistant HeLa or SiHa cells support that notion. It is further corroborated by the fact that not a single case of CPX-resistant fungi has been reported yet, although CPX has been used as an antimycotic

agent for more than 20 years [141]. Moreover, several attempts to induce CPX-resistance in fungi failed [297, 298].

Taken together, due to the high safety profile of CPX as a topical agent and the fact that resistance against CPX is not anticipated, CPX could serve as an agent to treat cancers that are located at the skin and mucosa. Furthermore, it seems possible that the concentrations which can be achieved with already existing formulations are sufficient to exhibit anti-tumourigenic effects.

3.7 Conclusions

Collectively, the data reveal that iron chelators are strong repressors of the HPV *E6* and *E7* oncogenes. Downregulation of the viral oncogenes is detectable both at the protein and mRNA levels. Moreover, CPX treatment induces senescence in HPV-positive cancer cells. Both viral oncogene repression and induction of senescence is caused by the depletion of iron through CPX, since it can be abrogated by the supplementation of iron. Importantly, CPX exhibits anti-tumourigenic effects under both normoxic and hypoxic conditions (Figure 29). Under normoxic conditions, CPX induces not only senescence but also apoptosis after prolonged treatment. In addition, CPX can also induce apoptosis under hypoxic conditions. Thus, CPX may not only be an interesting drug for the treatment of HPV-positive cancers as a monotherapy, but also in combination with CT and RT. Xenograft studies are planned to further strengthen the encouraging *in vitro* results.

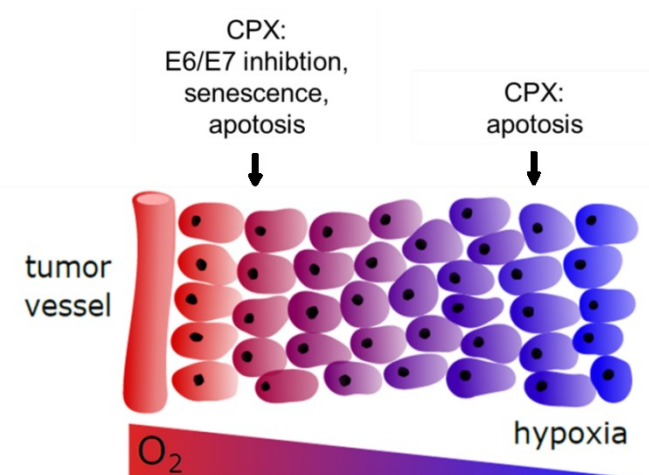


Figure 29: Anti-tumourigenic effects of CPX. Under normoxic conditions, CPX strongly represses E6/E7, induces senescence and apoptosis. Under hypoxia the anti-tumourigenic effects are mediated by the induction of apoptosis. Image modified from [40].

Taken together, CPX strongly represses HPV E6/E7, exhibits pronounced anti-tumourigenic effects under normoxic and hypoxic conditions and cooperates with CT/RT. Together with the fact that CPX can be applied topically and with its excellent safety profile, CPX appears to be a very promising candidate for the treatment of HPV-positive cervical (pre)neoplasias.

CHAPTER 4

MATERIAL AND METHODS

4. Material and Methods

4.1 Buffers and solutions

If not stated otherwise all buffers and solutions were prepared with water.

CSK-1 lysis buffer

10 mM PIPES (pH 6.8)

300 mM NaCl

1 mM EDTA

300 mM sucrose

1 mM MgCl₂

0.5% Triton X-100

100 µl PhosSTOP phosphatase inhibitor cocktail (Roche Diagnostics, Switzerland), 25 µl Pefablock (Merck, Germany) and 10 µl P8340 protease inhibitor cocktail (Sigma-Aldrich, USA) were added to 900 µl CSK-1 lysis buffer before use.

4x loading buffer (reducing)

8% SDS

250 mM Tris-HCl (pH 6.8)

20% β-mercaptoethanol

40% glycerol

PBS

137 mM NaCl

2.7 mM KCl

4.3 mM Na₂HPO₄

1.4 mM KH₂PO₄ (pH 7.4)

PBS/T

0.2% Tween®20

in PBS

Senescence assay buffer

40 mM citric acid

150 mM NaCl

2 mM MgCl₂

adjusted to pH 6.0 with Na₂HPO₄

5 mM $K_3[Fe(CN)_6]$, 5 mM $K_4[Fe(CN)_6]$ and 1 mg/ml X-gal in DMF were added freshly before use.

Senescence assay fixation buffer

2% PFA

0.2% glutaraldehyde

in PBS

Towbin transfer buffer pH 8.3

2.5 mM Tris

192 mM glycerol

20% methanol

Tris-Glycine running buffer

2.5 mM Tris (pH 8.6)

19.2 mM glycine

0.1% SDS

Colony Formation Assay (CFA) buffer

12 mM crystal violet

29 mM NaCl

3.7% PFA

22% EtOH

4.2 Chemicals

All chemicals were molecular biology grade where possible. All standard reagents for buffers and media were supplied by AppliChem (Germany), Applied Biosystems (USA), BD Biosciences (Germany), BioRad (USA), Carl Roth GmbH (Germany), Enzo Life Science (Germany), Fisher Scientific (USA), GE Healthcare (United Kingdom), Gerbu (Germany), Gibco (USA), Invitrogen (USA), Merck (Germany), Promega (USA), Roche Diagnostics (Switzerland), Saliter (Germany), Serva (Germany) and Sigma-Aldrich (USA). Manufacturers of specific reagents are named in the text.

4.3 Cell-based assays

4.3.1. Cell culture

HeLa and SiHa are HPV18 and HPV16- positive cervical cancer cell lines, respectively. HCT116 is a human colon carcinoma line. Cells were cultivated in media according to

Table 1, supplemented with 10% FCS, 100 U/ml penicillin, 100 µg/ml streptomycin and 2 mM L-glutamine. Standard cultivation of cells was performed at 37 °C, 5% CO₂ in a humidified incubator at 21% O₂ (normoxia). For experiments under hypoxic conditions (1% O₂, 5% CO₂), cells were transferred into a hypoxic chamber (InvivoO₂ 400 physiological oxygen workstation, Ruskin Technology Ltd, United Kingdom). For passaging, cells were washed with PBS, detached with 0.25% trypsin and resuspended in fresh medium. Cells were split twice a week.

Table 1: Cell lines and corresponding media and supplements (where applicable)

Cells	medium	supplements
HeLa	DMEM	
SiHa	DMEM	
HeLa “p53 null”	DMEM	700 µg/ml G418
HeLa mCherry H2B	DMEM	1 µg/ml puromycin
SiHa mCherry H2B	DMEM	1 µg/ml puromycin
HCT116	McCoy's	
HCT116 p53 ^{-/-}	McCoy's	
HCT116 p21 ^{-/-}	McCoy's	

In order to assess cell growth via the measurement of cell numbers, HeLa and SiHa cells were transduced with the pMOWS hH2B mCherry expression vector which fluorescently labels the cell nuclei red. The generated cell lines were called HeLa mCherry H2B and SiHa mCherry H2B. Transduction was kindly performed by Dr. Joschka Willemsen (Lab of Dr. Binder, DKFZ Heidelberg). HeLa “p53 null” cells were previously described by Hengstermann et al [189]. This cell line stably expresses a pSUPER-p53 vector encoding shRNA targeting *TP53* and thereby stably repressing p53. HCT116 p53^{-/-} and HCT116 p21^{-/-} were generated by the lab of Vogelstein [192, 193].

For experiments, cells were counted using trypan blue and CountessTM Automated Cell Counter (Invitrogen, USA) and seeded at the cell numbers given in Table 2 if not stated otherwise. 3 ml medium was used for 6 cm dishes and 100 µl/well for 96-well plates. For experiments performed under normoxic conditions, the medium was replaced with fresh medium before treatment. For experiments under hypoxic conditions, medium was replaced before the dishes were put in the hypoxic chamber. After the pre-incubation at 1% O₂ for 24 h, drugs were added directly to the medium.

Table 2: Cell numbers seeded for experiments

	6 cm dish	96-well plate (per well)
HeLa	5.5x10 ⁵	
SiHa	4x10 ⁵	
HeLa "p53 null"	4x10 ⁵	3000
HeLa mCherry H2B		4500
SiHa mCherry H2B		3000
HCT116		6000
HCT116 p53 ^{-/-}		6000
HCT116 p21 ^{-/-}		6000

4.3.1. Cryopreservation and thawing of cells

For cryopreservation, cells were trypsinised, pelleted by centrifugation (3 min, 800 x g) and resuspended in appropriate medium containing 30% FCS and 10% DMSO. Aliquots were transferred into an iso-propanol filled freezing container (Nalgene, Thermo Fisher Scientific, USA) and frozen at -80 °C. For long-term storage, cells were transferred to liquid nitrogen. For thawing, cells were rapidly warmed to 37 °C in a water bath, resuspended in pre-warmed medium and transferred into a new cell culture flask. Medium was changed 24 h later.

4.3.2. Treatment of cells

Drugs were prepared as stock solutions and diluted to final concentrations as indicated for each individual experiment. Some drugs were prepared freshly before treatment. For solvents and concentrations of stock solutions see Table 3.

Table 3: Compounds used

compound	manufacturer	stock solution	solvent	Remark
DFO	Sigma-Aldrich, USA	100 mM	water	prepared freshly
CPX	Sigma-Aldrich, USA	100 mM	EtOH	prepared freshly
etoposide	Enzo Life Science, Germany	5 mM	DMSO	stored at -20 °C
rapamycin	AdipoGen, USA	50 µM	DMSO	stored at -20 °C
CDDP	Merck, Germany	3.3 mM	0.9% NaCl	stored at RT
FAC	Sigma-Aldrich, USA	100 mM	water	prepared freshly
FeSO ₄	Sigma-Aldrich, USA	100 mM	water	prepared freshly
ZnSO ₄	Sigma-Aldrich, USA	100 mM	water	stored at 4 °C
ZnCl ₂	Sigma-Aldrich, USA	100 mM	water	stored at 4 °C

4.3.3. Irradiation of cells

Cell were seeded in 6 cm dishes and irradiated in a Gammacell® 40 Exactor Low Dose Rate Research Irradiator (Best Theratronics) with a Caesium-137 source at a constant rate of 0.933 Gy/min. To ensure the hypoxic environment, cells were transported from the hypoxia station to the irradiator in airtight boxes (Lock&Lock, South Korea).

4.3.4. Transfection of pSUPER constructs

HeLa cells were transfected using the calcium phosphate coprecipitation technique according to Chen and Okayama [299]. In short 6 µg of plasmid DNA was mixed with 150 µl 0.25 M CaCl₂ and 150 µl 2x BES buffer (50 mM BES, 280 mM NaCl, 1.5 mM Na₂HPO₄, pH 6.95). After 20 min incubation at RT the transfection mix was added dropwise to the cells and the cells were incubated at 35 °C and 3% CO₂ for 16-18 h. Then, cells were washed with PBS and fresh medium was added. In case of cell treatment, compounds were added approximately 4 h after medium change. The pSUPER constructs in Table 4 were used. The pSUPER plasmid served as empty vector (EV) control. For HIF-1α knockdown, 3 µg of each respective shRNA were used.

Table 4: pSUPER constructs

construct	target sequence (5'→ 3')
pSUPERshcontr-1	CAGUCGCGUUUGCGACUGG
pSUPERshHIF-1α-1	CUAACUGGACACAGUGUGU
psUPERshHIF-1α-2	CUGAUGACCAGCAACUUGA

4.3.5. Senescence Assay

This assay was described by Dimri et al. [184]. In senescent cells a β-galactosidase activity can be detected at pH 6. The so-called senescence-associated β-galactosidase (SA-β-gal) has a distinct enzymatic activity from the acidic β-galactosidase which is expressed in all cells and detectable at pH 4. SA-β-gal can be detected using the chromogenic substrate X-gal which results in blue staining of senescent cells. After treatment with drugs, cells were usually split at the ratio 1:2, 1:5 and 1:10 in 6 cm dishes in medium without drugs and cultivated under normoxic conditions. After 3-7 days, cells were washed with PBS, fixed with senescence assay fixation buffer for 3 min, washed and stained with senescence assay buffer. After 16-24 h of incubation at 37 °C, the senescence assay buffer was replaced by PBS and cells were stored at 4 °C until further analyses at the microscope. The used microscope is EVOSxl Core Cell Imaging System from Life Technologies (USA). Images with 20x magnification were acquired. Splits are indicated in the figures. Times between splitting and fixation are indicated in the figure legends.

4.3.6. Colony formation assay (CFA)

Similar as for the senescence assay, cells were split after treatment usually at ratios of 1:100 and 1:200, and incubated in drug-free medium under normoxic conditions. After colonies have formed (between 10 and 13 days after splitting, indicated in the figure legends), cells

were fixed and stained with CFA buffer for 5 min. After washing with water and drying at 37° C, dishes were scanned with Epson Perfection 4990 Photo scanner (Epson, Japan).

4.3.7. Cell cycle analysis

After treatment, cells were washed with PBS and trypsinised. To also include cells that have detached from the dish, both medium and wash were collected and joined with the harvested cells. After centrifugation (5 min, 100 x g) cells were resuspended in 300 µl cold PBS (in a 2 ml Eppendorf tube), 900 µl ice-cold 100% EtOH was added and cells were immediately vortexed. After incubation at 4 °C overnight, cells were pelleted, resuspended in 925 µl cold PBS and stained with 25 µl of 1 mg/ml PI (final concentration 25 µg/ml). 50 µl of 10 mg/ml RNase (final concentration 500 µg/ml) was added to degrade RNA. After incubation for 30 min at RT in the dark, cell cycle distribution could be analysed by flow cytometry at the BD LSR Fortessa (BD, Germany) with the BD FACS Diva Software version v8.0.1. Detectors were used according to Table 5. Analyses and image generation was done with FlowJo version 10. The Dean-Jett-Fox model was used for the distribution and quantification of the cells in G0/G1, S and G2/M phase.

Table 5: Detectors used at BD LSR Fortessa

Fluorochrome	detector	dichroic filter	bandpass filter
PI	D	600 LP	310/20
Eterneon-Red 645 Azide (EdU)	C	-	670/14
FITC (Annexin V)	B	505 LP	530/30

4.3.1. EdU assay

Two hours prior to harvesting, 10 µM EdU was added to the cells. Harvesting, fixation and staining was performed with the EdU-Flow cytometry 647 Kit from baseclick (Germany) according to the manufacturer's protocol. In short, cells were trypsinised and pelleted via centrifugation at 100 x g for 5 min at 4 °C. Cells were resuspended in 300 µl PBS (in a 2 ml Eppendorf tube) and 900 µl ice-cold 100% EtOH was added. The tubes were vortexed immediately. After incubation overnight or up to one week at -20 °C, cells were washed with 3 ml PBS, pelleted and resuspended in 100 µl 1x saponin-based permeabilisation and wash buffer in PBS. Then, 500 µl click assay cocktail was added and incubated for 30 min at RT in the dark. After washing two times with 1.3 ml saponin-based permeabilisation and wash buffer the cells were resuspended in 925 µl PBS and 25 µl of 1 mg/ml PI was added (final concentration 25 µg/ml). 50 µl of 10 mg/ml RNase was also added (final concentration: 500 µg/ml) and cells were incubated for 30 min at RT in the dark. Then, cells were filtered through gauze into FACS tubes and analysed at the BD LSR Fortessa (BD, Germany) with

the BD FACS Diva Software version v8.0.1. Analyses and image generation was done with FlowJo version 10. Detectors were used according to Table 5.

4.3.1. Proliferation assay

For real-time analysis of cell proliferation cells were seeded in 96-well plates and analysed with the IncuCyte® system. Usually, 4 images per well were acquired every 3-4 hours at a magnification of 10x. Analysis was performed with the IncuCyte® S3 2018A software.

4.3.2. Caspase-3/7 assay

Cells were seeded in a 96-well plate. 24 h (HeLa) or 48 h (HCT116) after seeding, medium was replaced with medium containing 5 µM IncuCyte® Caspase-3/7 Green Reagents for Apoptosis (Sartorius, Germany) and the drugs of interest. Images were taken every 3 h at the IncuCyte® for approximately 7 days. The Caspase-3/7 Green Reagent couples a recognition motif for activated caspase-3/7 to a DNA intercalating dye. The non-fluorescent substrate can be cleaved by activated caspase 3/7 and subsequently releases a fluorescent dye that can bind to the DNA. Thus, apoptotic cells emit green fluorescence.

4.3.3. TUNEL assay

During apoptosis, DNA double strands are cleaved by endonucleases. The 3'-hydroxyl termini that are exposed after cleavage can be detected using the terminal deoxynucleotidyl transferase dUTPS nick end labelling (TUNEL) assay. Cells were seeded in 6 cm dishes containing glass coverslips. At the given points of time, coverslips were removed from the dish and fixed in 4% PFA in PBS for 30 min at RT. After washing with PBS coverslips could be stored in 70% EtOH at -20 °C for several weeks. Usually coverslips from all points of time were gathered and stained together. For staining, coverslips were washed with PBS, permeabilised in 0.1% Triton, 0.1% sodium citrate in PBS for 2 min at 4 °C. Then cells were washed twice with PBS and stained with the in situ cell death detection kit, fluorescein (Roche, Germany). Cells were incubated with 25 µl TUNEL solution (mix: enzyme solution:label solution = 1:10) for 1 h at 37 °C in a humidified chamber. Then, cells were washed with PBS (2x 10 min) and incubated with DAPI (1 µg/ml, Roche, Germany) for 5 min in the dark. After washing with PBS (2x 10 min) the coverslips were dipped into water, then 100% EtOH and air-dried. The coverslips were then mounted with Vectashield (Vector Laboratories Inc., USA) onto microscope slides. Representative images are shown in the Figures. Images were acquired using the motorised inverted Zeiss Cell Observer with LED module Colibri.2 470 nm for excitation and the 20x / 0.4 LD PlnN Ph2 DICII objective.

4.3.4. γ -H2AX staining

Cells were grown on glass coverslips in 6 cm dishes and removed from the dish at the given points of time. Cells were fixed in 4% PFA for 5 min at RT and washed with PBS. Fixed cells could be stored in PBS at 4 °C for a couple of days. For staining, cells were permeabilised with 0.1% Triton X-100 in PBS for 5 min at RT. Cells were washed and subsequently blocked in 5% BSA in PBS containing 0.1% Triton X-100 and 0.3 M glycine for 20 min at RT. Then cells were incubated with mouse anti- γ H2AX-antibody (P-Ser139 H2AX No. 05-636 from Millipore, Germany) in 3% BSA, 0.1% Triton X-100 in PBS at a dilution of 1:100 for 1 h at RT in a humidified chamber. After washing four times with PBS, cells were incubated with anti-mouse Cy3 (dilution: 1:400, donkey α -mouse, Cy3-conjugate from Pierce Antibodies) and DAPI (1 μ g/ml) in PBS for 1 h at RT in a humidified chamber. Cells were then washed five times with PBS and mounted with Vectashield onto microscope slides. Images were acquired using the motorised inverted Zeiss Cell Observer with LED module Colibri.2 555 nm for excitation and the 40x / 0.75 EC PlnN Ph2 objective.

4.3.5. Annexin V apoptosis detection

Both cell culture supernatant and PBS wash were collected to include cells that have detached from the dish and joined with the trypsinised cells. After centrifugation (136 x g for 5 min at 4 °C) staining was performed using the FITC Annexin V Apoptosis detection Kit I from BD Pharmingen (USA) according to the manufacturer's protocol with slight changes. In short, after washing two times with ice-cold PBS, cells were counted and resuspended in 1x Annexin Binding Buffer to reach a concentration of approximately 2×10^6 cells/ml. Then 100 μ l (= 2×10^5 cells) were transferred into a new tube and 5 μ l FITC Annexin V and 5 μ l PI were added. After incubation for 15 min at RT in the dark, 400 μ l 1x Annexin Binding buffer was added, cells were filtered through gauze and analysed at the BD LSR Fortessa (BD, Germany) with the BD FACS Diva Software version v8.0.1. Analyses and image generation was done with FlowJo version 10. PI single stained cells and Annexin V single stained cells were used for compensation. Detectors were used according to Table 5.

4.3.6. Generation of spheroids

3D cell spheroids more closely mimic the heterogeneity of a tumour since cells in the outer layer of the spheroid have access to nutrients and oxygen, whereas in the core of the spheroid waste accumulates and (depending on the size of the spheroid) a hypoxic region forms. To generate spheroids 5000 HeLa or SiHa cells were cultivated in 200 μ l medium in 96-well low attachment U-bottom plates for suspension cells. To further inhibit the cells from attaching to

the plastic, the medium was supplemented with 30% methylcellulose stock solution. For the generation of methylcellulose stock solution, 250 ml DMEM (without supplements) was heated to 60 °C. Then 6 g methylcellulose powder (sterile) was added and an emulsion formed under heavy stirring for 20 min. Then, 250 ml DMEM (without supplements) at RT was added followed by FCS, penicillin, streptomycin and L-glutamine at the standard concentrations (see paragraph 4.3). During stirring at 4 °C overnight the powder dissolves in the medium. To remove any undissolved methylcellulose powder the solution was centrifuged for 2 h at 4500 x g and 90% of the supernatant were collected, aliquoted and stored at -20 °C for up to one year. If possible, the solution was thawed overnight at 4 °C.

Using the cultivation in low attachment plates and 30% methylcellulose stock solution, spheroids formed after 2-3 days. For treatment of spheroids, 100 µl of medium was removed and 100 µl medium with drugs at twice the final concentration was added.

4.3.7. Histological staining of spheroids

Spheroids were collected in a 15 ml falcon tube and within minutes gravity pulled them to the bottom of the tube. The supernatant was removed and PBS was added. After spheroids settled at the bottom, PBS was removed and the spheroids were fixed in 10 ml 4.5% phosphate-buffered PFA at 4 °C overnight. Spheroids were briefly washed two times with PBS and then incubated in water for 30 min. Dehydration was performed using ascending alcohols. In specific, spheroids were incubated for 45-60 min in 10 ml 70% EtOH, then 85% EtOH and 100% EtOH. Finally, spheroids were incubated in 10 ml xylene for 45-60 min. For embedding, the spheroids in xylene were transferred into a metal base mold. After removing xylene, 60 °C hot paraffin was added and the mold incubated at 70 °C until the paraffin melted. The paraffin was exchanged trice in order to remove any xylene residue (one incubation at 70 °C was performed overnight). Then the paraffin was left to solidify. Sections of 2 µm were stained with a BOND-MAX automated IHC/ISH Stainer (Leica Biosystems, Germany) in collaboration with Prof. Dr. Mathias Heikenwalder, DKFZ Heidelberg. The following primary and secondary antibodies (Table 6 and Table 7) were used. Images were acquired with a Leica DM1000 LED microscope (Leica, Germany).

Table 6: Primary antibodies for IHC

antibody	company	no.	species	dilution	BOND epitope retrieval solution
ferritin H1	Santa Cruz Biotechnology, USA	#376594	mouse	1:100	1 (citrate-based) (30 min, 95 °C)
Ki-67	Thermo Scientific, USA	RM-9106-S1	rabbit	1:200	2 (EDTA-based) (30 min, 95 °C)

Table 7: Secondary antibodies for IHC

antibody	company	no.	dilution
α -mouse IgG-HRP	Abcam, United Kingdom	ab125904	1:500
α -rabbit IgG-HRP	Leica Biosystems, Germany	DS9800	1:1

4.4 Protein-based assays

4.4.1. Protein extraction

For extraction of proteins, cells were scraped in 500 μ l ice-cold PBS and centrifuged for 10 sec at 10000 x g. PBS was removed and cells were either subsequently lysed in an appropriate amount of lysis buffer or stored at -20 °C. The cells were lysed with CSK-1 lysis buffer for 30 min on ice and centrifuged for 5 min at 13000 x g at 4 °C. The supernatant was removed and subjected to protein concentration determination via Bradford.

4.4.2. Protein concentration determination and preparation of samples

1 μ l of protein lysate was added to 1 ml of Bradford solution (1 ml of protein assay dye reagent concentrate plus 4 ml water; BioRad, USA). Absorption at 595 nm was measured with a photometer (BioPhotometer D30; Eppendorf, Germany) and protein concentration was determined using a BSA standard curve of absorptions plotted against known protein concentrations. The lysates were adjusted to a desired concentration and 4x protein loading buffer was added. After boiling the samples for 5 min at 95 °C, the denatured and reduced proteins could be further subjected to western blot analyses or stored at -80 °C.

4.4.3. SDS-PAGE, western blot and immunodetection of proteins

Table 8: SDS-PAGE recipe

components	for 2 separation gels (12.5%)	for 2 stacking gels (5%)
H ₂ O	4.5 ml	3.5 ml
30% acrylamide/bisacrylamide	4.2 ml	830 μ l
0.47 M Tris-HCl (pH 6.7)	-	620 μ l
3 M Tris HCl (pH 8.9)	1.2 ml	-
10% SDS	100 μ l	50 μ l
10% APS	10 μ l	100 μ l
TEMED	50 μ l	5 μ l

Gels were cast according to Table 8 between two glass plates and installed into the Xcell SureLock™ Mini-Cell Electrophoresis System (Life Technologies) filled with Tris-Glycine running buffer. Proteins were separated during gel electrophoresis at 120 V for approximately 2 h. Then proteins were transferred onto a methanol-activated PVDF membrane using the Trans-Blot® SD Semi-Dry Transfer Cell (BioRad, USA). The gel and membrane were sandwiched between four sheets of Whatman filter paper soaked with Towbin transfer buffer and blotted for 1 h at 20 V. In order to detect several proteins of different sizes from the same

membrane, the membrane was cut in horizontal pieces according to the size of the protein of interest. Then, membranes were blocked in blocking solution for 1 h at RT. Usually, the blocking solution consists of 5% milk powder and 1% BSA in PBS/T. An exception was made for p53 phospho (Ser15) detection, for which the membranes were blocked in 5%BSA in PBS/T.

For immunodetection of proteins, the membrane stripe was incubated in blocking solution containing the primary antibody at the indicated concentrations (Table 9) over night at 4 °C. Then, the membrane was washed 3x 10 min with PBS/T, incubated with secondary antibody (Table 10) in blocking solution for 1 h at RT and washed for at least 1 h with PBS/T. All antibodies were diluted 5% milk powder, 1% BSA in PBS/T (blocking solution), except for β -actin which was diluted in PBS/T and p53 phospho (Ser15) which was diluted in 5% BSA in PBS/T. Enhanced chemiluminescence (ECL) was used to detect the proteins. ECLTM Prime Western Blotting Detection Reagent (GE Healthcare, United Kingdom) was applied to the membrane, incubated for 1 min and then images were acquired with the Fusion SL Detection System (Vilber Lourmat, Germany).

Table 9: Primary antibodies for immunodetection

antibody	company	no.	species	dilution
16E6	Arbor Vita Corporation, USA	#849	mouse	1:2000
16E7	kind gift of Dr. Müller, DKFZ Heidelberg, Germany	NM2	mouse	1:1000
18E6	Arbor Vita Corporation, USA	#399	mouse	1:2000
18E7	Zentgraf, DKFZ Heidelberg, Germany	B (28) #47 31.10-11.11.95	chicken	1:1000
ferritin H1	Santa Cruz Biotechnology, USA	#376594	mouse	1:1000
HIF-1 α	BD Pharmingen, USA	#610959	mouse	1:500
p21	Santa Cruz Biotechnology, USA	#397	rabbit	1:500
P-4E-BP1	Cell Signaling, USA	#9451	rabbit	1:1000
p53 (DO-1)	Santa Cruz Biotechnology, USA	#126	mouse	1:1000
p53 phospho (Ser15)	Cell Signaling, USA	# 9284	rabbit	1:1000
S6K(p70S6K)	Cell Signaling, USA	#9202	rabbit	1:1000
PARP (Asp214)	Cell Signaling, USA	#9546	mouse	1:1000
P-S6K (P-p70S6K)	Cell Signaling, USA	#9234	rabbit	1:1000
REDD1	Proteintech, USA	# 10638-1-AP	rabbit	1:2000
β -actin	Sigma-Aldrich, USA	#A2228	mouse	1:50000
tubulin	Calbiochem, Germany	#CP06	mouse	1:5000
vinculin	Santa Cruz Biotechnology, USA	#73614	mouse	1:4000

Table 10: Secondary antibodies for immunodetection

secondary antibody	company	no.	dilution
α -chicken IgG-HRP	Santa Cruz Biotechnology, USA	#2428	1:5000
α -mouse IgG-HRP	Santa Cruz Biotechnology, USA	#2005	1:5000
α -rabbit IgG-HRP	Santa Cruz Biotechnology, USA	#2004	1:5000

4.4.4. Proteome analysis (TMT10plex method)

Proteome analyses were kindly performed by Bianca Kuhn in the lab of Prof. Jeroen Krijgsveld (DKFZ, Heidelberg). Upon treatment proteins were labelled using the Thermo Fischer Scientific's tandem mass tags (TMTs). Since the labelling is isobaric the tags all have similar weights although they differ in the distribution of heavy and light isotopes which then generates a unique reporter. Up to 10 samples could be measured simultaneously with this approach (TMT10plex) using liquid chromatography combined with mass spectrometry (LC)-MS/MS. A relative quantification of proteins can be determined by measuring the intensities of the unique reporters.

For proteome analyses SiHa cells were seeded in 6 cm dishes according to Table 2 and treated with 10 μ M CPX for 48 h. Then cells were harvested by scraping in ice-cold PBS, pelleted and stored at -80 °C until further processing.

The following protocol was kindly provided by Bianca J. Kuhn and describes the sample preparation and analysis of the proteins: "Cell pellets were suspended in 0.1% (w/v) RapiGest-SF (Waters) in 100 mM triethylammonium bicarbonate (TEAB, pH 8). Cell lysis and shearing of chromatin was performed in a Bioruptor Pico (Diagenode) in a final volume of max. 300 μ l, 15-20 cycles of 30''/30'' (ON/OFF) at 4 °C. Protein concentration was determined by BCA-assay following the manufacturer's protocol (Thermo Fisher Scientific). Prior to protein digestion disulfide bonds were reduced by 5 mM DTT for 30 min at 60 °C and subsequently alkylated with 15 mM 2-chloroacetamide for 30 min at RT. Proteolytic digestion was performed with trypsin (sequencing grade modified, Promega) in a protease-to-protein ratio of 1:50 (w/w) overnight at 37 °C, shaking at 700 rpm. Following digestion, 1% trifluoroacetic acid was added (pH < 2) to stop digestion and break down RapiGest by incubation at 37 °C for 30 min followed by centrifugation at 20000 x g for 10 min. Supernatants were transferred to a new tube and dried in a vacuum centrifuge.

Isobaric labeling of the peptides was performed with 10-plex TMT reagents according to the manufacturer's protocol (Thermo Fisher Scientific). In brief, 10 μ g of sample was dissolved in 10 μ l, 100 mM TEAB, vortexed and incubated for 10 min at RT. TMT10-plex reagents (0.8 mg) were dissolved in 41 μ l of acetonitrile (ACN, LC-MS grade). 4.1 μ L of TMT reagent

was combined with sample and incubated for 1 h at RT. The reaction was quenched by adding 8 μ l of 5% hydroxylamine and incubation for 15 min. Labeling efficacy was checked for each sample by MS prior to combining equal amounts and drying in a vacuum centrifuge prior to fractionation.

Dried samples were dissolved in 20 mM ammonium formate (pH 10), prior to fractionation on a 1200 Infinity HPLC system (Agilent) with a Gemini C18 column (3 μ m, 110 Å, 100 \times 1.0 mm; Phenomenex) using a linear 60 min gradient from 0% to 35% (v/v) ACN in 20 mM ammonium formate (pH 10) at a flow rate of 0.1 ml/min. Sixty 1-min fractions were collected and pooled into twelve fractions, dried and reconstituted in 0.1% formic acid (FA). Fractions were injected by an Easy-nLC 1200 nano-UPLC (Thermo Fisher Scientific) onto a trap column (Pepmap, 100 μ m \times 2 cm, C18, 5 μ m 100 Å pores) and separated on an analytical column (PepMap RSLC 75 μ m \times 50 cm, nanoViper, C18, 2 μ M, 100 Å) by applying a multistep gradient (Solvent A: 0.1% FA in water, Solvent B: 0.1% FA, 80% ACN 29.9% water) from : 3-50% B over 90 min. Eluting peptides were electro-sprayed by applying 2 kV on a 10 μ m Picotip coated emitter (New Objective) into an Orbitrap Fusion™ Tribrid™ (Thermo Fisher Scientific) mass spectrometer operated in data-dependent mode of acquisition using the vendor supplied default settings for synchronous precursor selection (SPS) MS3 fragmentation [300].

The mass spectra were analysed using Proteome Discoverer 2.1.0.81 (Thermo Fisher Scientific), using the SEQUEST search engine against UniProtKB/Swiss-Prot databases of Homo sapiens (21.06.2018), and human papillomavirus 16 (21.06.2018) proteome databases. Search settings: digestion reagent: trypsin, precursor and product ion tolerances were set at 20 ppm and 0.5 Da, respectively. Carbamidomethylation of cysteine was set as a fixed modification, oxidation of methionine as a variable modification. For TMT labels, TMT6-plex on lysine and peptide N-termini were set as a static modification. The percolator algorithm was used as the false discovery rate (FDR) calculator, and all peptides were filtered at a 'strict' target FDR level of 0.01. Proteins were tested for differential expression with Linear Models for Microarray Data (limma [301], version 3.36.2; R, version 3.5.1). Significant events (FDR < 0.05, $|\log FC| \geq 1$) were identified after adjusting for multiple testing according to Benjamini & Hochberg. The mass spectrometry proteomics data have been deposited to the ProteomeXchange Consortium via the PRIDE [302] partner repository with the dataset identifier PXD011095." (F. Bossler, B. J. Kuhn, T. Günther, S. J. Kraemer, P. Khalkar, S. Adrian, C. Lohrey, A. Holzer, M. Shimobayashi, M. Dürst, A. Mayer, F. Rösl,

Adam Grundhoff, J. Krijgsveld, K. Hoppe-Seyler, F. Hoppe-Seyler, submitted for publication).

Volcano Plots were generated using GraphPad Prism Software. For gene set enrichment analyses the gene set enrichment analysis software GSEA Desktop v3.0 was used. Only genes with a p-value less than 0.05 were used. Genes were ranked according to their log₂ fold change and a preranked GSEA was run against the current molecular signature database (MSigDB) gene sets (gene symbols) from 16.04.18 (msigdb.v6.2.symbols.gmt).

4.5 RNA-based assays

4.5.1. RNA isolation

For RNA isolation the column-based PureLink RNA Mini Kit (Invitrogen, USA) was used according to the manufacturer's protocol. In short 600 µl lysis buffer complemented with β-mercaptoethanol (100 µl per 10 ml lysis buffer) was used to lyse cells grown in a 6 cm dish. The lysate could either be stored at -80 °C or subjected to further RNA purification. To further process the RNA, 600 µl of 70% EtOH was added and the RNA was transferred onto the column followed by washing. To remove unwanted DNA the PureLink DNase Set (Invitrogen, USA) was applied. For this 80 µl of DNase I reaction mix (8 µl 10x DNase I Reaction Buffer, 10 µl DNase (~3 U/µl) and 62 µl water) were added to the column and incubated for 15 min at RT. After washing, the RNA was eluted in 40-80 µl water.

4.5.2. Reverse transcription (RT) and quantitative real-time PCR (qRT-PCR)

The ProtoScript® II First Strand cDNA Synthesis Kit (NEB, USA) was used according to the manufacturer's protocol. cDNA was synthesised using 500 ng RNA and oligodT primers. The samples were incubated at 42 °C for 1 h, were heated up to 80 °C for 5 min and then cooled down to 4 °C. After the addition of 40 µl water, the samples could be used for qRT-PCR or stored at -20 °C.

For qRT-PCR 2 µl of cDNA, 10 µl SYBR® Green PCR master mix (Applied Biosystems, USA), 0.4 µl of 5 pM forward and reverse primer (final concentration 0.1 pM each) and 7.2 µl water were analysed with a 7300 Real Time PCR System. The PCR cycles are summarised in Table 11. Sequences of primers are listed in Table 12. HPV16 and HPV18 *E6/E7* primers recognise all three transcript classes of HPV16 and HPV18 *E6/E7*.

Table 11: PCR cycles

	step 1 (primer annealing)	step 2 (DNA denaturation)	step 3 (elongation)	step 4 (dissociation)
no. of cycles	1	1	40	1
temperature (°C)	50	95	95/60	95/60/95
time (min)	2:00	10:00	0:15/1:00	0:15/1:00/0:15

Table 12: Primer for qRT-PCR

primer	sequence (5' → 3')
HPV16 E6/E7 forward	CAATGTTTCAGGACCCACAGG
HPV16 E6/E7 reverse	CTCACGTCGCAGTAACTGTTG
HPV18 E6/E7 forward	ATGCATGGACCTAAGGCAAC
HPV18 E6/E7 reverse	AGGTCGTCTGCTGAGCTTTC
β -actin forward	GGACTTCGAGCAAGAGATGGC
β -actin reverse	GCAGTGATCTCCTTCTGCATC
transferrin receptor 1 forward	TGCTGGAGACTTTGGATCGG
transferrin receptor 1 reverse	TATACAACAGTGGGCTGGCA

Relative quantification was performed using the comparative Ct ($2^{\Delta\Delta C_t}$) method [303]. Ct values of *E6/E7* or *TFRI* were normalised to the reference β -actin. For statistical analysis of fold changes, values were transformed logarithmically.

4.6 Statistical analyses

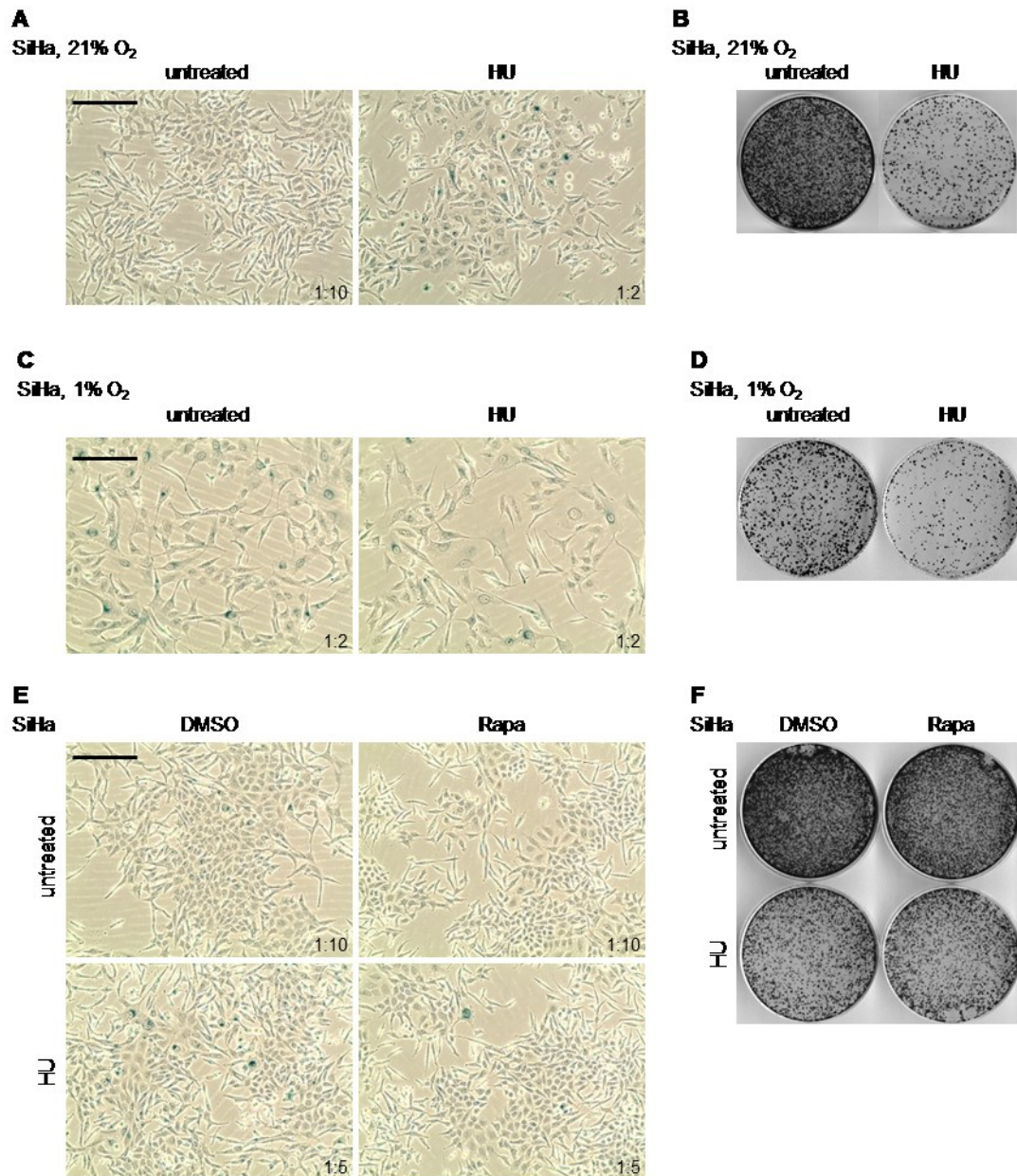
SigmaPlot version 12.5 was used to perform statistical tests. For comparison of relative mRNA levels upon CPX treatment a One-Sample t-test was performed with the test mean set to zero. Shapiro-Wilk was used for normality statistic and the alpha value was set to 0.05. For the comparison of EdU incorporation in EtOH- and CPX-treated cells a t-test was performed with the same settings.

CHAPTER 5

APPENDIX

5. Appendix

Supplementary figure



Supplementary Figure 1: HU induces senescence in SiHa cells. SiHa cells according to Figure 27. **(A)** SiHa cells were treated under normoxic conditions with 1 mM HU for 48 h. SA-β-gal was stained 4 days after splitting (scale bar: 200 μm). **(B)** Concomitant CFAs to (A), 11 days after splitting. **(C)** SiHa cells were cultivated under hypoxic conditions for 24 h. Then cells were treated with 1 mM HU for another 96 h under hypoxic conditions. Senescence assays were performed 3 days after splitting (scale bar: 200 μm). **(D)** Concomitant CFAs (13 days after splitting). **(E)** Senescence assays after HU treatment in the presence of rapamycin (24 h pre-incubation with 50 nM rapamycin, then addition of 1 mM HU for another 48 h). Staining was performed 4 days after splitting (scale bar: 200 μm). **(F)** Concomitant CFAs to (E), 10 days after splitting.

List of Figures

Figure 1: HPV-induced carcinogenesis.....	5
Figure 2: Cooperation of HPV E6 and E7 oncoproteins during oncogenesis.....	6
Figure 3: Possible strategies to target normoxic and hypoxic HPV-positive cancer cells.....	10
Figure 4: Cellular iron metabolism.....	12
Figure 5: The IRE/IRP system.....	14
Figure 6: Complexes of iron chelators and iron ions.....	16
Figure 7: Ribonucleotide reductase.....	19
Figure 8: Iron chelators repress HPV16 and HPV18 E6 and E7 expression.....	26
Figure 9: CPX represses HPV oncogene expression.....	28
Figure 10: Excess iron prevents CPX-induced E7 repression.....	29
Figure 11: CPX inhibits proliferation.....	31
Figure 12: CPX induces cell cycle arrest and senescence.....	32
Figure 13: CPX induces phosphorylation of p53 at Ser15.....	33
Figure 14: CPX causes DNA damage.....	34
Figure 15: Senescence and cell cycle arrest induced by CPX are p53-independent.....	36
Figure 16: E6/E7 repression by CPX is HIF-1 α -independent.....	37
Figure 17: Senescence induction by CPX is caused by iron deprivation.....	38
Figure 18: CPX induces apoptosis.....	41
Figure 19: CPX induces PARP cleavage.....	42
Figure 20: Apoptosis induction by CPX is delayed in HeLa "p53 null" cells.....	43
Figure 21: The lack of p53 delays CPX-induced apoptosis in HCT116 cells.....	44
Figure 22: CPX induces mTORC1-independent senescence.....	45
Figure 23: Iron chelators repress mTORC1 signalling.....	47
Figure 24: CPX treatment under hypoxic conditions.....	49
Figure 25: CPX cooperates with RT and CT.....	51
Figure 26: Proteome analyses of CPX treatment.....	53
Figure 27: HU induces senescence.....	54
Figure 28: Apoptosis assays upon HU treatment.....	55
Figure 29: Anti-tumourigenic effects of CPX.....	73

List of Tables

Table 1: Cell lines and corresponding media and supplements (where applicable).....	79
Table 2: Cell numbers seeded for experiments	80
Table 3: Compounds used	80
Table 4: pSUPER constructs	81
Table 5: Detectors used at BD LSR Fortessa	82
Table 6: Primary antibodies for IHC	85
Table 7: Secondary antibodies for IHC	86
Table 8: SDS-PAGE recipe	86
Table 9: Primary antibodies for immunodetection	87
Table 10: Secondary antibodies for immunodetection	88
Table 11: PCR cycles	91
Table 12: Primer for qRT-PCR	91

Abbreviations

(d)ATP	(deoxy)adenosine triphosphate
(d)CTP	(deoxy)cytidine triphosphate
(d)GTP	(deoxy)guanosine triphosphate
(d)TTP	(deoxy)thymidine triphosphate
3-AP	3-aminopyridine-2-carboxaldehyde thiosemicarbazone
4E-BP1	eukaryotic translation initiation factor 4E binding protein 1
AMPK	AMP-activated protein kinase
AP-1	activator protein 1
APS	ammonium persulfate
ARF	alternate reading frame
ARNT	aryl hydrocarbon receptor nuclear translocator
ATM	ataxia telangiectasia mutated
ATR	ataxia telangiectasia and Rad3 related
BAK	Bcl-2 homologous antagonist killer
BAX	Bcl-2-associated X protein
BCL-2	B-cell lymphoma 2
BCL-XL	B-cell lymphoma-extra large
BSA	bovine serum albumin
C/EBP β	CCAAT/enhancer binding protein- β
Caspase	cysteine-aspartic protease
Cdc25A	cell division cycle 25 homolog A
CDDP	cis-diamminedichloridoplatinum(II)/ cisplatin
CDK	cyclin-dependent kinase
CDKN1A	cyclin-dependent kinase inhibitor 1 A
CFA	colony formation assay
CHK1/2	checkpoint kinase 1/2
CIN	cervical intraepithelial neoplasia
CO ₂	carbon dioxide
CPX	ciclopirox (olamine)
CT	chemotherapy
Ct	cycle threshold
DAPI	4',6-diamidino-2-phenylindole
DFO	deferoxamine
DMEM	Dulbecco's minimal essential medium
DMF	dimethylformanid
DMSO	dimethyl sulfoxide
DMT1	divalent metal transporter 1
DNA	deoxyribonucleic acid
dNDP	deoxyribonucleoside diphosphates
dNTP	deoxyribonucleoside triphosphates
DOHH	deoxyhypusine hydroxylase
DTT	dithiothreitol

e. g.	<i>exempli gratia</i>
E2F	elongation factor 2
E6AP	E6-associated protein
ECL	enhanced chemoluminescence
EDTA	ethylenediaminetetraacetic acid
EdU	5-ethynyl-2'-deoxyuridine
EGF	epidermal growth factor
eIF5A	eukaryotic initiation factor 5A protein
et al.	<i>et alii</i>
Eto	etoposide
EtOH	ethanol
FAC	ferric ammonium citrate
FACS	fluorescence-activated cell sorting
FCS	fetal calf serum
FDA	Food and Drug Administration
FDR	false discovery rate
Fe ²⁺	ferrous iron
Fe ³⁺	ferric irons
FeSO ₄	iron(II) sulphate
FITC	fluorescein isothiocyanate
FPN1	ferroportin
Fra	Fos related antigen
FTH	ferritin heavy chain
FTL	ferritin light chain
G418	geneticin
GSK3 β	glycogen synthase kinase 3 beta
H2B	histone 2 B
H ₂ O	water
H ₂ O ₂	hydrogen peroxide
HAMP	hepcidin antimicrobial peptide
HIF	hypoxia-inducible factor
HPV	human papillomavirus
HRP	horseradish peroxidase
HU	hydroxyurea
i. e.	<i>id est</i>
Ig	immunoglobuline
IL	interleukin
INK4	inhibitors of CDK4
IRE	iron responsive element
IRP	iron regulatory protein
LC	liquid chromatography
LIP	labile iron pool
log ₂	binary logarithm
MAPK	mitogen-activated protein kinase

MDM2	mouse double minute 2 homolog
mRNA	messenger RNA
MS	mass spectrometry
mTOR	mechanistic/mammalian target of rapamycin
mTORC1/mTORC2	mTOR complex 1/mTOR complex 2
NAC	N-acetylcysteine
NDRG-1	N-myc downstream regulated gene 1
NF-IL6	nuclear factor for IL-6 expression
NTBI	non-transferrin bound iron
O ₂	oxygen
ORF	open reading frame
p53R2	p53 inducible ribonucleotide reductase
PARP	poly (adenosine diphosphate-ribose) polymerase
PBS	phosphate-buffered saline
PCR	polymerase chain reaction
PFA	paraformaldehyde
PHD	prolyl hydroxylase domain enzyme
PI	propidium iodide
PIPES	piperazine-N,N'-bis(2-ethanesulfonic acid) sodium salt
pRb	retinoblastoma protein
PVDF	polyvinylidene difluoride
qPCR	quantitative real-time polymerase chain reaction
qRT-PCR	quantitative real-time reverse transcription-polymerase chain reaction
Rapa	rapamycin
RAPTOR	regulatory-associated protein of mTOR
REDD1	protein regulated in development and DNA damage response 1
RICTOR	rapamycin-insensitive companion of mTOR
RNA	ribonucleic acid
RNAse	ribonuclease
rNDP	ribonucleoside diphosphates
rNTP	ribonucleoside triphosphates
ROS	reactive oxygen species
RR	ribonucleotide reductase
RRM1/2	ribonucleotide reductase subunit M1/2
RT	room temperature
RT	radiotherapy
RT	reverse transcription
S6K/p70S6K	p70 S6 kinase
SASP	senescence-associated secretory phenotype
SA-β-gal	senescence-associated β-galactosidase
SDS	sodium dodecyl sulphate
SDS-PAGE	sodium dodecyl sulphate-polyacrylamide gel electrophoresis
Ser	serine
siRNA	small interfering RNA

STEAP	six-transmembrane epithelial antigen of prostate
TEMED	tetramethylethylenediamine
TF	transferrin
TFR	transferrin receptor
TMT	tandem mass tag
tris	tris(hydroxymethyl)aminomethane
TSC	tuberous sclerosis complex
TUNEL	terminal desoxynucleotidyl transferase dUTP nick end labelling
URR	upstream regulatory region
UTR	untranslated region
VEGF	vascular endothelial growth factor
VHL	von Hippel-Lindau tumour suppressor
Wnt	Wingless/Integrated
X-gal	5-bromo-4-chloro-3-indolyl- β -D-galactopyranoside
ZnCl ₂	zinc chloride
ZnSO ₄	zinc sulphate
z-VAD-FMK	carbobenzoxy-valyl-alanyl-aspartyl-[O-methyl]-fluoromethylketone
γ H2AX	phosphorylated histone 2AX (serine 139)

The one-letter code for nucleotides was applied according to declarations by the International Union of Pure and Applied Chemistry (IUPAC).

Units and prefixes

%	percent
°C	degree Celsius
Å	angstrom
g	centrifugal acceleration
g	gram
h	hour
l	litre
M	molar
m	metre
min	minute
sec	second
U	unit
V	volt

symbol	prefix	factor
c	centi	10^{-2}
m	milli	10^{-3}
μ	micro	10^{-6}
n	nano	10^{-9}
p	piko	10^{-12}

References

1. de Villiers, E.-M., et al., *Classification of papillomaviruses*. Virology, 2004. **324**(1): p. 17-27.
2. Malik, H., F.H. Khan, and H. Ahsan, *Human papillomavirus: current status and issues of vaccination*. Archives of Virology, 2014. **159**(2): p. 199-205.
3. Walboomers, J.M., et al., *Human papillomavirus is a necessary cause of invasive cervical cancer worldwide*. J Pathol, 1999. **189**(1): p. 12-9.
4. zur Hausen, H., *Papillomaviruses in the causation of human cancers — a brief historical account*. Virology, 2009. **384**(2): p. 260-265.
5. zur Hausen, H., et al., *Attempts to detect virus-specific DNA in human tumors. I. Nucleic acid hybridizations with complementary RNA of human wart virus*. Int J Cancer, 1974. **13**(5): p. 650-6.
6. Durst, M., et al., *A papillomavirus DNA from a cervical carcinoma and its prevalence in cancer biopsy samples from different geographic regions*. Proc Natl Acad Sci U S A, 1983. **80**(12): p. 3812-5.
7. de Araújo Catão Zampronha, R., et al., *Human papillomavirus types 16 and 18 and the prognosis of patients with stage I cervical cancer*. Clinics, 2013. **68**(6): p. 809-814.
8. Lowy, D.R., R. Kirnbauer, and J.T. Schiller, *Genital human papillomavirus infection*. Proc Natl Acad Sci U S A, 1994. **91**(7): p. 2436-40.
9. de Martel, C., et al., *Worldwide burden of cancer attributable to HPV by site, country and HPV type*. Int J Cancer, 2017. **141**(4): p. 664-670.
10. Hasche, D., S.E. Vinzón, and F. Rösl, *Cutaneous Papillomaviruses and Non-melanoma Skin Cancer: Causal Agents or Innocent Bystanders?* Frontiers in Microbiology, 2018. **9**: p. 874.
11. Zhai, L. and E. Tumban, *Gardasil-9: A global survey of projected efficacy*. Antiviral Res, 2016. **130**: p. 101-9.
12. Bruni, L., et al., *Global estimates of human papillomavirus vaccination coverage by region and income level: a pooled analysis*. The Lancet Global Health, 2016. **4**(7): p. e453-e463.
13. Doorbar, J., *The papillomavirus life cycle*. J Clin Virol, 2005. **32 Suppl 1**: p. S7-15.
14. Doorbar, J., et al., *Human papillomavirus molecular biology and disease association*. Reviews in Medical Virology, 2015. **25**(Suppl Suppl 1): p. 2-23.
15. Schiffman, M., et al., *Carcinogenic human papillomavirus infection*. Nature Reviews Disease Primers, 2016. **2**: p. 16086.
16. Roman, A. and K. Munger, *The papillomavirus E7 proteins*. Virology, 2013. **445**(1): p. 138-168.
17. Vande Pol, S.B. and A.J. Klingelutz, *Papillomavirus E6 oncoproteins*. Virology, 2013. **445**(1): p. 115-137.
18. Schwarz, E., et al., *Structure and transcription of human papillomavirus sequences in cervical carcinoma cells*. Nature, 1985. **314**: p. 111.
19. Lambert, P.F., et al., *Epidermal cancer associated with expression of human papillomavirus type 16 E6 and E7 oncogenes in the skin of transgenic mice*. Proc Natl Acad Sci U S A, 1993. **90**(12): p. 5583-7.
20. Trimble, C.L., et al., *Spontaneous Regression of High-Grade Cervical Dysplasia: Effects of Human Papillomavirus Type and HLA Phenotype*. Clinical Cancer Research, 2005. **11**(13): p. 4717-4723.

21. Sotlar, K., et al., *Detection of high-risk human papillomavirus E6 and E7 oncogene transcripts in cervical scrapes by nested RT-polymerase chain reaction*. Journal of Medical Virology, 2004. **74**(1): p. 107-116.
22. Bernard, B.A., et al., *The human papillomavirus type 18 (HPV18) E2 gene product is a repressor of the HPV18 regulatory region in human keratinocytes*. Journal of Virology, 1989. **63**(10): p. 4317-4324.
23. McBride, A.A. and A. Warburton, *The role of integration in oncogenic progression of HPV-associated cancers*. PLOS Pathogens, 2017. **13**(4): p. e1006211.
24. Wentzensen, N., S. Vinokurova, and M. von Knebel Doeberitz, *Systematic review of genomic integration sites of human papillomavirus genomes in epithelial dysplasia and invasive cancer of the female lower genital tract*. Cancer Res, 2004. **64**(11): p. 3878-84.
25. Cullen, A.P., et al., *Analysis of the physical state of different human papillomavirus DNAs in intraepithelial and invasive cervical neoplasm*. J Virol, 1991. **65**(2): p. 606-12.
26. Münger, K., *The molecular biology of cervical cancer*. Journal of Cellular Biochemistry, 1995. **59**(23): p. 55-60.
27. Schiffman, M. and N. Wentzensen, *Human Papillomavirus Infection and the Multistage Carcinogenesis of Cervical Cancer*. Cancer Epidemiology Biomarkers & Prevention, 2013. **22**(4): p. 553-560.
28. zur Hausen, H., *Human genital cancer: synergism between two virus infections or synergism between a virus infection and initiating events?* Lancet, 1982. **2**(8312): p. 1370-2.
29. Duensing, S. and K. Münger, *Mechanisms of genomic instability in human cancer: Insights from studies with human papillomavirus oncoproteins*. International Journal of Cancer, 2004. **109**(2): p. 157-162.
30. Shanmugasundaram, S. and J. You, *Targeting Persistent Human Papillomavirus Infection*. Viruses, 2017. **9**(8): p. 229.
31. Dyson, N., et al., *The human papilloma virus-16 E7 oncoprotein is able to bind to the retinoblastoma gene product*. Science, 1989. **243**(4893): p. 934-7.
32. Giacinti, C. and A. Giordano, *RB and cell cycle progression*. Oncogene, 2006. **25**: p. 5220.
33. Evan, G.I. and K.H. Vousden, *Proliferation, cell cycle and apoptosis in cancer*. Nature, 2001. **411**: p. 342.
34. Jones, D.L., D.A. Thompson, and K. Munger, *Destabilization of the RB tumor suppressor protein and stabilization of p53 contribute to HPV type 16 E7-induced apoptosis*. Virology, 1997. **239**(1): p. 97-107.
35. Martinez-Zapien, D., et al., *Structure of the E6/E6AP/p53 complex required for HPV-mediated degradation of p53*. Nature, 2016. **529**(7587): p. 541-5.
36. Scheffner, M., et al., *The E6 oncoprotein encoded by human papillomavirus types 16 and 18 promotes the degradation of p53*. Cell, 1990. **63**(6): p. 1129-1136.
37. Hawley-Nelson, P., et al., *HPV16 E6 and E7 proteins cooperate to immortalize human foreskin keratinocytes*. The EMBO Journal, 1989. **8**(12): p. 3905-3910.
38. Münger, K., et al., *The E6 and E7 genes of the human papillomavirus type 16 together are necessary and sufficient for transformation of primary human keratinocytes*. Journal of Virology, 1989. **63**(10): p. 4417-4421.
39. Hoppe-Seyler, K., et al., *Induction of dormancy in hypoxic human papillomavirus-positive cancer cells*. Proceedings of the National Academy of Sciences, 2017. **114**(6): p. E990-E998.

40. Hoppe-Seyler, K., et al., *The HPV E6/E7 Oncogenes: Key Factors for Viral Carcinogenesis and Therapeutic Targets*. Trends in Microbiology, 2018. **26**(2): p. 158-168.
41. Stern, P.L., et al., *Therapy of Human Papillomavirus-Related Disease*. Vaccine, 2012. **30**: p. F71-F82.
42. Skeate, J.G., et al., *Current therapeutic vaccination and immunotherapy strategies for HPV-related diseases*. Human Vaccines & Immunotherapeutics, 2016. **12**(6): p. 1418-1429.
43. Brinkman, J.A., et al., *Therapeutic Vaccination for HPV Induced Cervical Cancers*. Disease Markers, 2007. **23**(4): p. 337-352.
44. Ashrafi, G.H., et al., *E5 protein of human papillomavirus 16 downregulates HLA class I and interacts with the heavy chain via its first hydrophobic domain*. Int J Cancer, 2006. **119**(9): p. 2105-12.
45. Butz, K., et al., *siRNA targeting of the viral E6 oncogene efficiently kills human papillomavirus-positive cancer cells*. Oncogene, 2003. **22**: p. 5938.
46. Yuan, C.H., et al., *Flavonol and imidazole derivatives block HPV16 E6 activities and reactivate apoptotic pathways in HPV+ cells*. Cell Death & Disease, 2016. **7**: p. 2060.
47. Sterlinko Grm, H., et al., *Inhibition of E6-induced Degradation of its Cellular Substrates by Novel Blocking Peptides*. Journal of Molecular Biology, 2004. **335**(4): p. 971-985.
48. Cherry, J.J., et al., *Structure Based Identification and Characterization of Flavonoids That Disrupt Human Papillomavirus-16 E6 Function*. PLOS ONE, 2013. **8**(12): p. e84506.
49. Han, K., et al., *Measurement of Tumor Hypoxia in Patients With Locally Advanced Cervical Cancer Using Positron Emission Tomography with ¹⁸F-Fluoroazomyin Arabinoside*. International Journal of Radiation Oncology • Biology • Physics.
50. Teicher, B.A., *Hypoxia and drug resistance*. Cancer Metastasis Rev, 1994. **13**(2): p. 139-68.
51. Bertout, J.A., S.A. Patel, and M.C. Simon, *The impact of O(2) availability on human cancer*. Nature reviews. Cancer, 2008. **8**(12): p. 967-975.
52. Carmeliet, P. and R.K. Jain, *Angiogenesis in cancer and other diseases*. Nature, 2000. **407**: p. 249.
53. Hoppe-Seyler, K., et al., *Virus/Host Cell Crosstalk in Hypoxic HPV-Positive Cancer Cells*. Viruses, 2017. **9**(7).
54. Guzy, R.D., et al., *Mitochondrial complex III is required for hypoxia-induced ROS production and cellular oxygen sensing*. Cell Metab, 2005. **1**(6): p. 401-8.
55. Bristow, R.G. and R.P. Hill, *Hypoxia and metabolism. Hypoxia, DNA repair and genetic instability*. Nat Rev Cancer, 2008. **8**(3): p. 180-92.
56. Eales, K.L., K.E. Hollinshead, and D.A. Tennant, *Hypoxia and metabolic adaptation of cancer cells*. Oncogenesis, 2016. **5**: p. e190.
57. Erler, J.T., et al., *Hypoxia-mediated down-regulation of Bid and Bax in tumors occurs via hypoxia-inducible factor 1-dependent and -independent mechanisms and contributes to drug resistance*. Mol Cell Biol, 2004. **24**(7): p. 2875-89.
58. Leontieva, O.V., et al., *Hypoxia suppresses conversion from proliferative arrest to cellular senescence*. Proc Natl Acad Sci U S A, 2012. **109**(33): p. 13314-8.
59. Rouschop, K.M., et al., *The unfolded protein response protects human tumor cells during hypoxia through regulation of the autophagy genes MAP1LC3B and ATG5*. J Clin Invest, 2010. **120**(1): p. 127-41.

60. Krock, B.L., N. Skuli, and M.C. Simon, *Hypoxia-induced angiogenesis: good and evil*. Genes Cancer, 2011. **2**(12): p. 1117-33.
61. Xu, H., et al., *Hypoxia stimulates invasion and migration of human cervical cancer cell lines HeLa/SiHa through the Rab11 trafficking of integrin alphavbeta3/FAK/PI3K pathway-mediated Rac1 activation*. J Biosci, 2017. **42**(3): p. 491-499.
62. Gray, L.H., et al., *The Concentration of Oxygen Dissolved in Tissues at the Time of Irradiation as a Factor in Radiotherapy*. The British Journal of Radiology, 1953. **26**(312): p. 638-648.
63. Tredan, O., et al., *Drug resistance and the solid tumor microenvironment*. J Natl Cancer Inst, 2007. **99**(19): p. 1441-54.
64. Rohwer, N. and T. Cramer, *Hypoxia-mediated drug resistance: novel insights on the functional interaction of HIFs and cell death pathways*. Drug Resist Updat, 2011. **14**(3): p. 191-201.
65. Kaanders, J.H., J. Bussink, and A.J. van der Kogel, *ARCON: a novel biology-based approach in radiotherapy*. Lancet Oncol, 2002. **3**(12): p. 728-37.
66. Dische, S., *Hyperbaric oxygen: the Medical Research Council trials and their clinical significance*. Br J Radiol, 1978. **51**(611): p. 888-94.
67. Rademakers, S.E., et al., *Molecular aspects of tumour hypoxia*. Molecular Oncology, 2008. **2**(1): p. 41-53.
68. Vaupel, P., M. Hockel, and A. Mayer, *Detection and characterization of tumor hypoxia using pO2 histography*. Antioxid Redox Signal, 2007. **9**(8): p. 1221-35.
69. Lee, M. and J.-S. Lee, *Exploiting tumor cell senescence in anticancer therapy*. BMB Reports, 2014. **47**(2): p. 51-59.
70. Hayflick, L. and P.S. Moorhead, *The serial cultivation of human diploid cell strains*. Exp Cell Res, 1961. **25**: p. 585-621.
71. Harley, C.B., A.B. Futcher, and C.W. Greider, *Telomeres shorten during ageing of human fibroblasts*. Nature, 1990. **345**(6274): p. 458-60.
72. Kuilman, T., et al., *The essence of senescence*. Genes Dev, 2010. **24**(22): p. 2463-79.
73. Ben-Porath, I. and R.A. Weinberg, *The signals and pathways activating cellular senescence*. Int J Biochem Cell Biol, 2005. **37**(5): p. 961-76.
74. el-Deiry, W.S., et al., *WAF1, a potential mediator of p53 tumor suppression*. Cell, 1993. **75**(4): p. 817-25.
75. Harper, J.W., et al., *The p21 Cdk-interacting protein Cip1 is a potent inhibitor of G1 cyclin-dependent kinases*. Cell, 1993. **75**(4): p. 805-16.
76. Kruiswijk, F., C.F. Labuschagne, and K.H. Vousden, *p53 in survival, death and metabolic health: a lifeguard with a licence to kill*. Nature Reviews Molecular Cell Biology, 2015. **16**: p. 393.
77. Purvis, J.E., et al., *p53 dynamics control cell fate*. Science, 2012. **336**(6087): p. 1440-4.
78. Gil, J. and G. Peters, *Regulation of the INK4b-ARF-INK4a tumour suppressor locus: all for one or one for all*. Nat Rev Mol Cell Biol, 2006. **7**(9): p. 667-77.
79. Zhang, Y. and Y. Xiong, *Control of p53 ubiquitination and nuclear export by MDM2 and ARF*. Cell Growth Differ, 2001. **12**(4): p. 175-86.
80. Weber, J.D., et al., *Nucleolar Arf sequesters Mdm2 and activates p53*. Nature Cell Biology, 1999. **1**: p. 20.
81. Bracken, A.P., et al., *The Polycomb group proteins bind throughout the INK4A-ARF locus and are disassociated in senescent cells*. Genes & Development, 2007. **21**(5): p. 525-530.
82. Krishnamurthy, J., et al., *Ink4a/Arf expression is a biomarker of aging*. The Journal of Clinical Investigation, 2004. **114**(9): p. 1299-1307.

83. Hengstermann, A., et al., *Complete switch from Mdm2 to human papillomavirus E6-mediated degradation of p53 in cervical cancer cells*. Proceedings of the National Academy of Sciences of the United States of America, 2001. **98**(3): p. 1218-1223.
84. Tam, S.W., J.W. Shay, and M. Pagano, *Differential expression and cell cycle regulation of the cyclin-dependent kinase 4 inhibitor p16Ink4*. Cancer Res, 1994. **54**(22): p. 5816-20.
85. Sritippho, T., et al., *p16 - a Possible Surrogate Marker for High-Risk Human Papillomaviruses in Oral Cancer?* Asian Pac J Cancer Prev, 2016. **17**(8): p. 4049-57.
86. Blagosklonny, M.V., *Geroconversion: irreversible step to cellular senescence*. Cell Cycle, 2014. **13**(23): p. 3628-3635.
87. Herranz, N. and J. Gil, *Mechanisms and functions of cellular senescence*. The Journal of Clinical Investigation, 2018. **128**(4): p. 1238-1246.
88. Nelson, G., et al., *A senescent cell bystander effect: senescence-induced senescence*. Aging Cell, 2012. **11**(2): p. 345-9.
89. Krtolica, A., et al., *Senescent fibroblasts promote epithelial cell growth and tumorigenesis: a link between cancer and aging*. Proc Natl Acad Sci U S A, 2001. **98**(21): p. 12072-7.
90. Laberge, R.M., et al., *MTOR regulates the pro-tumorigenic senescence-associated secretory phenotype by promoting IL1A translation*. Nat Cell Biol, 2015. **17**(8): p. 1049-61.
91. Papanikolaou, G. and K. Pantopoulos, *Iron metabolism and toxicity*. Toxicology and Applied Pharmacology, 2005. **202**(2): p. 199-211.
92. Mackenzie, E.L., K. Iwasaki, and Y. Tsuji, *Intracellular Iron Transport and Storage: From Molecular Mechanisms to Health Implications*. Antioxidants & Redox Signaling, 2008. **10**(6): p. 997-1030.
93. Przybyszewska, J. and E. Zekanowska, *The role of hepcidin, ferroportin, HCP1, and DMT1 protein in iron absorption in the human digestive tract*. Prz Gastroenterol, 2014. **9**(4): p. 208-13.
94. Vashchenko, G. and R.T. MacGillivray, *Multi-copper oxidases and human iron metabolism*. Nutrients, 2013. **5**(7): p. 2289-313.
95. Luck, A.N. and A.B. Mason, *Transferrin-mediated cellular iron delivery*. Curr Top Membr, 2012. **69**: p. 3-35.
96. Chung, M.C.-M., *Structure and function of transferrin*. Biochemical Education, 1984. **12**(4): p. 146-154.
97. Ohgami, R.S., et al., *Identification of a ferrireductase required for efficient transferrin-dependent iron uptake in erythroid cells*. Nat Genet, 2005. **37**(11): p. 1264-9.
98. Dautry-Varsat, A., A. Ciechanover, and H.F. Lodish, *pH and the recycling of transferrin during receptor-mediated endocytosis*. Proceedings of the National Academy of Sciences of the United States of America, 1983. **80**(8): p. 2258-2262.
99. Beguin, Y., et al., *Epidemiological and nonclinical studies investigating effects of iron in carcinogenesis--a critical review*. Crit Rev Oncol Hematol, 2014. **89**(1): p. 1-15.
100. Kakhlon, O. and Z.I. Cabantchik, *The labile iron pool: characterization, measurement, and participation in cellular processes1*. Free Radical Biology and Medicine, 2002. **33**(8): p. 1037-1046.
101. Arosio, P., R. Ingrassia, and P. Cavadini, *Ferritins: a family of molecules for iron storage, antioxidation and more*. Biochim Biophys Acta, 2009. **1790**(7): p. 589-99.
102. Harrison, P.M. and P. Arosio, *The ferritins: molecular properties, iron storage function and cellular regulation*. Biochim Biophys Acta, 1996. **1275**(3): p. 161-203.

103. Lawson, D.M., et al., *Identification of the ferroxidase centre in ferritin*. FEBS Lett, 1989. **254**(1-2): p. 207-10.
104. Levi, S., et al., *Evidence of H- and L-chains have co-operative roles in the iron-uptake mechanism of human ferritin*. Biochem J, 1992. **288 (Pt 2)**: p. 591-6.
105. Martsev, S.P., A.P. Vlasov, and P. Arosio, *Distinct stability of recombinant L and H subunits of human ferritin: calorimetric and ANS binding studies*. Protein Eng, 1998. **11**(5): p. 377-81.
106. Muckenthaler, M.U., B. Galy, and M.W. Hentze, *Systemic Iron Homeostasis and the Iron-Responsive Element/Iron-Regulatory Protein (IRE/IRP) Regulatory Network*. Annual Review of Nutrition, 2008. **28**(1): p. 197-213.
107. Rouault, T.A., *The role of iron regulatory proteins in mammalian iron homeostasis and disease*. Nature Chemical Biology, 2006. **2**: p. 406.
108. Wilkinson, N. and K. Pantopoulos, *The IRP/IRE system in vivo: insights from mouse models*. Frontiers in Pharmacology, 2014. **5**: p. 176.
109. Hentze, M.W., et al., *Identification of the iron-responsive element for the translational regulation of human ferritin mRNA*. Science, 1987. **238**(4833): p. 1570-3.
110. Casey, J.L., et al., *Iron-responsive elements: regulatory RNA sequences that control mRNA levels and translation*. Science, 1988. **240**(4854): p. 924-8.
111. Binder, R., et al., *Evidence that the pathway of transferrin receptor mRNA degradation involves an endonucleolytic cleavage within the 3' UTR and does not involve poly(A) tail shortening*. The EMBO Journal, 1994. **13**(8): p. 1969-1980.
112. Rouault, T.A., *Iron metabolism in the CNS: implications for neurodegenerative diseases*. Nat Rev Neurosci, 2013. **14**(8): p. 551-64.
113. Brazzolotto, X., et al., *Human cytoplasmic aconitase (Iron regulatory protein 1) is converted into its [3Fe-4S] form by hydrogen peroxide in vitro but is not activated for iron-responsive element binding*. J Biol Chem, 1999. **274**(31): p. 21625-30.
114. Guo, B., et al., *Iron regulates the intracellular degradation of iron regulatory protein 2 by the proteasome*. J Biol Chem, 1995. **270**(37): p. 21645-51.
115. Eckard, J., K. Frenkel, and X. Huang, *Iron metabolism and oxygen tension: effect on hypoxia inducible factor (HIF) stabilization*. Cancer Research, 2005. **65**(9 Supplement): p. 264-264.
116. Bruick, R.K. and S.L. McKnight, *A conserved family of prolyl-4-hydroxylases that modify HIF*. Science, 2001. **294**(5545): p. 1337-40.
117. Semenza, G.L., *Hypoxia-inducible factor 1 (HIF-1) pathway*. Sci STKE, 2007. **2007**(407): p. cm8.
118. Sanchez, M., et al., *Iron-regulatory proteins limit hypoxia-inducible factor-2[alpha] expression in iron deficiency*. Nat Struct Mol Biol, 2007. **14**(5): p. 420-426.
119. Nicolas, G., et al., *The gene encoding the iron regulatory peptide hepcidin is regulated by anemia, hypoxia, and inflammation*. J Clin Invest, 2002. **110**(7): p. 1037-44.
120. Pinto, J.P., et al., *Erythropoietin mediates hepcidin expression in hepatocytes through EPOR signaling and regulation of C/EBPalpha*. Blood, 2008. **111**(12): p. 5727-33.
121. Xu, M.M., J. Wang, and J.X. Xie, *Regulation of iron metabolism by hypoxia-inducible factors*. Sheng Li Xue Bao, 2017. **69**(5): p. 598-610.
122. Torti, S.V. and F.M. Torti, *Iron and cancer: more ore to be mined*. Nat Rev Cancer, 2013. **13**(5): p. 342-55.
123. Habeshaw, J.A., et al., *Correlation of transferrin receptor expression with histological class and outcome in non-Hodgkin lymphoma*. Lancet, 1983. **1**(8323): p. 498-501.
124. Prior, R., G. Reifenberger, and W. Wechsler, *Transferrin receptor expression in tumours of the human nervous system: relation to tumour type, grading and tumour growth fraction*. Virchows Arch A Pathol Anat Histopathol, 1990. **416**(6): p. 491-6.

125. Kondo, K., et al., *Transferrin receptor expression in adenocarcinoma of the lung as a histopathologic indicator of prognosis*. Chest, 1990. **97**(6): p. 1367-71.
126. Yang, D.C., et al., *Expression of transferrin receptor and ferritin H-chain mRNA are associated with clinical and histopathological prognostic indicators in breast cancer*. Anticancer Res, 2001. **21**(1b): p. 541-9.
127. Brookes, M.J., et al., *Modulation of iron transport proteins in human colorectal carcinogenesis*. Gut, 2006. **55**(10): p. 1449-1460.
128. Pinnix, Z.K., et al., *Ferroportin and Iron Regulation in Breast Cancer Progression and Prognosis*. Science translational medicine, 2010. **2**(43): p. 43ra56-43ra56.
129. Cheng, J., et al., *Systematic evaluation of connectivity map for disease indications*. Genome Medicine, 2014. **6**: p. 95.
130. Maffettone, C., et al., *Tumorigenic properties of iron regulatory protein 2 (IRP2) mediated by its specific 73-amino acids insert*. PLoS One, 2010. **5**(4): p. e10163.
131. Wang, W., et al., *IRP2 regulates breast tumor growth*. Cancer Res, 2014. **74**(2): p. 497-507.
132. Wu, K.J., A. Polack, and R. Dalla-Favera, *Coordinated regulation of iron-controlling genes, H-ferritin and IRP2, by c-MYC*. Science, 1999. **283**(5402): p. 676-9.
133. Keberle, H., *THE BIOCHEMISTRY OF DESFERRIOXAMINE AND ITS RELATION TO IRON METABOLISM*. Ann N Y Acad Sci, 1964. **119**: p. 758-68.
134. Alta, E.C.P., et al., *Desferrioxamine-caffeine (DFCAF) as a cell permeant moderator of the oxidative stress caused by iron overload*. BioMetals, 2014. **27**(6): p. 1351-1360.
135. Doulias, P.-T., et al., *Endosomal and lysosomal effects of desferrioxamine: protection of HeLa cells from hydrogen peroxide-induced DNA damage and induction of cell-cycle arrest*. Free Radical Biology and Medicine, 2003. **35**(7): p. 719-728.
136. Vermynen, C., *What is new in iron overload?* Eur J Pediatr, 2008. **167**(4): p. 377-81.
137. Caro, J., K.F. Huybrechts, and T.C. Green, *Estimates of the effect on hepatic iron of oral deferiprone compared with subcutaneous desferrioxamine for treatment of iron overload in thalassemia major: a systematic review*. BMC Blood Disord, 2002. **2**(1): p. 4.
138. Haghpanah, S., et al., *Compliance and satisfaction with deferasirox (Exjade(R)) compared with deferoxamine in patients with transfusion-dependent beta-thalassemia*. Hematology, 2014. **19**(4): p. 187-91.
139. Mobarra, N., et al., *A Review on Iron Chelators in Treatment of Iron Overload Syndromes*. International Journal of Hematology-Oncology and Stem Cell Research, 2016. **10**(4): p. 239-247.
140. Abrams, B.B., H. Hänel, and T. Hoehler, *Ciclopirox olamine: A hydroxypyridone antifungal agent*. Clinics in Dermatology, 1991. **9**(4): p. 471-477.
141. Subissi, A., et al., *Ciclopirox: recent nonclinical and clinical data relevant to its use as a topical antimycotic agent*. Drugs, 2010. **70**(16): p. 2133-52.
142. Ghannoum, M.A. and L.B. Rice, *Antifungal Agents: Mode of Action, Mechanisms of Resistance, and Correlation of These Mechanisms with Bacterial Resistance*. Clinical Microbiology Reviews, 1999. **12**(4): p. 501-517.
143. Jue, S.G., G.W. Dawson, and R.N. Brogden, *Ciclopirox olamine 1% cream. A preliminary review of its antimicrobial activity and therapeutic use*. Drugs, 1985. **29**(4): p. 330-41.
144. Bohn, M. and K.T. Kraemer, *Dermatopharmacology of ciclopirox nail lacquer topical solution 8% in the treatment of onychomycosis*. J Am Acad Dermatol, 2000. **43**(4 Suppl): p. S57-69.
145. Leem, S.H., et al., *The possible mechanism of action of ciclopirox olamine in the yeast Saccharomyces cerevisiae*. Mol Cells, 2003. **15**(1): p. 55-61.

146. Linden, T., et al., *The antimycotic ciclopirox olamine induces HIF-1 α stability, VEGF expression, and angiogenesis*. The FASEB Journal, 2003. **17**(6): p. 761-763.
147. Eberhard, Y., et al., *Chelation of intracellular iron with the antifungal agent ciclopirox olamine induces cell death in leukemia and myeloma cells*. Blood, 2009. **114**(14): p. 3064-3073.
148. Clement, P.M.J., et al., *The antifungal drug ciclopirox inhibits deoxyhypusine and proline hydroxylation, endothelial cell growth and angiogenesis in vitro*. International Journal of Cancer, 2002. **100**(4): p. 491-498.
149. Zhou, H., et al., *The antitumor activity of the fungicide ciclopirox*. International journal of cancer. Journal international du cancer, 2010. **127**(10): p. 2467-2477.
150. Coombs, G.S., et al., *Modulation of Wnt/ β -catenin signaling and proliferation by a ferrous iron chelator with therapeutic efficacy in genetically engineered mouse models of cancer*. Oncogene, 2011. **31**: p. 213.
151. Kim, Y., et al., *Targeting the Wnt/ β -catenin pathway with the antifungal agent ciclopirox olamine in a murine myeloma model*. In Vivo, 2011. **25**(6): p. 887-93.
152. Luo, Y., et al., *The fungicide ciclopirox inhibits lymphatic endothelial cell tube formation by suppressing VEGFR-3-mediated ERK signaling pathway*. Oncogene, 2011. **30**(18): p. 2098-2107.
153. Sen, S., et al., *Novel mTOR inhibitory activity of ciclopirox enhances parthenolide antileukemia activity*. Exp Hematol, 2013. **41**(9): p. 799-807 e4.
154. Yang, J., et al., *Targeting histone demethylases in MYC-driven neuroblastomas with ciclopirox*. Cancer Res, 2017.
155. Mihailidou, C., et al., *Superior efficacy of the antifungal agent ciclopirox olamine over gemcitabine in pancreatic cancer models*. Oncotarget, 2018. **9**(12): p. 10360-10374.
156. Weir, S.J., et al., *Preclinical development of ciclopirox prodrug for the treatment of non-muscle invasive and muscle invasive bladder cancer*. Journal of Clinical Oncology, 2018. **36**(15_suppl): p. e14576-e14576.
157. Minden, M.D., et al., *Oral ciclopirox olamine displays biological activity in a phase I study in patients with advanced hematologic malignancies*. Am J Hematol, 2014. **89**(4): p. 363-8.
158. Nair, A.B., et al., *Skin uptake and clearance of ciclopirox following topical application*. Biopharmaceutics & Drug Disposition, 2013. **34**(9): p. 540-549.
159. Kellner, H.M., et al., *[Pharmacokinetics and biotransformation of the antimycotic drug ciclopiroxolamine in animals and man after topical and systemic administration]*. Arzneimittelforschung, 1981. **31**(8a): p. 1337-53.
160. Eberhard, Y., et al., *The off-Patent Anti-Fungal Ciclopirox Olamine Displays Preclinical Activity in Leukemia and Myeloma*. Blood, 2008. **112**(11): p. 944-944.
161. Zhou, B., et al., *A small-molecule blocking ribonucleotide reductase holoenzyme formation inhibits cancer cell growth and overcomes drug resistance*. Cancer research, 2013. **73**(21): p. 10.1158/0008-5472.CAN-13-1094.
162. Crona, M., et al., *A ribonucleotide reductase inhibitor with deoxyribonucleoside-reversible cytotoxicity*. Molecular Oncology, 2016. **10**(9): p. 1375-1386.
163. Aird, K.M., et al., *Identification of ribonucleotide reductase M2 as a potential target for pro-senescence therapy in epithelial ovarian cancer*. Cell Cycle, 2014. **13**(2): p. 199-207.
164. Kuo, M.-L., et al., *RRM2B Suppresses Activation of the Oxidative Stress Pathway and is Up-regulated by P53 During Senescence*. Scientific Reports, 2012. **2**: p. 822.

165. Grusch, M., et al., *Activation of caspases and induction of apoptosis by novel ribonucleotide reductase inhibitors amidox and didox*. *Exp Hematol*, 2001. **29**(5): p. 623-32.
166. Raje, N., et al., *Didox, a ribonucleotide reductase inhibitor, induces apoptosis and inhibits DNA repair in multiple myeloma cells*. *Br J Haematol*, 2006. **135**(1): p. 52-61.
167. Wang, N., Y. Li, and J. Zhou, *Downregulation of ribonucleotide reductase subunits M2 induces apoptosis and G1 arrest of cervical cancer cells*. *Oncology Letters*, 2018. **15**(3): p. 3719-3725.
168. Mathews, C.K., *Deoxyribonucleotide metabolism, mutagenesis and cancer*. *Nat Rev Cancer*, 2015. **15**(9): p. 528-539.
169. Nordlund, P. and P. Reichard, *Ribonucleotide Reductases*. *Annual Review of Biochemistry*, 2006. **75**(1): p. 681-706.
170. Gräslund, A., M. Sahlin, and B.M. Sjöberg, *The tyrosyl free radical in ribonucleotide reductase*. *Environmental Health Perspectives*, 1985. **64**: p. 139-149.
171. Reichard, P., *Interactions between deoxyribonucleotide and DNA synthesis*. *Annu Rev Biochem*, 1988. **57**: p. 349-74.
172. Sjöberg, B.M., et al., *The tyrosine free radical in ribonucleotide reductase from Escherichia coli*. *J Biol Chem*, 1978. **253**(19): p. 6863-5.
173. Tanaka, H., et al., *A ribonucleotide reductase gene involved in a p53-dependent cell-cycle checkpoint for DNA damage*. *Nature*, 2000. **404**: p. 42.
174. Grossi, F., et al., *Expression of Ribonucleotide Reductase Subunit-2 and Thymidylate Synthase Correlates with Poor Prognosis in Patients with Resected Stages I–III Non-Small Cell Lung Cancer*. *Disease Markers*, 2015. **2015**: p. 302649.
175. Guittet, O., et al., *Mammalian p53R2 protein forms an active ribonucleotide reductase in vitro with the R1 protein, which is expressed both in resting cells in response to DNA damage and in proliferating cells*. *J Biol Chem*, 2001. **276**(44): p. 40647-51.
176. Yamaguchi, T., et al., *p53R2-dependent Pathway for DNA Synthesis in a p53-regulated Cell Cycle Checkpoint*. *Cancer Research*, 2001. **61**(22): p. 8256-8262.
177. Bourdon, A., et al., *Mutation of RRM2B, encoding p53-controlled ribonucleotide reductase (p53R2), causes severe mitochondrial DNA depletion*. *Nat Genet*, 2007. **39**(6): p. 776-80.
178. Aye, Y., et al., *Ribonucleotide reductase and cancer: biological mechanisms and targeted therapies*. *Oncogene*, 2015. **34**(16): p. 2011-21.
179. Mannargudi, M.B. and S. Deb, *Clinical pharmacology and clinical trials of ribonucleotide reductase inhibitors: is it a viable cancer therapy?* *Journal of Cancer Research and Clinical Oncology*, 2017. **143**(8): p. 1499-1529.
180. Lassmann, G., L. Thelander, and A. Gräslund, *EPR stopped-flow studies of the reaction of the tyrosyl radical of protein R2 from ribonucleotide reductase with hydroxyurea*. *Biochem Biophys Res Commun*, 1992. **188**(2): p. 879-87.
181. Chapman, T.R. and T.J. Kinsella, *Ribonucleotide reductase inhibitors: a new look at an old target for radiosensitization*. *Front Oncol*, 2011. **1**: p. 56.
182. von Knebel Doeberitz, M., et al., *Inhibition of tumorigenicity of cervical cancer cells in nude mice by HPV E6-E7 anti-sense RNA*. *Int J Cancer*, 1992. **51**(5): p. 831-4.
183. Yu, Y., et al., *EdU incorporation is an alternative non-radioactive assay to [³H]thymidine uptake for in vitro measurement of mice T-cell proliferations*. *J Immunol Methods*, 2009. **350**(1-2): p. 29-35.
184. Dimri, G.P., et al., *A biomarker that identifies senescent human cells in culture and in aging skin in vivo*. *Proc Natl Acad Sci U S A*, 1995. **92**(20): p. 9363-7.
185. El-Deiry, W.S., et al., *WAF1/CIP1 Is Induced in p53-mediated G1 Arrest and Apoptosis*. *Cancer Research*, 1994. **54**(5): p. 1169-1174.

186. Shieh, S.Y., et al., *DNA damage-induced phosphorylation of p53 alleviates inhibition by MDM2*. Cell, 1997. **91**(3): p. 325-34.
187. Loughery, J., et al., *Critical role for p53-serine 15 phosphorylation in stimulating transactivation at p53-responsive promoters*. Nucleic Acids Research, 2014. **42**(12): p. 7666-7680.
188. Kuo, L.J. and L.X. Yang, *Gamma-H2AX - a novel biomarker for DNA double-strand breaks*. In Vivo, 2008. **22**(3): p. 305-9.
189. Hengstermann, A., et al., *Growth suppression induced by downregulation of E6-AP expression in human papillomavirus-positive cancer cell lines depends on p53*. J Virol, 2005. **79**(14): p. 9296-300.
190. Blase, J.I., *Influence of iron metabolism on human papillomavirus oncogene expression*. Unpublished master's thesis. University of Lübeck, Germany, 2017.
191. Fridman, J.S. and S.W. Lowe, *Control of apoptosis by p53*. Oncogene, 2003. **22**: p. 9030.
192. Bunz, F., et al., *Requirement for p53 and p21 to Sustain G₂ Arrest After DNA Damage*. Science, 1998. **282**(5393): p. 1497-1501.
193. Waldman, T., K.W. Kinzler, and B. Vogelstein, *p21 Is Necessary for the p53-mediated G₁ Arrest in Human Cancer Cells*. Cancer Research, 1995. **55**(22): p. 5187-5190.
194. Zheng, Y. and Y. Jiang, *mTOR Inhibitors at a Glance*. Molecular and cellular pharmacology, 2015. **7**(2): p. 15-20.
195. Sarbassov, D.D., et al., *Prolonged Rapamycin Treatment Inhibits mTORC2 Assembly and Akt/PKB*. Molecular Cell, 2006. **22**(2): p. 159-168.
196. Choo, A.Y., et al., *Rapamycin differentially inhibits S6Ks and 4E-BP1 to mediate cell-type-specific repression of mRNA translation*. Proceedings of the National Academy of Sciences of the United States of America, 2008. **105**(45): p. 17414-17419.
197. Brugarolas, J., et al., *Regulation of mTOR function in response to hypoxia by REDD1 and the TSC1/TSC2 tumor suppressor complex*. Genes Dev, 2004. **18**(23): p. 2893-904.
198. Leontieva, O.V. and M.V. Blagosklonny, *Hypoxia and gerosuppression: the mTOR saga continues*. Cell Cycle, 2012. **11**(21): p. 3926-31.
199. Brown, J.M., *Tumor Hypoxia in Cancer Therapy*, in *Methods in Enzymology*. 2007, Academic Press. p. 295-321.
200. Herrmann, A.L., *Cooperative Effects of Iron Chelation with Chemo- and Radiotherapy in HPV-Positive Tumour Cells*. Unpublished master's thesis. Faculty of Biosciences, Faculty of Chemistry and Earth Sciences, University of Heidelberg, Germany, 2018.
201. Hoppe-Seyler, F. and K. Butz, *Cellular control of human papillomavirus oncogene transcription*. Molecular Carcinogenesis, 1994. **10**(3): p. 134-141.
202. Huang, X., et al., *Deferoxamine synergistically enhances iron-mediated AP-1 activation: a showcase of the interplay between extracellular-signal-regulated kinase and tyrosine phosphatase*. Free Radic Res, 2007. **41**(10): p. 1135-42.
203. Vollgraf, U., M. Wegner, and C. Richter-Landsberg, *Activation of AP-1 and Nuclear Factor- κ B Transcription Factors Is Involved in Hydrogen Peroxide-Induced Apoptotic Cell Death of Oligodendrocytes*. Journal of Neurochemistry, 2002. **73**(6): p. 2501-2509.
204. Kyo, S., et al., *Expression of AP1 during cellular differentiation determines human papillomavirus E6/E7 expression in stratified epithelial cells*. J Gen Virol, 1997. **78** (Pt 2): p. 401-11.

205. Rösl, F., et al., *Antioxidant-induced changes of the AP-1 transcription complex are paralleled by a selective suppression of human papillomavirus transcription*. Journal of Virology, 1997. **71**(1): p. 362-370.
206. Angel, P. and M. Karin, *The role of Jun, Fos and the AP-1 complex in cell-proliferation and transformation*. Biochim Biophys Acta, 1991. **1072**(2-3): p. 129-57.
207. Prusty, B.K. and B.C. Das, *Constitutive activation of transcription factor AP-1 in cervical cancer and suppression of human papillomavirus (HPV) transcription and AP-1 activity in HeLa cells by curcumin*. International Journal of Cancer, 2005. **113**(6): p. 951-960.
208. Soto, U., et al., *Genetic complementation to non-tumorigenicity in cervical-carcinoma cells correlates with alterations in AP-1 composition*. International Journal of Cancer, 2000. **86**(6): p. 811-817.
209. Henken, F.E., et al., *The functional role of Notch signaling in HPV-mediated transformation is dose-dependent and linked to AP-1 alterations*. Cell Oncol (Dordr), 2012. **35**(2): p. 77-84.
210. Talora, C., et al., *Specific down-modulation of Notch1 signaling in cervical cancer cells is required for sustained HPV-E6/E7 expression and late steps of malignant transformation*. Genes Dev, 2002. **16**(17): p. 2252-63.
211. Kyo, S., et al., *NF-IL6 represses early gene expression of human papillomavirus type 16 through binding to the noncoding region*. Journal of Virology, 1993. **67**(2): p. 1058-1066.
212. Dlaska, M. and G. Weiss, *Central role of transcription factor NF-IL6 for cytokine and iron-mediated regulation of murine inducible nitric oxide synthase expression*. J Immunol, 1999. **162**(10): p. 6171-7.
213. Campillos, M., et al., *SIREs: searching for iron-responsive elements*. Nucleic Acids Research, 2010. **38**(Web Server issue): p. W360-W367.
214. Rosenberger, S., et al., *Alternative splicing of human papillomavirus type-16 E6/E6* early mRNA is coupled to EGF signaling via Erk1/2 activation*. Proceedings of the National Academy of Sciences of the United States of America, 2010. **107**(15): p. 7006-7011.
215. Shen, T., et al., *Ciclopirox inhibits cancer cell proliferation by suppression of Cdc25A*. Genes Cancer, 2017. **8**(3-4): p. 505-516.
216. Simonart, T., et al., *Antiproliferative and apoptotic effects of iron chelators on human cervical carcinoma cells*. Gynecol Oncol, 2002. **85**(1): p. 95-102.
217. Simonart, T., et al., *Iron withdrawal strategies fail to prevent the growth of SiHa-induced tumors in mice*. Gynecologic Oncology, 2003. **90**(1): p. 91-95.
218. Pahl, P.M.B. and L.D. Horwitz, *Cell Permeable Iron Chelators as Potential Cancer Chemotherapeutic Agents*. Cancer Investigation, 2005. **23**(8): p. 683-691.
219. Mémin, E., et al., *Blocking eIF5A Modification in Cervical Cancer Cells Alters the Expression of Cancer-Related Genes and Suppresses Cell Proliferation*. Cancer research, 2014. **74**(2): p. 552-562.
220. Urbani, L., S.W. Sherwood, and R.T. Schimke, *Dissociation of nuclear and cytoplasmic cell cycle progression by drugs employed in cell synchronization*. Exp Cell Res, 1995. **219**(1): p. 159-68.
221. Szüts, D. and T. Krude, *Cell cycle arrest at the initiation step of human chromosomal DNA replication causes DNA damage*. Journal of Cell Science, 2004. **117**(21): p. 4897-4908.
222. Yoon, G., et al., *Iron chelation-induced senescence-like growth arrest in hepatocyte cell lines: association of transforming growth factor beta1 (TGF-beta1)-mediated p27Kip1 expression*. Biochem J, 2002. **366**(Pt 2): p. 613-21.

223. Pai, C.-C. and S.E. Kearsey, *A Critical Balance: dNTPs and the Maintenance of Genome Stability*. Genes, 2017. **8**(2): p. 57.
224. Eriksson, S., et al., *Cell cycle-dependent regulation of mammalian ribonucleotide reductase. The S phase-correlated increase in subunit M2 is regulated by de novo protein synthesis*. J Biol Chem, 1984. **259**(19): p. 11695-700.
225. Bianchi, V., E. Pontis, and P. Reichard, *Changes of deoxyribonucleoside triphosphate pools induced by hydroxyurea and their relation to DNA synthesis*. J Biol Chem, 1986. **261**(34): p. 16037-42.
226. Petermann, E., et al., *Hydroxyurea-Stalled Replication Forks Become Progressively Inactivated and Require Two Different RAD51-Mediated Pathways for Restart and Repair*. Molecular Cell, 2010. **37**(4): p. 492-502.
227. Coyle, M.B. and B. Strauss, *Cell Killing and the Accumulation of Breaks in the DNA of HEp-2 Cells Incubated in the Presence of Hydroxyurea*. Cancer Research, 1970. **30**(9): p. 2314-2319.
228. Cimprich, K.A. and D. Cortez, *ATR: an essential regulator of genome integrity*. Nat Rev Mol Cell Biol, 2008. **9**(8): p. 616-27.
229. Ganeshaguru, K., et al., *Effect of various iron chelating agents on DNA synthesis in human cells*. Biochemical Pharmacology, 1980. **29**(9): p. 1275-1279.
230. Shen, T., et al., *Ciclopirox activates ATR-Chk1 signaling pathway leading to Cdc25A protein degradation*. Genes & Cancer, 2018. **9**(1-2): p. 39-52.
231. Mannava, S., et al., *Depletion of Deoxyribonucleotide Pools Is an Endogenous Source of DNA Damage in Cells Undergoing Oncogene-Induced Senescence*. The American Journal of Pathology, 2013. **182**(1): p. 142-151.
232. Aird, Katherine M., et al., *Suppression of Nucleotide Metabolism Underlies the Establishment and Maintenance of Oncogene-Induced Senescence*. Cell Reports, 2013. **3**(4): p. 1252-1265.
233. R L Blakley, a. and E. Vitols, *The Control of Nucleotide Biosynthesis*. Annual Review of Biochemistry, 1968. **37**(1): p. 201-224.
234. Wells, S.I., et al., *Papillomavirus E2 induces senescence in HPV-positive cells via pRB- and p21^{CIP}-dependent pathways*. The EMBO Journal, 2000. **19**(21): p. 5762-5771.
235. DeFilippis, R.A., et al., *Endogenous Human Papillomavirus E6 and E7 Proteins Differentially Regulate Proliferation, Senescence, and Apoptosis in HeLa Cervical Carcinoma Cells*. Journal of Virology, 2003. **77**(2): p. 1551-1563.
236. Tibbetts, R.S., et al., *A role for ATR in the DNA damage-induced phosphorylation of p53*. Genes Dev, 1999. **13**(2): p. 152-7.
237. Canman, C.E., et al., *Activation of the ATM Kinase by Ionizing Radiation and Phosphorylation of p53*. Science, 1998. **281**(5383): p. 1677-1679.
238. Rebbaa, A., et al., *The role of histone acetylation versus DNA damage in drug-induced senescence and apoptosis*. Cell Death And Differentiation, 2006. **13**: p. 1960.
239. Jacobs, J.J. and T. de Lange, *Significant role for p16INK4a in p53-independent telomere-directed senescence*. Curr Biol, 2004. **14**(24): p. 2302-8.
240. Yamakoshi, K., et al., *Real-time in vivo imaging of p16(Ink4a) reveals cross talk with p53*. The Journal of Cell Biology, 2009. **186**(3): p. 393-407.
241. Wang, W., et al., *Sequential Activation of the MEK-Extracellular Signal-Regulated Kinase and MKK3/6-p38 Mitogen-Activated Protein Kinase Pathways Mediates Oncogenic *ras*-Induced Premature Senescence*. Molecular and Cellular Biology, 2002. **22**(10): p. 3389-3403.

242. Ye, X., et al., *Downregulation of Wnt signaling is a trigger for formation of facultative heterochromatin and onset of cell senescence in primary human cells*. Mol Cell, 2007. **27**(2): p. 183-96.
243. Song, S., et al., *Wnt inhibitor screen reveals iron dependence of beta-catenin signaling in cancers*. Cancer Res, 2011. **71**(24): p. 7628-39.
244. Veeman, M.T., et al., *Zebrafish prickles, a modulator of noncanonical Wnt/Fz signaling, regulates gastrulation movements*. Curr Biol, 2003. **13**(8): p. 680-5.
245. Iavarone, A. and J. Massague, *Repression of the CDK activator Cdc25A and cell-cycle arrest by cytokine TGF-beta in cells lacking the CDK inhibitor p15*. Nature, 1997. **387**(6631): p. 417-22.
246. Saha, P., et al., *p21CIP1 and Cdc25A: competition between an inhibitor and an activator of cyclin-dependent kinases*. Mol Cell Biol, 1997. **17**(8): p. 4338-45.
247. Gautier, J., et al., *cdc25 is a specific tyrosine phosphatase that directly activates p34cdc2*. Cell, 1991. **67**(1): p. 197-211.
248. Nguyen, D.X., T.F. Westbrook, and D.J. McCance, *Human Papillomavirus Type 16 E7 Maintains Elevated Levels of the cdc25A Tyrosine Phosphatase during Dereglulation of Cell Cycle Arrest*. Journal of Virology, 2002. **76**(2): p. 619-632.
249. Katich, S.C., K. Zerfass-Thome, and I. Hoffmann, *Regulation of the Cdc25A gene by the human papillomavirus Type 16 E7 oncogene*. Oncogene, 2001. **20**(5): p. 543-50.
250. Wu, L., et al., *E2F-Rb Complexes Assemble and Inhibit cdc25A Transcription in Cervical Carcinoma Cells following Repression of Human Papillomavirus Oncogene Expression*. Molecular and Cellular Biology, 2000. **20**(19): p. 7059-7067.
251. Lane, D.J.R., et al., *N-myc Downstream Regulated 1 (NDRG1) Is Regulated by Eukaryotic Initiation Factor 3a (eIF3a) during Cellular Stress Caused by Iron Depletion*. PLOS ONE, 2013. **8**(2): p. e57273.
252. Ellen, T.P., et al., *NDRG1, a growth and cancer related gene: regulation of gene expression and function in normal and disease states*. Carcinogenesis, 2008. **29**(1): p. 2-8.
253. Wang, J., et al., *Expression and biological function of N-myc down-regulated gene 1 in human cervical cancer*. Journal of Huazhong University of Science and Technology [Medical Sciences], 2010. **30**(6): p. 771-776.
254. Demidenko, Z.N., et al., *Rapamycin decelerates cellular senescence*. Cell Cycle, 2009. **8**(12): p. 1888-95.
255. Zhou, H., et al., *Ciclopirox Olamine inhibits mTORC1 signaling by activation of AMPK*. Biochemical pharmacology, 2016. **116**: p. 39-50.
256. Shoshani, T., et al., *Identification of a Novel Hypoxia-Inducible Factor 1-Responsive Gene, RTP801, Involved in Apoptosis*. Molecular and Cellular Biology, 2002. **22**(7): p. 2283-2293.
257. Hardie, D.G., *AMP-activated protein kinase: an energy sensor that regulates all aspects of cell function*. Genes Dev, 2011. **25**(18): p. 1895-908.
258. Sarbassov, D.D., et al., *Phosphorylation and regulation of Akt/PKB by the rictor-mTOR complex*. Science, 2005. **307**(5712): p. 1098-101.
259. Yang, H.W., et al., *mTORC2 facilitates endothelial cell senescence by suppressing Nrf2 expression via the Akt/GSK-3beta/C/EBPalpha signaling pathway*. Acta Pharmacol Sin, 2018.
260. Garcia-Martinez, J.M., et al., *Ku-0063794 is a specific inhibitor of the mammalian target of rapamycin (mTOR)*. Biochem J, 2009. **421**(1): p. 29-42.
261. Li, W., et al., *Hypoxia-induced endothelial proliferation requires both mTORC1 and mTORC2*. Circ Res, 2007. **100**(1): p. 79-87.

262. Stegeman, H., et al., *Interaction between hypoxia, AKT and HIF-1 signaling in HNSCC and NSCLC: implications for future treatment strategies*. Future Science OA, 2016. **2**(1): p. FSO84.
263. Leszczynska, K.B., et al., *Hypoxia-induced p53 modulates both apoptosis and radiosensitivity via AKT*. The Journal of Clinical Investigation, 2015. **125**(6): p. 2385-2398.
264. Coppé, J.-P., et al., *The Senescence-Associated Secretory Phenotype: The Dark Side of Tumor Suppression*. Annual review of pathology, 2010. **5**: p. 99-118.
265. Hanauske-Abel, H.M., et al., *Drug-induced reactivation of apoptosis abrogates HIV-1 infection*. PLoS One, 2013. **8**(9): p. e74414.
266. Kim, J.L., et al., *Iron chelator-induced apoptosis via the ER stress pathway in gastric cancer cells*. Tumour Biol, 2016. **37**(7): p. 9709-19.
267. Hileti, D., P. Panayiotidis, and A.V. Hoffbrand, *Iron chelators induce apoptosis in proliferating cells*. Br J Haematol, 1995. **89**(1): p. 181-7.
268. Greene, B.T., et al., *Activation of caspase pathways during iron chelator-mediated apoptosis*. J Biol Chem, 2002. **277**(28): p. 25568-75.
269. Kamihara, Y., et al., *The iron chelator deferasirox induces apoptosis by targeting oncogenic Pyk2/ β -catenin signaling in human multiple myeloma*. Oncotarget, 2016. **7**(39): p. 64330-64341.
270. Tait, S.W.G. and D.R. Green, *Caspase independent cell death: leaving the set without the final cut*. Oncogene, 2008. **27**(50): p. 6452-6461.
271. Lee, S.J., et al., *Ciclopirox protects mitochondria from hydrogen peroxide toxicity*. Br J Pharmacol, 2005. **145**(4): p. 469-76.
272. Robb, S.J., et al., *Influence of calcium and iron on cell death and mitochondrial function in oxidatively stressed astrocytes*. J Neurosci Res, 1999. **55**(6): p. 674-86.
273. Yoon, Y.S., et al., *Mitochondrial dysfunction via disruption of complex II activity during iron chelation-induced senescence-like growth arrest of Chang cells*. Ann N Y Acad Sci, 2004. **1011**: p. 123-32.
274. Hanauske-Abel, H.M., et al., *Drug-Induced Reactivation of Apoptosis Abrogates HIV-1 Infection*. PLoS ONE, 2013. **8**(9): p. e74414.
275. Hoque, M., et al., *Inhibition of HIV-1 gene expression by Ciclopirox and Deferiprone, drugs that prevent hypusination of eukaryotic initiation factor 5A*. Retrovirology, 2009. **6**: p. 90-90.
276. Sun, Z., et al., *Apoptosis induction by eIF5A1 involves activation of the intrinsic mitochondrial pathway*. J Cell Physiol, 2010. **223**(3): p. 798-809.
277. Gartel, A.L. and A.L. Tyner, *The Role of the Cyclin-dependent Kinase Inhibitor p21 in Apoptosis 1 Supported in part by NIH Grant R01 DK56283 (to A. L. T.) for the p21 research and Campus Research Board and Illinois Department of Public Health Penny Severns Breast and Cervical Cancer grants (to A. L. G.)*. [Molecular Cancer Therapeutics](#), 2002. **1**(8): p. 639-649.
278. Baar, M.P., et al., *Targeted Apoptosis of Senescent Cells Restores Tissue Homeostasis in Response to Chemotoxicity and Aging*. Cell, 2017. **169**(1): p. 132-147.e16.
279. Wang, E., *Senescent human fibroblasts resist programmed cell death, and failure to suppress bcl2 is involved*. Cancer Res, 1995. **55**(11): p. 2284-92.
280. Gui, C.Y., et al., *The apoptosis of HEL cells induced by hydroxyurea**. Cell Research, 1997. **7**: p. 91.
281. Olmos, G., et al., *Quantitation of apoptosis induction by etoposide or hydroxyurea in mouse interleukin 3-dependent lymphoma cells*. In Vivo, 2005. **19**(2): p. 455-64.

282. Kuo, M.L., et al., *The interaction of hydroxyurea and ionizing radiation in human cervical carcinoma cells*. *Cancer J Sci Am*, 1997. **3**(3): p. 163-73.
283. Johnson, C.A., et al., *Hydroxyurea induces apoptosis and regular DNA fragmentation in a Burkitt's lymphoma cell line*. *Biochim Biophys Acta*, 1992. **1136**(1): p. 1-4.
284. Greijer, A.E. and E. van der Wall, *The role of hypoxia inducible factor 1 (HIF-1) in hypoxia induced apoptosis*. *Journal of Clinical Pathology*, 2004. **57**(10): p. 1009-1014.
285. Saikumar, P., et al., *Role of hypoxia-induced Bax translocation and cytochrome c release in reoxygenation injury*. *Oncogene*, 1998. **17**(26): p. 3401-15.
286. Kim, J.-Y. and J.-H. Park, *ROS-dependent caspase-9 activation in hypoxic cell death*. *FEBS Letters*, 2003. **549**(1-3): p. 94-98.
287. Sendoel, A. and M.O. Hengartner, *Apoptotic Cell Death Under Hypoxia*. *Physiology*, 2014. **29**(3): p. 168-176.
288. Chen, D., et al., *Direct interactions between HIF-1 alpha and Mdm2 modulate p53 function*. *J Biol Chem*, 2003. **278**(16): p. 13595-8.
289. van Moorsel, C.J., et al., *Combination chemotherapy studies with gemcitabine and etoposide in non-small cell lung and ovarian cancer cell lines*. *Biochem Pharmacol*, 1999. **57**(4): p. 407-15.
290. Hreshchyshyn, M.M., et al., *Hydroxyurea or placebo combined with radiation to treat stages iib and iv cervical cancer confined to the pelvis*. *International Journal of Radiation Oncology*Biology*Physics*, 1979. **5**(3): p. 317-322.
291. Kunos, C.A., et al., *Modulating Radiation Resistance by Inhibiting Ribonucleotide Reductase in Cancers with Virally or Mutationally Silenced p53 Protein*. *Radiation research*, 2009. **172**(6): p. 666.
292. Kunos, C.A., et al., *Ribonucleotide Reductase Inhibition Enhances Chemoradiosensitivity of Human Cervical Cancers*. *Radiation research*, 2010. **174**(5): p. 574-581.
293. Zhen, S., et al., *In Vitro and In Vivo Synergistic Therapeutic Effect of Cisplatin with Human Papillomavirus16 E6/E7 CRISPR/Cas9 on Cervical Cancer Cell Line*. *Transl Oncol*, 2016. **9**(6): p. 498-504.
294. Jung, H.S., et al., *The synergistic therapeutic effect of cisplatin with Human papillomavirus E6/E7 short interfering RNA on cervical cancer cell lines in vitro and in vivo*. *International Journal of Cancer*, 2012. **130**(8): p. 1925-1936.
295. Ceschin-Roques, C.G., et al., *Ciclopiroxolamine cream 1%: in vitro and in vivo penetration into the stratum corneum*. *Skin Pharmacol*, 1991. **4**(2): p. 95-9.
296. Housman, G., et al., *Drug Resistance in Cancer: An Overview*. *Cancers*, 2014. **6**(3): p. 1769-1792.
297. Ghelardi, E., et al., *In vitro evaluation of the potential of ciclopirox to induce resistance in Trichophyton rubrum, in comparison to terbinafine, amorolfine, and itraconazole*. *Journal of the American Academy of Dermatology*, 2013. **68**(4): p. AB106.
298. Niewerth, M., et al., *Ciclopirox Olamine Treatment Affects the Expression Pattern of Candida albicans Genes Encoding Virulence Factors, Iron Metabolism Proteins, and Drug Resistance Factors*. *Antimicrobial Agents and Chemotherapy*, 2003. **47**(6): p. 1805-1817.
299. Chen, C. and H. Okayama, *High-efficiency transformation of mammalian cells by plasmid DNA*. *Mol Cell Biol*, 1987. **7**(8): p. 2745-52.
300. McAlister, G.C., et al., *MultiNotch MS3 enables accurate, sensitive, and multiplexed detection of differential expression across cancer cell line proteomes*. *Anal Chem*, 2014. **86**(14): p. 7150-8.

301. Smyth, G.K., *Linear models and empirical bayes methods for assessing differential expression in microarray experiments*. Stat Appl Genet Mol Biol, 2004. **3**: p. Article3.
302. Vizcaino, J.A., et al., *2016 update of the PRIDE database and its related tools*. Nucleic Acids Res, 2016. **44**(D1): p. D447-56.
303. Livak, K.J. and T.D. Schmittgen, *Analysis of relative gene expression data using real-time quantitative PCR and the 2(-Delta Delta C(T)) Method*. Methods, 2001. **25**(4): p. 402-8.